Aus Klinik für Kardiologie und Pneumologie

(Prof. Dr. med. G. Hasenfuß)

der Medizinischen Fakultät der Universität Göttingen

The role of SFRP5 in cardiomyocyte function

INAUGURAL-DISSERTATION

zur Erlangung des Doktorgrades

der Medizinischen Fakultät der

Georg-August-Universität zu Göttingen

vorgelegt von

Frederike Weber

aus

Gehrden

Göttingen 2020

Hiermit erkläre ich, die Dissertation mit dem Titel "The role of SFRP5 in cardiomyocyte function" eigenständig angefertigt und keine anderen als die von mir angegebenen Quellen und Hilfsmittel verwendet zu haben.

Göttingen, den ……………   ……………………………………………………

Contents

List of figures

List of tables

List of abbreviations

18S	18S ribosomal RNA
AAV	Adeno associated virus
BSA	Bovine serum albumin
CAMKII	Calcium-calmodulin dependent kinase II
CaspaseI	Cysteinyl-aspartate specific protease
cDNA	Complementary DNA
CH	Compensated hypertrophy
CICR	Calcium-induced calcium-release
Control^{OE}	AAV-Basic treated
CRISPR/Cas9	Clustered Regularly Interspaced Short Palindromic Repeats and Cas9 nuclease
cTnT	Cardiac troponin T
Cx43	Connexin 43
DMEM	Dulbecco's Modified Eagle Medium
DNA	Deoxyribonucleic acid
DSB	Double strand breaks
EDTA	Ethylenediaminetetraacetic acid
ER	Endoplasmic reticulum
FACS	Fluorescence activated cell sorting
FCS	Fetal calf serum
gDNA	Genomic DNA
gRNA	Guide ribonucleic acid
hESC	Human embryonic stem cells
hiPSC	Human induced embryonic stem cells
hiPSC-CM	hiPSC derived cardiomyocytes
LB-Agar	Lysogeny broth agar
LTCC	L-type calcium channel
MEF	Mouse embryonic fibroblasts
MOI	Multiplicity of infection
mPTP	Mitochondrial permeability transition pore
mRNA-seq	mRNA-sequencing
NCX	Sodium-calcium exchanger
NHEJ	Non-homologous end joining
NKA	Sodium-potassium ATPase
pAAV	Overexpression plasmid of AAV
PCA	Principal component analysis
PCR	Polymerase chain reaction
Pen/Strep	Penicillin-Streptomycin solution
PKA	Protein kinase A
PKCε	Protein kinase C isoform ε

ROS	Reactive oxygen species
RT	Room temperature
RYR2	Ryanodine receptor 2
SDS-PAGE	Sodium dodecyl sulfate-polyacrylamide gel electrophoresis
SERCA2A	Sarcoplasmic/endoplasmic reticulum ATPase 2A
SFRP5^{KO}	CRISPR/Cas9-mediated SFRP5 knock out
SFRP5^{OE}	AAV-mediated SFRP5 overexpression
SFRP5^{WT}	Wild type SFRP5
SFRPs	Secreted-frizzled-related proteins
SR	Sarcoplasmic reticulum
TAC	Transverse aortic constriction
TBS-T	Tris-buffered saline with Tween20
TNFα	Tumor necrosis factor α
TZV	Thiazovin
UPR	Unfolded protein response

1   Introduction

1.1 The transition from cardiac hypertrophy to heart failure in the pressure-overloaded heart

In Europe, cardiovascular diseases cause 47 % of all deaths and thereby represent the most common cause of death in European countries. There are many risk factors for developing cardiovascular diseases, including ischemic heart diseases, alcohol abuse, high blood cholesterol, hypertension, smoking, obesity, and diabetes. Therefore, the disease prevalence is widespread among the European population (all reviewed in Nichols et al. 2014).

Heart failure is an end-stage disease resulting from a prior process of cardiac remodeling. This cardiac remodeling is "defined as a group of molecular, cellular and interstitial changes that manifest clinically as changes in size, mass, geometry and function of the heart after injury" (Azevedo et al. 2016). For example, aortic stenosis patients develop pressure-overload in the left ventricle resulting in concentric hypertrophy with preserved ejection fraction, cardiac function, and blood pressure, also known as compensated hypertrophy (CH). Despite preserved cardiac function, hypertrophied hearts already displayed a reduced contractile reserve and reduced chronotropic response during exercise (Lam et al. 2010). The occurring cardiac remodeling process leads to a decompensation of concentric hypertrophy into eccentric hypertrophy and terminally into systolic heart failure (HF) with reduced ejection fraction and cardiac function, and left ventricle dilation (Kannel et al. 1969; Levy et al. 1990; Vakili et al. 2001; Frey and Olson 2003). Due to the reduced stroke volume, the metabolic demands of the heart are insufficiently fulfilled and the additional development of cardiac arrhythmias can lead to sudden death of HF patients (Mozaffarian et al. 2007). Despite intensive research, the molecular mechanisms underlying the transition from reversible CH to irreversible HF with significantly reduced ejection fraction are still poorly understood. Additionally, there is a lack of new drugs that specifically and efficiently prevent the transformation towards irreversible HF (reviewed in Ponikowski et al. 2014 and Schirone et al. 2017).

The mechanical stretch during pathologic hypertrophy stimulates neurohumoral signaling, facilitating contractile dysfunction in the pressure-overloaded heart. Contrarily, in hypertrophy induced by gravidity or extensive exercise, growth hormones and insulin-like growth factors stimulate physiological hypertrophy of the heart through the PI3K-pathway. The physiological hypertrophic state is associated with normal or increased cardiac function and normal survival. The differences between physiological and pathological remodeling are reviewed in detail by Nakamura and Sadoshima (2018).

Cardiac remodeling is characterized by cardiomyocyte hypertrophy, cardiomyocyte loss and myocardial fibrosis (reviewed in Schirone et al. 2017). Multiple mechanisms and pathways are involved in the development of cardiac hypertrophy. One known pathological neurohumoral stimulus inducing cardiac remodeling occurs by angiotensin II. Through the G-protein coupled receptor the downstream phospholipase C and PI3K pathways are activated, mediating NFAT-induced transcription of the hypertrophic gene program (reviewed in Schirone et al. 2017). Additionally, the increase in volume, mass, and shape in hypertrophic cardiomyocytes is related to the re-expression of a fetal gene program (Michalak and Agellon 2018). Further repression of contractile function occurs by the disrupted homeostasis of contractile filaments, e.g. between the α and β isoform of myosin (Herron and McDonald 2002). Contrarily, it is known that cardioprotective natriuretic peptides (ANP, BNP) are also upregulated during cardiac remodeling, antagonizing cardiac hypertrophic growth and cardiac fibrosis (Calderone et al. 1998; Silberbach et al. 1999; Tamura et al. 2000). Further complex pathways are involved in hypertrophy induction, e.g. MAPK/ERK1/2/JNK/p38 pathway and calcium-calmodulin dependent kinase II (CAMKII) mediated protein regulation, whereas especially the last one seems to play a major role in the detrimental process of cardiac remodeling (reviewed in Luo and Anderson 2013 and Schirone et al. 2017).

Further processes promoting cardiac decompensation leading to HF involve cardiomyocyte loss, inflammation, and fibrosis. During cardiac remodeling, cardiomyocyte loss is mediated by apoptosis, autophagy, and necroptosis (a form of programmed necrosis, reviewed in Schirone et al. 2017). Additionally, only recently it was shown that in an early phase of the pressure-overloaded heart the inflammation through neutrophils and macrophages is required to induce cardiac hypertrophy (Wang

et al. 2019). As a result of occurring inflammation and myocardial apoptosis the cardiac fibroblasts produce collagen type I and III that increases myocardial fibrosis and leads to passive stiffness with subsequent diastolic dysfunction (reviewed in Segura et al. 2014). The interaction between hypertrophy, apoptosis, and fibrosis may also depend on mitochondrial dysfunction. To meet the metabolic demand of the pressure-overloaded heart, energy production via oxidative phosphorylation is strained, thereby leading to increased reactive oxygen species (ROS)-production in mitochondria. Mitochondrial ROS physiologically function as transcriptional regulators of mitochondrial genes and are involved in excitation-contraction-coupling and cell differentiation (Burgoyne et al. 2012). However, pathologically increased ROS concentration is detrimental for energy production via induced mitochondrial DNA damage (Burgoyne et al. 2012). In angiotensin II-treated mice, the hypertrophic cardiomyocytes display increased mitochondrial ROS, which facilitates cardiac fibrosis and hypertrophy while fibrosis is associated with cardiomyocyte loss, as described above (Dai et al. 2011).

Current therapies decelerating the transition from CH to HF involve the blockage of the renin-angiotensin-aldosterone system, β-adrenergic blockage of the heart, and the implantation of electrical devices such as cardiac resynchronization therapy and mechanical ventricular assist devices (reviewed in Luo and Anderson 2013). Despite improving the clinical state of the patients by using current therapies, cardiac remodeling advances resulting in irreversible decompensated HF with life-threatening symptoms. The incomplete understanding of the complex mechanisms resulting in the transition from CH to HF has prevented the development of new drugs and therapies so far (reviewed in Ponikowski et al. 2014). Therefore, current research focuses on the identification of involved molecular pathways to elaborate new drugs and therapies inhibiting or reversing cardiac remodeling, thereby preventing irreversible end-stage HF.

1.1.1 Cardiac contraction and impaired calcium handling in cardiac remodeling and heart failure

Cardiomyocyte contraction is a complex process initiated through calcium-induced calcium release (CICR) leading to crossbridging between actin and myosin, which results in cardiomyocyte contraction. An action potential depolarizes the membrane by opening of voltage-dependent sodium channels along the T-tubule system.

Subsequently, voltage-dependent L-type calcium channels (LTCC) open and cause an influx of calcium into the cytosol. This calcium influx triggers an additional calcium release from the sarcoplasmic reticulum (SR) through ryanodine receptor 2 (RYR2). This leads to an extensive increase of the cytosolic calcium concentration by a mechanism known as CICR. Consequently, conformation change of troponin induced by calcium binding uncovers the myosin binding site for crossbridging of actin and myosin facilitating myocardial contraction. Cytosolic calcium reuptake in the diastole occurrs within the SR or extracellular space by sarcoplasmic/endoplasmic reticulum calcium ATPase 2a (SERCA2a) or sodium-calcium exchanger (NCX) (reviewed in Luo and Anderson 2013).

The described excitation-contraction-coupling is essential for cardiomyocyte function, whereas its dysregulation diminishes cardiac contractile force and is associated with CH and HF (Gómez et al. 1997). Calcium is the important mediator for signaling pathways and cardiac contraction, therefore experimental techniques visualizing cardiomyocyte calcium handling e.g. by using calcium dyes and confocal calcium imaging, have gained a lot of interest over the last years. During cardiac contraction, extensive cytosolic calcium concentration increase is displayed as calcium transients, whereas the accumulation of local calcium, e.g. due to leaky RYR2, is recorded as calcium spark. Calcium transients of hypertrophic, non-failing cardiomyocytes displayed a normal or increased amplitude associated with delayed calcium reuptake resulting in slowed cardiomyocyte relaxation (reviewed in Berridge 2006). However, these changes are controversially reported in literature depending on the experimental model and the respective hypertrophy stimulus (Balke and Shorofsky 1998). In failing cardiomyocytes, calcium transient amplitude as well as calcium outflow of the SR and calcium reuptake are reduced (reviewed in Lou et al. 2012), which attenuates contractile force and impairs relaxation as well as force-frequency relationship (reviewed in Luo and Anderson 2013). In addition, the role of calcium sparks during disease progression is controversially reported in the literature (Balke and Shorofsky 1998; Jiang et al. 2002; Kohlhaas et al. 2006; van Oort et al. 2010; Sedej et al. 2014). Recently, the impact of calcium sparks-mediated diastolic calcium leak in arrhythmias but not in the transition to HF was reported (Mohamed et al. 2018). The structural, functional, and molecular mechanisms

associated with alterations in calcium transients and diastolic calcium leak are displayed in the following:

The CICR and the organization of sarcomere structure are crucial for contractile force development. In the failing heart the organization of T-tubules is disrupted as well as the functional coupling of RYR2 and LTCC leading to impaired CICR and reduced SR calcium outflow during the systole (Song et al. 2006). The regulation of LTCC by CAMKII, protein kinase A (PKA) and β-adrenergic stimulation results in a longer channel opening and increased open frequency promoting HF as well as arrhythmias by early afterdepolarization (Yue et al. 1990; Wu et al. 1999; Koval et al. 2010). Moreover, the regulation of RYR2 plays a key role in the development of HF. RYR2 activity is modified by PKA, CAMKII, protein phosphatase 1 and 2a, calmodulin and FKBP12.6 (reviewed in Luo and Anderson 2013). The diastolic calcium release mediated by CAMKII-phosphorylated RYR2 is associated with spontaneous diastolic sarcomere contractions. Consequently cardiomyocytes reveal reduced contractile force during the systole; which could further contribute to the reduced inotropic reserve in failing cardiomyocytes (reviewed in Luo and Anderson 2013). Complementary, transcriptional expression changes in failing cardiomyocytes, such as the increase of CAMKII expression and decrease of RYR2 expression, might also reduce contractile force (Ai et al. 2005). A further regulator of contractile force is the sarcomere protein titin, which is also involved in the development of HF. The titin expression is reported to be upregulated in CH and downregulated in HF resulting in reduced compliance and contractile function that is intensified by CAMKII phosphorylation (Hein et al. 1994; Collins et al. 1996; Hamdani et al. 2013). Collectively, the regulation of calcium channels via CAMKII, especially of RYR2, LTCC and voltage-dependent sodium channels, and the aberrant sarcomere structure play an important role in the pathophysiology of failing cardiomyocytes.

Next to the sarcomere organization and cytosolic calcium homeostasis, microdomain calcium and sodium homeostasis in the T-tubules is dysregulated in failing cardiomyocytes. The excitation-contraction-coupling in cardiomyocytes directly depends on sodium homeostasis regulated by sodium-potassium ATPase (NKA) and NCX. In failing myocardium elevated sodium influx during membrane depolarization interferes with calcium homeostasis through NCX by sodium sequestration and calcium

influx during the systole (Pieske et al. 2002). Additionally, CAMKII-mediated phosphorylation of sodium channels intensifies this effect and can further evoke arrhythmias (Khoo et al. 2006; Ashpole et al. 2012). The disrupted sodium homeostasis in failing hearts is also displayed by the reduction of NKA concentration to about 40 % (Bundgaard and Kjeldsen 1996). Thus, the dysregulation of sarcomere microdomain sodium and calcium interaction via NCX and NKA may also contribute to maladaptive cardiac remodeling leading to HF.

Calcium pumps as NCX and SERCA2a are responsible for calcium reuptake after cardiomyocyte contraction. SERCA2a activity and expression in HF is controversially discussed in literature, although studies consistently demonstrated enhanced SERCA2a inhibition by dephosphorylated phospholamban in failing hearts (Mercadier et al. 1990; Meyer et al. 1995; Schwinger et al. 1995; Schmidt et al. 1999; Mishra et al. 2002). As compensation of enhanced SERCA2a inhibition, NCX may sequestrate cytosolic calcium resulting in an increased sodium influx, which impairs sodium and calcium homeostasis. The overexpression of SR luminal histidine-rich calcium binding protein, a suggested cross-talk protein between RYR2 and SERCA2a, is also known to induce cardiac hypertrophy by delayed calcium reuptake (reviewed in Arvanitis et al. 2011). Thus, cytosolic calcium sequestration and cross-talking between NCX, RYR2 and sarcoplasmic/endoplasmic reticulum ATPase 2A (SERCA2A) is crucial for cardiomyocyte function, whereas its dysregulation is often observed in failing cardiomyocytes.

Impaired calcium homeostasis regulating the contraction in cardiomyocytes may be one of the main triggers for cardiac remodeling leading to HF. Aberrant transcription or posttranslational modifications of calcium channels e.g. via CAMKII diminishes cardiac contractile function. Furthermore, sarcomere disorganization leading to functional aberrations and the dysregulation of calcium and sodium homeostasis accelerate cardiac remodeling. Therapeutic strategies maintaining calcium homeostasis may be essential to alleviate, prevent or even reverse cardiac remodeling.

1.1.2   Apoptosis in cardiac remodeling and heart failure

Cell death is either mediated by programmed apoptosis, necrosis, or lysosome-mediated autophagy. In cardiac remodeling and end-stage HF, increased myocyte

apoptosis was reported in literature, whereas the role of cell death in cardiac remodeling is still controversially discussed (reviewed in Kim and Kang 2010). Apoptosis is sub-grouped in a) the cysteinyl-aspartate specific protease (caspase)-dependent intrinsic apoptosis pathway initiated by endoplasmic reticulum (ER) stress and DNA damage, b) extrinsic induction of apoptotic events by direct or indirect receptor mediated activation of caspases and c) an initially caspase-independent pathway through the mitochondria.

Caspase-mediated pathways are triggered by initiator caspases, which are activated by extrinsic or intrinsic signaling pathways. Initiator caspases induce the activation of effector caspases executing apoptosis by destroying different cellular proteins. The "extrinsic-death receptor pathway" is activated by binding of Fas ligand or tumor necrosis factor α (TNFα) to their specific membrane-bound receptor. This thereby induces cleavage and activation of initiator caspase 8 and downstream mitochondrial cytochrome c release resulting in the activation of effector caspases (all reviewed in Kim and Kang 2010). In HF, several studies reported a detrimental role of highly expressed TNFα and thereby activation of the death receptor mediated extrinsic apoptosis pathway (Doyama et al. 1996; Torre-Amione et al. 1996; Kubota et al. 1997; Bryant et al. 1998). Thus, the extrinsic apoptosis pathway is activated in failing cardiomyocytes, whereas the role of extrinsic pathway activation during cardiac remodeling is not fully understood.

The coupling of intrinsic and extrinsic apoptosis pathways is mediated by the cytosolic BID. The BID protein is cleaved into truncated BID by either extrinsic or intrinsic apoptosis pathway activated caspases. Truncated BID can translocate to the mitochondria facilitating cytochrome c release via pro-apoptotic BCL2 family members (Li et al. 1998). These BCL-2 family members can either function as pro-apoptotic (e.g. BAD, BAK and BAX) or anti-apoptotic (e.g. BCL-2, BCL-XL) proteins regulating the mitochondrial cytochrome c release (all reviewed in Kim and Kang 2010).

The intrinsic apoptosis pathway is known to be introduced by e.g. ROS-mediated DNA damage activating p53 protein or ER stress. Downstream pro-apoptotic gene expression results in mitochondrial cytochrome c release, forming the apoptosome together with APAF-1 and auto-processing procaspase 9. The apoptosome complex activates caspase 9, which induces the cleavage of effector pro-caspase 3 into its activated form, which

eventually executes apoptosis. Hypoxia, dysregulation of mitochondrial calcium handling and unfolded protein response (UPR) are the main trigger for ER stress-induced apoptosis. The induced transcription factors, e.g. CHOP/GADD, can lead to cardiomyocyte death via activation of initiator caspase 12 and downstream pro-apoptotic protein activation. These pro-apoptotic proteins accelerate mitochondrial cytochrome c release or activate directly effector caspases (all reviewed in Kim and Kang 2010).

Furthermore, the important role of caspase-independent apoptosis in cardiac remodeling via mitochondrial release of pro-apoptotic proteins like apoptosis inducing factors was reported in hypertrophic and failing cardiomyocytes (Chen et al. 2004; Choudhury et al. 2010). An additional caspase-independent activation of apoptosis pathway is the mitochondrial permeability transition pore (mPTP). As an important part of apoptosis induction in cardiomyocytes, mPTP leads to extensive mitochondrial calcium efflux leading to membrane depolarization, uncoupling of the respiratory chain, and mitochondrial swelling resulting in cell death (reviewed in Kwong and Molkentin 2015). CAMKII, elevated after cardiac ischemic insult, is known to facilitate mPTP opening leading to myocardial death (Joiner et al. 2012). Cardiomyocyte depletion of mPTP regulator gene *Slc25a3*, coding for a mitochondrial phosphate carrier, desensitizes mPTP's response to ischemia/reperfusion injury and calcium overload induced death (Kwong et al. 2014), underlining the role of mPTP-mediated cardiomyocyte loss during cardiac remodeling. The mPTP pore formation can be inhibited by cardioprotective protein kinase C isoform ε (PKCε), known to be induced via NO/cGMP/PKG signaling (Ping et al. 1999; Baines et al. 2003; Joiner et al. 2012).

Apoptosis inhibition as a therapeutic tool for the treatment of cardiac remodeling is comprehensively discussed. The intrinsic, extrinsic, and caspase-independent apoptosis pathways are proceeded especially in failing cardiomyocytes. Regarding a therapeutic approach of cardiomyocyte death repression, the promotion of carcinogenesis and autoimmune diseases due to apoptosis inhibition should be considered (reviewed in Kim and Kang 2010). Further long-term consequences in the heart and non-cardiac organs are not yet studied in detail.

1.1.3   WNT pathway in cardiac remodeling and heart failure

In general, WNT signaling pathways regulate organogenesis, tissue homeostasis and regeneration. Additionally, WNT signaling pathways are known to play an important role in apoptosis, cardiac function and regulation of cardiac remodeling leading to HF. Two downstream pathway concepts of WNT-activated frizzled transmembrane receptors are known: The canonical WNT pathway mediates downstream gene transcription through stabilized β-catenin that translocate into the nucleus acting as a transcription factor. The non-canonical signaling pathway mediates the activation of calcium-dependent kinases, such as CAMKII, and is involved in planar cell and polarity pathways by Rho A/RAC (all reviewed in Bergmann 2010).

Both the canonical and the non-canonical WNT-mediated pathways play important roles during cardiac development (reviewed in Gessert and Kühl 2010). The biphasic role of WNT pathway activity in cardiac organogenesis is required to obtain functional cardiomyocytes. Ueno et al. (2007) demonstrated for the first time that activation of canonical WNT signaling in human embryonic stem cells (hESCs) induces mesodermal differentiation and subsequently cardiac specification is accomplished by inhibition of the WNT pathway using DKK1. In later stages of cardiac development, WNT signaling regulates cell-cell adhesion via non-canonical WNT5A signaling, morphological arrangement by canonical WNT-frizzled-2 signaling and the conduction system through WNT11 and WNT7a signaling (Toyofuku et al. 2000; Bond et al. 2003; Fujio et al. 2004). These data outline the unique role of WNT signaling in early and late cardiogenesis and display its diverse influence in the development of the heart. Furthermore, the WNT pathway regulation of the fetal gene program in early cardiogenesis was also reported in the process of cardiac remodeling leading to HF.

The induction of cardiac hypertrophy can be mediated by non-canonical WNT signaling pathway activation via WNT5A, WNT11 and Dapper-1 (Eisenberg et al. 1997; Pandur et al. 2002; Hagenmueller et al. 2014). Additionally, the activation of canonical WNT pathway via stabilized β-catenin and the repression of its inhibitor GSK3β was shown to induce cardiac hypertrophy, whereas canonical WNT signaling activation in HF is also associated with improved cardiomyocyte function (Haq et al. 2003; Hirotani et al. 2007). In contrast, Baurand et al. (2007) reported that stabilized β-catenin attenuates cardiac

function after angiotensin II induced CH in mice. The complex role of canonical and non-canonical WNT pathway regulation in CH and HF demonstrates its role in the process of cardiac remodeling. Canonical and non-canonical WNT signaling can induce cardiac hypertrophy, and canonical WNT signaling is further active in HF, whereas its impact on cardiac function is controversially reported in the literature.

Secreted-frizzled-related proteins (SFRPs) are modulators of WNT signaling molecules activating canonical and non-canonical WNT pathway. Several studies reported the anti-hypertrophic role of SFRPs by modulating WNT signaling pathways in cardiac remodeling. In detail, SFRP1 depletion was shown to be detrimental for cardiac function and promoted cardiac fibrosis (Sklepkiewicz et al. 2015). Moreover, calcium extrusion pump PMCA4-depleted cardiac fibroblasts attenuated cardiomyocyte hypertrophy by local SFRP2 secretion (Mohamed et al. 2016), underlining the predicted anti-hypertrophic role of SFRPs. Additionally, SFRP5 was also described to play an anti-hypertrophic role in angiotensin II treated rat cardiomyocytes (Jin et al. 2015). In contrast to the predicted anti-hypertrophic role of SFRP1, SFRP2 and SFRP5, the repression of previously reported beneficial canonical pathway in failing cardiomyocytes by SFRP3 and SFRP4 can consequently be associated with reduced cardiac function (Schumann et al. 2000). Regarding the role of WNT signaling in the process of cardiac remodeling, SFRPs as WNT modulators display an anti-hypertrophic stimulus and SFRP3 and SFRP4 were also active in failing cardiomyocytes, probably diminishing cardiac function by canonical WNT pathway repression.

Besides cardiac hypertrophy induction, WNT signaling and its modulators were also involved in the transition to HF. Several studies demonstrated the dysregulation of WNT pathways in HF, which were associated with decompensation of cardiac function, increased cardiomyocyte apoptosis, and fibrosis. Myocyte degradation plays a crucial role in the decompensation of cardiac function in failing cardiomyocytes. As anti-apoptotic regulators, WNT1 and WNT2b are known to inhibit apoptosis by activation of canonical WNT signaling repressing cytochrome c release from mitochondria or the expression of FAS, a pro-apoptotic NF-κB target gene, respectively (Spiegelman et al. 2000; Chen et al. 2001; Noubissi et al. 2006). Additionally, repression of canonical WNT pathway inhibitor GSK3β leads to reduced cardiomyocyte apoptosis and fibrosis (Hirotani et al. 2007). In the murine heart, hypoxic cardiomyocytes displayed Wnt3a

upregulation, which was also associated with enhanced apoptosis, whereas treatment with Sfrp1 and Sfrp2 protects these murine cardiomyocytes from apoptosis probably by activation of canonical Wnt signaling (Barandon et al. 2003; Mirotsou et al. 2007). Moreover, angiotensin II treated murine hypertrophic cardiomyocytes were protected against apoptosis by Sfrp5 treatment (Nakamura et al. 2016). These results suggest the anti-apoptotic role of SFRP1, SFRP2 and SFRP5 together with canonical WNT pathway activation in cardiomyocytes. In contrast, pro-apoptotic stimuli of SFRPs were also reported. SFRP3 and SFRP4 were associated with apoptosis in failing ventricular tissue and SFRP5 promotes apoptosis in cardiac fibroblasts (Schumann et al. 2000; Bie et al. 2016). The anti-apoptotic role of canonical WNT pathway activation and its modulation by SFRPs were reported in cardiomyocytes, whereas SFRPs were also known to induce apoptosis in failing cardiac tissue, especially in cardiac fibroblasts. Therefore, the role of WNT pathway in apoptosis might be cell type-specific and stimulus-dependent.

Until now, the complex role of WNT pathway regulation and its modulators in cardiomyocyte function and apoptosis are not completely understood and partially controversely reported in literature. The reactivation of essential embryonic cardiac development WNT pathways can contribute to cardiac hypertrophy, as well as preserving cardiac function in the failing heart. Additionally, an anti-apoptotic stimulus via canonical WNT pathway activation by SFRPs was reported in cardiomyocytes, whereas SFRPs were also known to induce apoptosis in cardiac fibroblasts. In conclusion, WNT signaling pathways play an important role in cardiac remodeling via regulation of cardiac function and apoptosis, whereas the precise mechanisms need to be explored further in human cardiomyocytes.

1.1.4   Deep RNA sequencing of myocardial biopsies from different stages of pressure-overload in human and mouse identified the conserved candidate secreted-frizzled-related protein 5

Initially, next generation sequencing of human myocardial samples of aortic stenosis patients suffering from CH and decompensated HF was performed to elucidate molecular mechanisms that may regulate cardiac remodeling. Myocardial biopsies from patients with preserved ejection fraction were grouped in a CH group and biopsies from patients with reduced ejection fraction were grouped in a HF group comprising five

replicates each (figure 1A). Healthy donor hearts were used as control group. To identify conserved candidates in the transition from CH to HF, a comparable mouse model treated with transverse aortic valve constriction (TAC) was used. One week after TAC treatment, mouse hearts were comparable with human CH and 8 weeks after TAC surgery mouse hearts developed a human HF like state (figure 1B). The comparative deep RNA sequencing (RNA-seq) screening identified a set of significantly up- and downregulated genes at different stages of pressure-overload compared to healthy controls. Grouped in expression profiles of transcriptional changes from non-failing control (C) to CH to HF, 25 conserved candidates between mice and human were identified (figure 1C). Interestingly, SFRP5 was the only conserved candidate gene significantly decreasing from C to CH and is re-expressed in the failing heart (figure 1D). Therefore, SFRP5 was chosen for further investigation in this thesis.
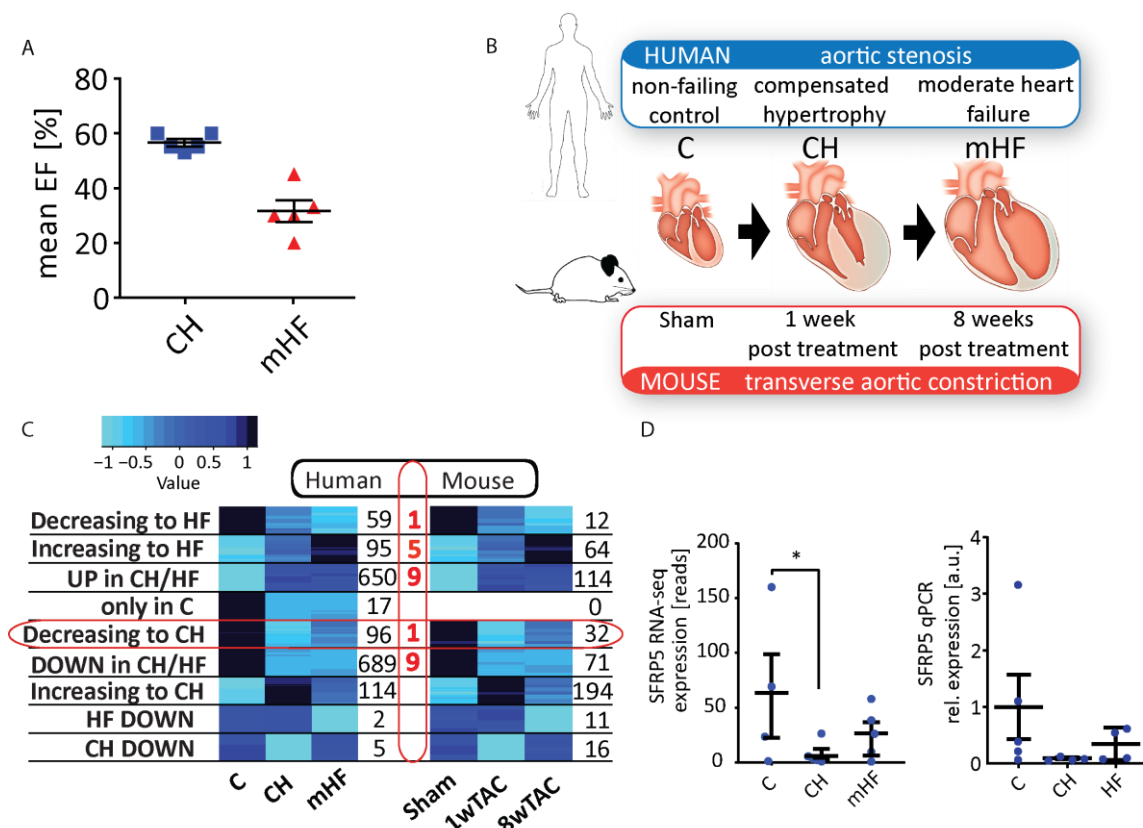
Figure 1: Identifying conserved candidates regulating the transition from CH to HF. Myocardial biopsies from patients with different stage of aortic stenosis and healthy hearts from organ donors (C) were obtained to perform deep RNA-seq. To identify conserved candidate genes involved in the transition to HF samples from the comparative TAC mice model were additionally analyzed. **(A)** Myocardial samples of patients with AS were grouped in CH with preserved ejection fraction (EF) and in HF with reduced EF. **(B)** Myocardial samples from the stage of CH were compared to TAC-mouse samples one week after surgery and HF samples were compared to TAC-mouse samples 8 weeks after surgery. **(C)** Deep RNA-seq of different stages of pressure-overload in the human and murine samples identified differentially up and

downregulated genes during disease progression. Grouped in gene expression profiles from C to CH to HF, 25 differentially expressed conserved candidates were displayed. SFRP5, as the only candidate significantly decreasing from C to CH, was chosen for further analysis. **(D)** SFRP5 is expressed in human non-failing myocardium, decreases during CH (log2 fold change -3.5) and shows a stable upregulation in HF, but does not reach the basal expression level in control. RNA-sequencing data of human tissue was validated via qPCR. The illustration was adapted from Khadjeh et al (2020), Creative Common International License: CC BY 4.0.

1.1.5 Secreted-frizzled-related protein 5

SFRP5 is a secreted modulator of WNT and BMP signaling (Stuckenholz et al. 2013). The SFRP family consist of five secreted glycoproteins, which directly bind and regulate WNT proteins by a homologous cysteine-rich domain (Lin et al. 1997). Due to sequence homology, SFRP5 is subclassified together with SFRP1 and 2, whereas SFRP3 and 4 display more similarities among each other compared to the other three family members (Jones and Jomary 2002). The SFRP5 gene is located on chromosome 10 and consists of 3 exons (Chang et al. 1999). The 37 kDa protein is known to directly inhibit WNT5A and WNT11 consequently modulates canonical and non-canonical WNT pathway (Li et al. 2008). Multiple functions and interactions of SFRP5 were reported. In several tissues SFRP5 is described as fundamental for tissue homeostasis, because it has been shown that its expression is altered in different diseases and cancers (Zhao et al. 2009; Peng et al. 2014; Gutiérrez-Vidal et al. 2015). For example SFRP5 is a known tumor suppressor gene in many cancer types e.g. in renal cell cancer as well as expressed in murine cardiac progenitor cells, indicating involvement in cardiac differentiation (Kawakami et al. 2011; Fujii et al. 2017).

As a novel anti-inflammatory adipokine, SFRP5 is involved in the regulation of insulin-sensitizing, obesity and coronary artery disease (reviewed in Wang et al. 2020). As adipokine SFRP5 is highly expressed in white adipose tissue, and also endocrine effects of SFRP5 were reported (Ouchi et al. 2010; Ehrlund et al. 2013). Obesity, a multifactorial disease, is often associated with low-grade chronic inflammation of especially visceral white adipose tissue (Weisberg et al. 2003). These patients displayed lower SFRP5 serum levels and expression in inflammatory adipose tissue compared to non-obese patients (Ouchi et al. 2010; Hu et al. 2013; Akoumianakis et al. 2019). Consequently, SFRP5 may protect against adipose tissue inflammation and obesity via repression of pro-inflammatory WNT5A-mediated non-canonical WNT pathway.

Furthermore, SFRP5 as an insulin-sensitizing adipokine is involved in diabetes type 2 development. The pathophysiological mechanism of insulin resistance in diabetes type 2 involves macrophage-mediated inflammation of adipose white tissue (Xu et al. 2003). The macrophage inflammation may also occur by WNT5A-mediated non-canonical WNT signaling, which can be rescued by SFRP5 treatment restoring insulin sensitizing in white adipose tissue (Ouchi et al. 2010). Moreover, endogenous SFRP5 secretion is hypothesized as the underlying pharmacological mechanism to improve insulin sensitizing of anti-diabetes pharmaceuticals like rosiglitazone and metformin (Lv et al. 2012). The beneficial role of SFRP5 in the development and therapy of diabetes type 2 was confirmed in animal and cell models, whereas until today clinical data reported controversial results on SFRP5 serum levels (reviewed in Wang et al. 2020).

SFRP5 is further reported to diminish coronary artery disease due to metabolic dysfunction (reviewed in Wang et al. 2020). Coronary artery disease is based on atherosclerosis, a complex process of LDL storage in the vascular wall accompanied by macrophage migration and oxidative stress leading to endothelial dysfunction together with the proliferation and migration of vascular smooth muscle cells. Several studies reported the rescue of endothelial dysfunction and vascular smooth muscle cell proliferation, migration and inflammation by SFRP5 via inhibition of WNT5A/JNK pathway, canonical WNT pathway and p38/MAPK pathway and further increased nitric oxygen production of endothelial cells (Bretón-Romero et al. 2016; Cho et al. 2018; Teliewubai et al. 2018; Akoumianakis et al. 2019). Recent clinical studies reported that patients with coronary artery disease displayed low serum levels of anti-inflammatory SFRP5 and high serum levels of pro-inflammatory WNT5A, underlining its role in disease progression (Miyoshi et al. 2014; Akoumianakis et al. 2019). Moreover, the pathophysiological mechanisms of adverse macrophage inflammation was also reported in the heart after ischemia/reperfusion injury (Nakamura et al. 2016). In the murine heart Sfrp5 is known to inhibit cardiac inflammation and apoptosis by inhibition of Wnt5a-positive macrophage's migration, and cytokine as well as chemokine expression, thereby protecting the heart after ischemia/reperfusion injury (Nakamura et al. 2016). A recent study of Du et al. (2019) reported the association of SFRP5 serum levels with improved cardiac function after percutaneous coronary intervention within the scope of myocardial infarction and evaluated SFRP5 as novel therapeutic target after ST-

segment elevated myocardial infarct. Moreover, miR-125b was identified as regulator of SFRP5 expression in cardiac fibroblasts, promoting their growth and activation as well as repressing their apoptosis (Bie et al. 2016), indicating an anti-apoptotic and anti-fibrotic role of SFRP5 in cardiac fibroblasts. Regarding the anti-inflammatory role of SFRP5 in cardiac diseases, aberrant disease progression can be diminished by inhibition of WNT5A-mediated non-canonical pathway, displaying SFRP5 as novel cardioprotective adipocytokine.

Interestingly, despite macrophage migration after myocardial infarction the WNT5A protein is also involved in neutrophil recruitment in the pressure-overloaded heart (Wang et al. 2019). This study reported for the first time the obligatory role of neutrophil inflammation leading to macrophage migration and cytokine and chemokine expression which results in hypertrophy induction. They also demonstrated that WNT5A is required for chemotactic migration and chemokine production of neutrophil cells and is directly correlated to disease severity (Jung et al. 2013; Wang et al. 2019). Gene edited murine myeloid cells displayed the increase of cardiac hypertrophy, inflammation and cardiac dysfunction during Wnt5a overexpression, whereas Wnt5a depletion diminishes disease severity (Wang et al. 2019). Furthermore, elevated WNT5A serum levels of HF patients were associated with increased cardiac inflammation, cardiac fibrosis and disease progression (Abraityte et al. 2017), underlining the results of Wang et al. (2019). Because Wnt5a was only expressed in neutrophils isolated from the heart, Wang et al. (2019) hypothesized Wnt5a-mediated autocrine regulation of neutrophil function or endocrine regulation via SFRP5. These data, together with the known anti-inflammatory and protective role described after ischemia/reperfusion injury strongly indicates the involvement of SFRP5 in the regulation of WNT5A induced neutrophil recruitment after pressure-overload leading to cardiac hypertrophy, inflammation, and cardiac dysfunction.

The predicted role of SFRP5 in the inhibition of WNT5A-mediated cardiac inflammation via neutrophils and macrophages resulting in cardiac hypertrophy and cardiac dysfunction was described in the literature, whereas SFRP5 may also have a direct influence on cardiomyocyte function. Unfortunately, the function of SFRP5 in cardiomyocytes is still poorly understood. For example, Jin et al. (2015) published that Sfrp5 expression is upregulated due to an angiotensin II stimulus in rat cardiomyocytes

resulting in transcriptional downregulation of BNP and TNF-α in hypertrophic cardiomyocytes. Under these conditions SFRP5 displays an anti-hypertrophic role (Jin et al. 2015), whereas the underlying mechanisms of SFRP5 diminishing cardiac hypertrophy remained unknown. The publications by Jin et al. (2015) and Wang et al. (2019) together with preliminary RNA-seq of AS patients suggest a beneficial role of SFRP5 in cardiac remodeling, regarding hypertrophy stimulation, fibrosis and apoptosis. Nevertheless, the direct influence of SFRP5 on cardiomyocytes was not examined until today.

1.2   Human induced pluripotent stem cell derived cardiomyocytes: suitable model for human cardiovascular research

In 2007 Takahashi et al. reported the successful reprogramming of adult human fibroblasts towards the pluripotent state by retroviral transduction of four genes associated with pluripotent cells. In this study they used OCT4, SOX2, KLF4 and C-MYC. These so called induced pluripotent stem cells (iPSCs) were capable of unlimited proliferation under specific cultivation conditions, could differentiate into all cells of the three germ layers (endoderm, mesoderm, ectoderm) and were capable of teratoma formation in vivo (Takahashi et al. 2007). Shortly thereafter, Yu et al. (2007) published the generation of human iPSCs (hiPSCs) using the pluripotency transcription factors OCT4, SOX2, NANOG and LIN28. Human iPSCs displayed comparable functional properties to hESCs. These include especially hESC like morphology, proliferation ability, expression of surface antigens, promotor activities and telomerase activity (Takahashi et al. 2007). Less ethical concerns were raised using hiPSCs, because they can be derived from adult somatic cells in comparison to hESCs, which are derived from the inner cell mass of blastocyst by destroying it (Thomson et al. 1998). Over the last couple of years, intensive research focuses on the further development of the promising hiPSC-technology. Reprogramming methods were refined, and new culture conditions were established in case of future clinical application.

Human iPSCs gained strong attention in cardiovascular research due to the lack of suitable and efficient human model systems. Animal models often display pronounced differences in cardiac physiology, especially in channelopathies, therefore research has focused on hiPSC-derived models in the field of cardiovascular research (reviewed in

Mummery 2018). Human iPSCs can be effectively differentiated into hiPSC-derived cardiomyocytes (hiPSC-CMs) by modulation of the WNT signaling pathway with small molecules (Lian et al. 2013; Cyganek et al. 2018). Usage of a metabolic selection via lactate enables cardiomyocyte populations of > 99 % purity without detectable tumor formation *in vivo* after transplantation (Tohyama et al. 2013). These purified cardiomyocytes are a heterogeneous population of mainly ventricular-like cells and a minority of atrial- and nodal-like cells. Subtype differentiation of atrial- and nodal-like cells is performed by BMP signaling modulation and supplementation of retinoic acid during differentiation (Devalla et al. 2015; Protze et al. 2017). The unlimited source of hiPSC-CMs and their ability to differentiate in several cardiomyocyte subtypes is a further great advantage in comparison to the isolation of adult cardiomyocytes from biopsies, which results in only small quantities of non-proliferating cells, which are difficult to culture for longer time periods *in vitro*.

Patient-specific hiPSCs can be used for disease modeling, to elucidate new cellular and molecular disease mechanisms as well as to identify new disease associated genes. The first reported cardiac disease model was the LEOPARD syndrome in 2010 followed by numerous other patient-derived hiPSCs modeling specific cardiac disorders (Carvajal-Vergara et al. 2010). To date, many of the genetically determined hypertrophic and dilated cardiomyopathies were examined *in vitro* using hiPSC-CMs (reviewed in Eschenhagen and Carrier 2019). Human iPSC-CMs derived from patients with genetically caused hypertrophic or dilated cardiomyopathy revealed aberrations in phenotype and functionality, which could recapitulate the patient's disease *in vitro* (reviewed in Eschenhagen and Carrier 2019). Furthermore, hiPSC-CM disease models can refine the understanding of underlying disease mechanisms and promote the development of new therapeutic strategies or determine drug sensitivity. Unfortunately, in comparison to easily accessible clinical measurements of cardiac contractility and size in patients, there are certain difficulties to determine these parameters in hiPSC-CMs, which is based on culture conditions (all reviewed in Mummery 2018). Due to the introduction of CRISPR/Cas9 system, genetically modified hiPSC-CMs can be compared to isogenic control, minimizing cell line dependent bias (reviewed in Eschenhagen and Carrier 2019).

Limitations of these human model for cardiac diseases refer mainly to their immature fetal-like state regarding morphological, molecular, structural, metabolic and functional aspects compared to adult cardiomyocytes (Yang et al. 2014). Strategies for hiPSC-CM maturation propose prolonged culture periods of 60 to 120 days, supplementation of triiodothyronine, electric stimulation and generation of cardiac tissues (Martherus et al. 2010; Lieu et al. 2013; Lundy et al. 2013; Tiburcy et al. 2017). Future applications in regenerative medicine refer to transplantation of hiPSC-CMs engineered patches in injured myocardium and further *in vitro* extracellular matrix scaffold repopulation of whole hearts (Carvalho et al. 2012; Weinberger et al. 2016). The first transplantation of hESC-derived cardiac progenitor cells into humans was reported in 2015 (Menasché et al. 2015). Despite several differences in comparison with adult cardiomyocytes, hiPSC-CMs are considered a suitable human model for the field of cardiovascular research regarding disease modeling, functional analysis of proteins and drug toxicity.

1.3   Methods used in the study

To analyze the function of SFRP5 in hiPSC-CMs a gain of function system via adeno associated virus (AAV)-mediated overexpression and a loss of function system via Clustered Regularly Interspaced Short Palindromic Repeats and the Cas9 nuclease system (CRISPR/Cas9) was used.

Transcriptional overexpression of genes in post-mitotic cardiomyocytes using AAVs is a promising tool in cardiovascular research. Several characteristics of AAVs are beneficial for the use as a gene transfer system: AAVs are part of Parvoviridae family consisting of non-enveloped, single-stranded deoxyribonucleic acid (DNA) viruses (Rapti et al. 2015). Recombinant AAVs remain episomally, and each of the 13 serotypes demonstrated tissue specific tropism. The most cardiotropic serotypes are 1, 6 and 9 (Rapti et al. 2015). Several studies examined the transduction efficiency of different AAV serotypes in hiPSC-CMs. Rapti et al. (2015) displayed AAV2 and AAV6 as superior serotypes for transduction of postmitotic hiPSC-CMs. Moreover, low immunogenicity, the lack of pathogenicity, attenuated oncogenic risk and stable long term overexpression contribute to their promising role in gene therapy (Rapti et al. 2015). Limitations of AAVs include to their small genome capacity of only 4.7 kb (Hajjar 2013). Furthermore,

Balakrishnan et al. (2013) reported an increase of UPR via IRE1α, PERK and ATF6 due to AAV transduction. Pre-treatment with metformin, a UPR inhibitor, in an animal model was convenient to reduce transcriptional pro-apoptotic activation of UPR to a modest level and reduce inflammatory response (Balakrishnan et al. 2013).

The novel gene editing technology using CRISPR/Cas9 is a precise tool to induce e.g. a mutation at a specific site in the genome that leads to a gene disruption/ knock-out (KO). Therefore, truly causative lesions can be analyzed for specific molecular and cellular phenotypes. The Cas9 causes sequence specific double strand breaks (DSB) guided by the corresponding crRNA transcribed from the CRISPR-locus together with the sequence-independent tracrRNA, which are often transcribed as one "fusion-RNA", the so-called guide RNA (gRNA) in the CRISPR/Cas9 system. Several delivery systems were developed including inducible Cas9 plasmids, virus mediated transfer methods, Cas9 ribonucleoprotein complexes or mRNA transfection. The short gRNA consists of 20 nucleotides at its 5'-end, which are homologous to the targeted DNA sequence in the genome while the residual bases are for the correct localization within Cas9 protein. For Cas9 and gRNA interaction, the protospacer adjacent motif is essential, which must be localized directly adjacent to the desired target site. Within cells a Cas9 introduced DSB can be repaired due to non-homologous end joining (NHEJ) or homology directed repair. The NHEJ is an error-prone, non-template ligation of the two ends, while homology directed repair allows the precise repair of the DSB using the homologous DNA sequence of sister chromosome as template (all reviewed in Lino et al. 2018).

Depending on the cell cycle, the introduced DSBs are predominantly repaired by NHEJ (up to more than 90 %), which can cause insertions and deletions. This results mostly in frameshifts and the loss of function of the gene of interest. Introducing two simultaneous DSBs, NHEJ can ligate misfitting ends together, which can lead to inversions, deletions or translocations (Xiao et al. 2013; Torres et al. 2014). In consequence, pretermination codons are recognized by the cell activating nonsense mediated decay promoting mRNA degradation (reviewed in Hug et al. 2016). Due to a carefully chosen gRNA target site, partially reconstruction of the mRNA due to alternative promoters, alternative splicing, or altered polyadenylation signals can be avoided, minimizing the risk for translating a truncated, but partially functional protein (reviewed in Hug et al. 2016).

Further limitations of CRISPR/Cas9 induced gene KOs depend on clonal variability of the specific hiPSC line and mismatches of the gRNA to other sequences in the genome next to the intendent gene of interest, the so called off-target sites. Various online tools were developed to create gRNAs with a high specificity towards the gene of interest and reduced off-target sites, thereby minimizing potential artefacts in the genome edited hiPSC line. Currently, Digenome-seq is a "robust, sensitive, unbiased and cost-effective method for profiling genome-wide off-target effects", which identifies mutagenesis frequencies < 0.1 % (Kim et al. 2015).

AAV-mediated overexpression and CRISPR/Cas9-mediated gene KO are two promising model systems in cardiovascular research. Cardiac tropism and the preferential transduction of post-mitotic cells are desirable characteristics of AAVs in order to analyze the function of SFRP5 in hiPSC-CMs. Despite limitations and various cellular rescue systems, gene KO by the CRISPR/Cas9-mediated genome editing system is a reliable tool for the generation of hiPSC KO lines to e.g. identify specific protein functions in the process of cardiac differentiation and in the hiPSC-CMs.

1.4   Aim and description of the project

The aim of the project is the identification of potential roles of SFRP5 in the pathophysiology of cardiac remodeling and the investigation of the molecular and functional disease-causing mechanisms in a human in vitro system. Therefore, the candidate of interest (SFRP5) was analyzed in two-month-old hiPSC-CMs (from healthy donors) by AAV-mediated overexpression (SFRP5^{OE}) and CRISPR/Cas9-mediated KO (SFRP5^{KO}).

In order to reveal the induced changes due to the overexpression of SFRP5, the SFRP5^{OE} hiPSC-CMs were analyzed on the molecular and cell biological level in comparison to untreated control hiPSC-CMs (Control^{OE} hiPSC-CMs). For molecular analysis, quantitative PCR (qPCR) was assessed to validate the overexpression of SFRP5 as well as the expression level of cardiac specific marker genes. Expression analysis of AAV-treated hiPSC-CMs by mRNA-sequencing (mRNA-seq) and pathway analysis should reveal transcriptional and signaling pathway changes induced by SFRP5 overexpression. Changes in calcium handling were further examined using functional analysis via

confocal calcium imaging. CRISPR/Cas9-mediated SFRP5^{KO} in hiPSC was performed, validated, and these SFRP5^{KO} hiPSCs were consequently differentiated into SFRP5^{KO} hiPSC-CMs to reveal the role of SFRP5 for cardiac development.

The results gained in this study give novel insights into molecular mechanisms underlying cardiac remodeling and may provide a new potential drug-targeted candidate for the development of therapeutic strategies for the treatment of HF progression.

2 Materials and methods

2.1 Materials

2.1.1 Disposable items and laboratory equipment

Table 1: List of disposable items.

Name	Type	Provider and Order Number
Cell culture plates	6 cm culture dish	Thermo Fisher Scientific # 150462
	6-well plate, TC-treated	CytoOne Starlab #CC7682-7506
	12-well plate, TC-treated	CytoOne Starlab #CC7682-7512
	24-well plate, Tc-treated	CytoOne Starlab #CC7682-7524
	96-well plate, TC-treated	CytoOne Starlab #E2896-0600
Cell scraper	Cell scraper 16cm 2 pos.-blade	Sarstedt #83.1832
Cell strainer	40µm nylon cell strainer	Stemcell Technologies ##27305
Cryo-tubes	CRYO.S, 2 ml	Greiner #126263
Falcon tubes	15 ml	Greiner Bio-one #188271
	50 ml	Sarstedt #62.547.004
Filter tips	0.1-10 µl	Starlab #S1121-3810
	10-200 µl	#S1120-1840
	100-1000 µl	#S1126-7810
Flow cytometer tube	Falcon® Round-Bottom Polystyrene Tubes, 5 mL	BD Falcon #352058
Gel extraction	Disposable Scalpel fig. 11	Feather #02.001.30.011
Pasteur pipettes	Pasteur pipettes	LabSolute # 7691061
Pipette tips	0.1-10 µl	Starlab #S1111-3700
	10-200 µl	#S1111-1706
	100-1000 µl	#S1111-6811
Pipettes	5 ml	Sarstedt # 86.1253.001
	10 ml	#86.1254.001
	25 ml	#86.1685.001
qPCR	Hard-Shell® 96-Well PCR Plates	BioRad #HSP9601
	Microseal® 'B' PCR Plate Sealing Film	BioRad #MSB1001
Safe lock tubes	0.1 ml: PCR consumables	Starlab #I1402-3706
	0.5 ml	Eppendorf #0030 121.023
	1.5 ml	Eppendorf #0030 123.328
	2 ml	Eppendorf #0030 120.094
	1.5 ml brown	Sarstedt #72.706.001

Name	Type	Provider and Order Number
Slides and coverslips	Microscope Slides Round 25 mm	Thermo Fisher Scientific #J1800AMNZ #CB00250RA033MNT0
Sterile filters	Steriflip 50 ml 0.22 µm	Merck Millipore #SCGP00525
Tips for gel loading	MiniFlex Round Tips, 10µl MiniFlex Round Tips, 200µl	Biozym #728014 #728204

Table 2: List of laboratory equipment

Description	Name	Provider
Autoclave	Vx-150	Systec
Balances	Quintix Entris	Sartorius
Cell counter	CASY Model TT	Innovatis
Cell stimulator	MyoPacer cell stimulator	IonOptix
Centrifuge	Sprout Centrifuge 5418R Heraeus Megafuge 40RT	Heathrow Scientific Eppendorf Thermo Scientific
Chemiluminescence detection system	ChemiDoc XRS+ System	BioRad
Confocal microscope	LSM710 confocal microscopic system	Carl Zeiss
Controlled rate freezer	KRYO 560-16	Planer
Cooling units	4°C: LKevx 1800 -20°C: LGUex 1500 MediLine -80°C: TSX60086V -150°C: MDF-C2156VAN-PE	Liebherr Liebherr Thermo Fisher Scientific Panasonic
Counting chamber	Thoma neu	Mareinfeld #0640810
Electrophoresis	Wide Mini-Sub Cell GT Systems Sub-Cell GT UV-Transparent Gel Tray 20-Well Comb Gel documentation: BioDoc Analyze	BioRad #1704416 #1704448 Biometra
Flow cytometer	BD LSR II Flow Cytometer	BD Biosciences
Freezing container	Mr. Frosty	Nalgene, #C1562-1EA
Heat block	Thermomoxer F1.5	Eppendorf
Heated magnetic stirrer	RH basic	IKA
Ice machine	AF103	Scotsman
Incubator	Heracell VIOS 250i, CO_2 Incubator	Unity Lab Service by Thermo Fisher Scientific

Description	Name	Provider
Microscope	Axio Observer.A1 Inverted Microscope Primovert	Carl Zeiss #491206-0001-000
Microwave	NN-E201 WM	Panasonic
NanoDrop	NanoDrop One Nanodorp 2000/2000c	Thermo Fisher Scientific #ND-ONE-W #ND-2000
PCR Cycler	Mastercycler nexus gradient	Eppendorf
pH meter	pH7110	InoLab
Pipet controller	AccuJet Pro	Brand
Pipettes	Reference, Research plus (2.5/10/100/1000 µl)	Th. Geyer #9283228 #9283200
Power supply	PowerPac basic Power Supply	BioRad
qPCR cycler	CFX96 Touch Real-Time Detection System	BioRad
Shaker	GFL 3015 Shaker Unimax 1010	GFL Heidolph
Sterile work bench	SAFE 2020 Biological safety cabinet, class II	Thermo Fisher Scientific
Sterilisation	Heratherm OMH750 Advanced Lab Oven	Thermo Fisher Scientific
Transfection unit	Amaxa Nucleofector II device	Lonza
Vortexer	uniTEXER1	LLG Labware
Water bath	Shaking water bath 1083	GFL
Water preparation system	PURELAB flex, ElgaLC 197	Veolia
Western Blot	Mini-PROTEAN Tertra Cell Trans-Blot Turbo Transfer System	BioRad #1658000EDU BioRad

2.1.2   AAV6 vectors
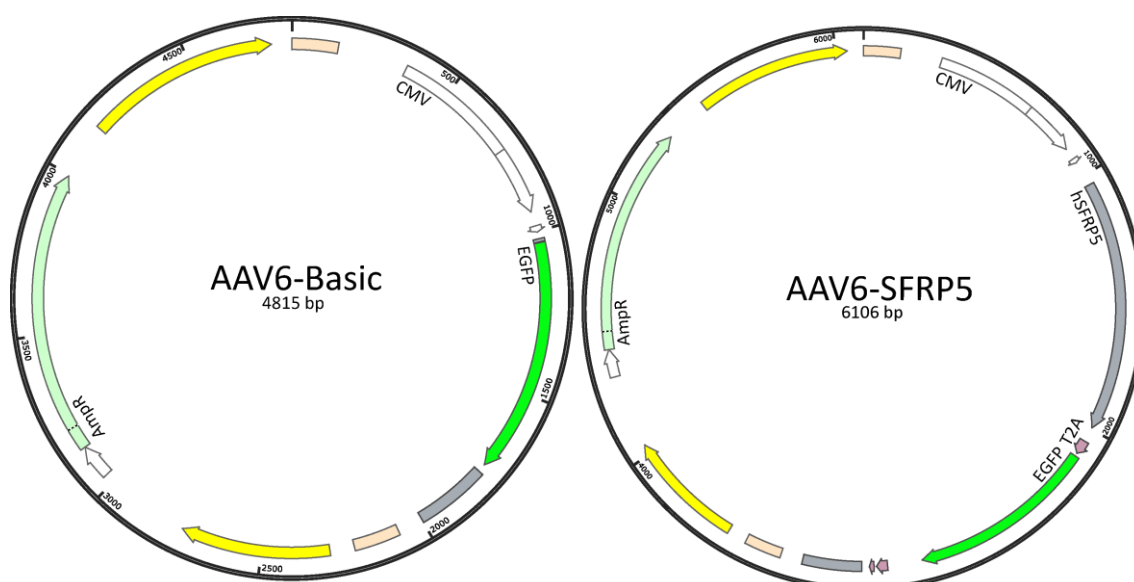
Figure 2: Design of AAV6 vectors. The AAV6-CMV-EGFP plasmid contains a ubiquitously active CMV promoter and the fluorescent marker EGFP. The overexpression vectors were designed with a CMV promoter and the human candidate gene (hSFRP5) linked with a T2A site to EGFP for co-translational expression of SFRP5 and EGFP from one mRNA. All vectors inherit an Ampicillin resistance (AmpR) for selection of transformed bacteria during cloning procedure. Illustration was created by visualizing the vector sequence (provided by Vector Biolabs) in snap gene and subsequently modified for better clarity.

AAV6-CMV-SFRP5-T2A-EGFP vector was custom-designed and purchased with the control vector AAV6-CMV-EGFP from Vector-Biolabs (figure 2).

2.1.3   CRISPR/Cas9 Sigma All-in-one plasmids
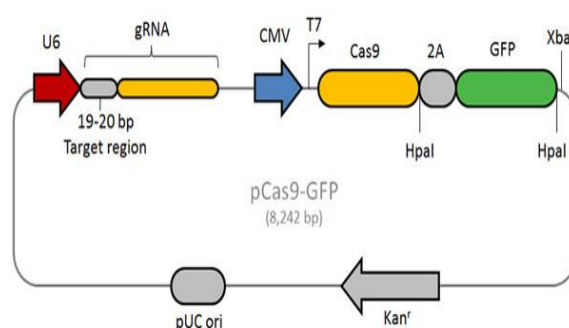
Figure 3: CRISPR/Cas9 plasmid map. The plasmid contains gRNA, Cas9 and the reporter GFP linked by a T2A site. Kanamycin resistance (Kan[r]) for transformed *E. Coli* selection is included (Sigma-Aldrich 2019).

Table 3: List of used CRISPR/Cas9 plasmids

Gene	Vector	CRISPR-binding site	Order number
SFRP5 Exon 1	U6gRNA-Cas9-2A-GFP	GGA TGT CAA GGC ACT GCG GCGG	HS0000269496
SFRP5 Exon 1	U6gRNA-Cas9-2A-GFP	CTG CATC GCC GTG CAG TTC GGG	HS0000269505

2.1.4 Primers

Table 4: List of primers for gDNA templates and for reverse transcription PCR

Name	Sequence	Product length (bp)
SFRP5_gDNA	For: GCTGGGTAGAGTCAGGGC Rev: GATGGGTACTGAGAGGGGTG	907
SFRP5_cDNA	For: GCTGCGAGGAGTACGACTAC Rev: CCACAAAGTCACTGGAGCAC	528

Table 5: List of primers for qPCR

Name	Sequence or order number Qiagen	Product length (bp)
18S	For: GAC ACG GAC AGG ATT GAC AG Rev: CTA GTT AGC ATG CCA GAG TCT C	132
CACNB2	PPH01623F	156
cTnT	For: AGC TGC TGT TCT GAG GTC AC Rev: AGG TAC AAA GGG AAG CCT GC	122
GAPDH	For: GTT CGT CAT GGG TGT GAA CC Rev: GGT CAT GAG TCC TTC CAC GA	139
Ryr2	PPH10458A	157
SFRP5	PPH15747A	146
WNT5A	PPH02410A	189

2.1.5 Antibodies

Primary antibodies used for immunofluorescence (IF) analysis and western blot (WB) analysis are listed in table 6. Corresponding secondary antibodies are listed in table 7.

Table 6: List of primary antibodies

Antigen	Host	Dilution	Blocking	Provider
A-actinin	Mouse (IgG1)	IF: 1:500 FACS: 1:1000	1 % BSA/DPBS	Sigma A7811 (EA-53)
RYR2	Rabbit (IgG1)	IF: 1:500	1 % BSA/DPBS	Sigma Prestige HPA020028
Cx43	Rabbit (IgG)	IF: 1:1000	1 % BSA/DPBS	Abcam ab11370 (GJA1)
GAPDH	Mouse (IgG1)	WB: 1:1000	3 % non-fat dry milk in TBS-T	Merck #MAB374
SFRP5	Mouse (IgG2b)	1:500	3 % non-fat dry milk in TBS-T	Santa Cruz Biotechnology #sc-374397
GFP	Rabbit (polyclonal)	WB: 1:10000	3 % BSA in TBS-T	Abcam #ab290
GFP	Sheep (polyclonal IgG)	IF: 1:1000	1 % BSA/DPBS	BioRad #4745-1051

Antigen	Host	Dilution	Blocking	Provider
Hoechst		IF: 1:2000 FACS: 1:1000	1 % BSA/DPBS	Thermo Fisher Scientific #H1399

Table 7: List of secondary antibodies

Fluorophore & Antigen	Host	Dilution	Company
Alexa Fluor 488, anti-mouse	Donkey (IgG)	1:500	Thermo Fisher Scientific #A-21202
Alexa Fluor 555, anti-rabbit	Donkey (IgG)	1:500	Thermo Fisher Scientific # A-31572
Alexa Fluor 647, anti-mouse	Goat (IgG)	1:500	Thermo Fisher Scientific # A-21235
Alexa Fluor 488, anti-sheep	Donkey (IgG)	1:400	Thermo Fisher Scientific #A-11015
HRP, anti-mouse	Sheep (IgG)	1:10000	Th. Geyer #NA931
HRP, anti-rabbit	Donkey (IgG)	1:10000	Th. Geyer #NA934

2.1.6 Chemicals and reagents

Table 8: List of chemicals and reagents

Name	Provider
200 µmol dNTPMix	Bioline #BIO-39029
4x Laemmli Sample Buffer	BioRad #1610747
6x DNA Loading dye	Thermo Fisher Scientific #R0611
Agarose	VWR #35-1020
Ammonium Persulfate	BioRad #1610700
Ampicillin sodium salt	Carl Roth #K029.1
Boric acid	Sigma Aldrich #15663
BSA	Sigma Aldrich # A9647
$CaCl_2$	Sigma Aldrich #21115
D(+)-Glucose	Carl Roth #HN06.2
Dithiothreitol	Life Technologies #R0861
Ethanol absolut	Merck Millipore #1.00983.1000
EDTA	Carl Roth #8040.3
Fluoromount-G	Invitrogen #00-4958-02
GeneRuler 100 bp Plus DNA Ladder	Thermo Fisher Scientific #SM0321
Glycin	Carl Roth #3908.2
GoTaq DNA Polymerase	Promega #M300B
HCl	Carl Roth #K025.1
HEPES	Carl Roth #HN77.1
Hoechst33342, trihydrochlorid, trihydrate	Life Technologies #H3570

Name	Provider
Isoprenaline hydrochloride	Sigma Aldrich #I5627
Isopropanol	Merck Millipore #1.09634.1000
Kanamycin sulfate	Carl Roth #T832.1
KCl	Carl Roth #HN02.1
LB-Agar	Carl Roth #X965.1
LB-medium (Luria/Miller)	Carl Roth +X968.1
MgCl	Carl Roth #KK36.2
Midori Green Advance	Biozym #617004
NaCl	Carl Roth #3957.1
NaOH 1 mol/l	Carl Roth #K021.1
Non-fat dry milk	Carl Roth #T145.2
Nuclease-free water	Ambion #AM9938
Phire Hot Start II DNA Polymerase	Thermo Fisher Scientific #F-122S
Phusion Green Hot Start II High-Fidelity DNA Polymerase	Thermo Fisher Scientific #F-5375
Pierce Protease Inhibitor Mini Tablets, EDTA free	Thermo Fisher Scientific #A32955
Pierce RIPA buffer	Thermo Fisher Scientific #89900
Pluronic F-127	Invitrogen #P3000MP
Ponceau S solution	Sigma Aldrich #P7170
Precision Plus Protein All Blue Standards	BioRad #1610373
Restore™ PLUS Western Blot Stripping Buffer	Thermo Fisher Scientific #46430
Rhod-2	Thermo Fisher Scientific #R1245MP
RNAse Erase	MP #821682
Roti-HistoFix	Carl Roth #P087.4
TEMED	BioRad #1610800
Tris	Carl Roth #5429.3
Triton X-100	Carl Roth #3051.4
Tween 20	Carl Roth #9127.1

Table 9: List of used Kits

Method	Kit	Provider and order number
cDNA Synthesis	RT^2 First strand Kit	Qiagen #330404
Gel extraction kit	QUIAquick Gel extraction kit	Qiagen #28706
Genomic DNA isolation	QIAamp DNA Mini kit	Qiagen #51306
Plasmid isolation	NucleoSpin® Plasmid EasyPure mini kit	Machery Nagel #740.727.250
qPCR	RT^2 SYBR Green qPCR Mastermix	Qiagen #330501

Method	Kit	Provider and order number
Total RNA isolation	SV Total RNA isolation and purification kit	Promega #Z3105
Western Blot	Pierce BCA protein assay kit	Life technologies #23227
	TGX StainFree FastCast Acrylamide Starter Kit 10 %	BioRad #161-0182
	TransBlot Turbo rta transfer kit kit, nitrocellulose membrane	BioRad #170-4270
	SuperSignal West Femto Maximum Sensitivity Substrate	Thermo Fisher Scientific #34094

2.1.7 Solutions, buffer, and bacteria material for molecular and protein analysis

Table 10: List of components for molecular biological methods and protein analysis

Solution	Components
0.1 % Triton-X/BSA	10 µl Triton-X 100 diluted in 10 ml 1 % BSA diluted in DPBS, stored at 4°C
10x Running buffer	60.4 g Tris 288 g Glycine 20 g SDS 2 l H_2O
10x TBS-buffer	24 g Tris 80 g NaCl add H_2O to a total volume of 1000 ml pH 7.6
1x TBS-T	900 ml H_2O 100 ml 10x TBS 1 ml Tween-20
BSA in TBST (5 % w/v)	5 g BSA dissolved in 100 ml 1x TBS-T buffer
Non-fat dry milk (5 % w/v)	5 g non-fat dry milk dissolved in 100 ml 1x TBS-T buffer
TBE buffer (5x)	54 g Tris 27.5 g Boric acid 20 ml 0.5 M EDTA pH 8.0 Ad 1 l ddH2O
Tyrode's solution	NaCl 140 mM, KCl 5.4 mM, $CaCl_2$ 1.8 mM, MgCl2 1 mM, HEPES 10 mM, Glucose 10 mM, pH 7.4
Staining solution	1 % BSA 0.1-0.5 % Triton X-100 in PBS

Table 11: List for competent E. coli

Competent cells	Provider
NEB® 10-beta Competent E. coli (High Efficiency)	New England BioLabs #C3019

2.1.8   Chemicals, solutions, and media for cell culture

Table 12: List of chemicals, solutions, and media for cell culture

Components	Provider
0.25 % Trypsin-EDTA	Thermo Fisher Scientific #25200056
Albumin, human recombinant	Sigma-Aldrich #A9731
B-27 serum free supplement (50x)	Gibco #17504-044
CHIR99021	Merck Millipore # 361571
Collagenase B	Worthington Biochemical, #CLS-AFB
DMEM	Thermo Fisher Scientific #11960044
DMEM/F-12, no phenol red	Thermo Fisher Scientific #21041025
DMSO D2650	Sigma Aldrich #D2660
FCS	Gibco #10270-106
Human Stem Cell Nucleofector Kit 2	Lonza #VPH-5022
IWP2	Merck Millipore #681671
L-ascobic acid 2-phosphate	Sigma-Aldrich #A8960
L-glutamine (200 mM, 100x)	Gibco #25030024
StemMACS iPS-Brew XT basal medium	Miltenyi Biotech # 130-107-086
StenMACS iPS-Brew XT supplement (50x)	Miltenyi Biotech #130-107-087
Matrigel	Corning #354230
Non-essential amino acids (NEAA, 100x)	Thermo Fisher Scientific #11140035
Opti MEM I	Gibco #31985062
DPBS (1x)	Gibco 14190-094
Pen/Strep (100x)	Sigma Aldrich #P4333
Recombinant human basic fibroblast growth factor (bFGF)	PeproTech #100-18B
RPMI 1640 with HEPES with GlutaMax	Gibco #72400-021
RPMI 1640 without HEPES without Glucose	Gibco #11879-020
Sodium DL-lactate solution 60 % (w/w)	Sigma-Aldrich #L4263
StemFlex basal medium	Gibco #A33493-01
StemFlex supplement (10x)	Gibco #A33492-01
StemPro Accutase Mix	Gibco #A11105-01
TZV	MerckMillipore #420220
Versene solution (0.48 mM EDTA)	Gibco #15040-033

Components	Provider
SOC outgrowth medium	NEB #B9035
Polyfect transfection reagent	Qiagen #301105
Hepes solution	Sigma Aldrich #H0887

Table 13: Preparation of chemicals for cell culture

Substance	Preparation
CHIR (4 mM)	5 mg CHIR99021 dissolved in 0.894 ml DMSO, stored at -20°C
Collagenase B	Working solution: 400 U/ml Dissolved in RPMI, sterile filtered, stored at -20°C
Matrigel	Aliquoted 0.5 ml in 50 ml falcon
hbFGF	Stock solution: 100 ng/µl 100 µg hbFGF dissolved in 1 ml Tris (5 mM), stored at -20°C Working solution: 5 ng/µl, diluted 1:20 in 0.1 % BSA, stored at 4°C
Isoprenaline	Stock solution: 1 mM Dissolved in ddH2O, stored at -20°C Working solution: 100 nM, diluted in RPMI1640
IWP2 (5 mM)	10 mg dissolved in 4.28 ml DMSO, incubated for 10 minutes at 37°C, stored at -20°C
TZV (2 mM)	10 mg TZV dissolved in 16.06 ml DMSO, stored at -20°C
Lactate/HEPES 1M	3 ml sodium DL-lactate dissolved in 18 ml 1 M HEPES solution
Cardio Digestion Mix	100 ml StemPro Accutase mixed with 5.26 ml 0.25 % Trypsin

Table 14: Preparation of media for cell culture

Medium	Components
B27 medium	500 ml RPMI 1640 with HEPES 1x B27 supplement with insulin (50x)
Cardio Cryopreservation medium	90 % FBS, 10 % DMSO, 2 µM TZV
Cardio Differentiation medium	500 ml RPMI 1640 with HEPES with GlutaMAX 250 mg Albumin, human recombinant 100 mg L-Ascorbic acid 2-phosphate, sterile filtered
Cardio Digestion Medium	80 ml B27 medium 20 ml FBS 100 µl TZV 10 µl/ml Pen/Strep

Medium	Components
FACS medium	1x DMEM/F-12, no phenol red 10 µl/ml Pen/Strep, 1.5 % heat-inactivated FBS, 4 µM TZV, 10 ng/ml bFGF
HEK medium	DMEM (1.5 g/l glucose, 1x NEAA, 1x l-glutamine, 10 % FBS
MEF-conditioned MACS medium	MACS medium was incubated for 24 hours on mitomycin C-treated MEFs
Stem Cell Freezing medium	Stem cell medium, 20 % DMSO, 4 µM TZV
StemFlex medium	500 ml StemFlex basal medium 1x StemFlex Supplement (10x)
StemMACS medium	500 ml StemMACS basal medium 1x StemMACS Supplement (50x)

2.1.9 Cells used in the study

Table 15: List of cells used in the study

Name	Number	origin	Reprogramming system	publication
ipWT1.3	GOEi014-B.3	Dermal fibroblast	4-in-1 CoMiP reprogramming plasmid, feeder-free culture conditions	(El-Battrawy et al. 2018)
iBM76.1	GOEi005-A.1; MSC3-iPS1	Mesenchymal stem cell	STEMCCA lentivirus	(Cyganek et al. 2018)
iWT.D2.1	GOEi001-A.1; FB2-iPS1	Dermal fibroblast	STEMCCA lentivirus	(Cyganek et al. 2018)

2.1.10 Databases

Table 16: List of software used in the study

Name	Purpose	Company/Author
Adobe Photoshop CS 6	Image processing	Adobe
Alpha Imager Software	Calculation of CRISPR/Cas9 cleavage efficacy	Alpha-Imager
AxioVision	Immunofluorescence images	Carl Zeiss
BioRad CFX Maestro	qPCR analysis	BioRad
BLAST	KO screening	NCBI
Chromas	Sequencing analysis	Technelysium
Ensemble.org	Gene ID reference	Ensemble

Name	Purpose	Company/Author
Graphpad Prism 6	Statistical data analysis and graph design	Graphpad Software, Inc.
ImageJ	Image processing	National Institutes of Health
ImageLab	Western Blot imaging and analysis	BioRad
LabChart 8	Calcium imaging analysis	AD Instruments
Microsoft Excel	qPCR analysis Calcium imaging analysis	Microsoft Office
Microsoft Word	Textualization of the results	Microsoft Office
SnapGene Viewer	Vector map processing	Snap Gene
Zen	Confocal images	Carl Zeiss

2.2   Methods

2.2.1   Cell biological methods

2.2.1.1 Cultivation and splitting of HEK293T cells

HEK293T cells were cultivated in uncoated 6 well plates. HEK medium was changed every second day. With a confluence of 80-90 %, cells were split by washing once with DPBS and resuspending in HEK Medium. Single cells and cell clusters were transferred to a new uncoated 6 well plate.

2.2.1.2 Cultivation of hiPSCs on Matrigel coated dishes and glass cover slips

Matrigel was thawed on ice and 0.5 ml were transferred into 50 ml falcons stored at -20°C. The aliquot was resuspended with 29.5 ml or 59.5 ml cold DPBS (1:60 or 1:120 dilution) and stored at 4°C. Dissolved Matrigel was transferred to the culture dish and incubated at 37°C for 45 min or at 4°C overnight (6 well plate: 17 $\mu g/cm^2$ or 0.5 $\mu g/cm^2$, 12 well plate: 21 $\mu g/cm^2$ or 0.6 $\mu g/cm^2$).

25 mm round glass cover slips were incubated with 0.1 % HCl overnight, subsequently washed with distilled water and incubated in 70 % ethanol for 12 hours. The cover slips were cleaned with lint-free papers and sterilized at 200°C for 2 hours. Glass cover slips were coated with 700 µl Matrigel 1:60 dilution in an uncoated 6 well plate and incubated for 45 min at 37°C.

With a confluency of 80-90 % hiPSC were passaged to a new Matrigel coated plate. Human iPSCs were washed twice with Versene and incubated with prewarmed Versene (37°C). The hiPSCs were washed using stem cell medium (StemMACS or StemFlex) containing 2 µM Thiazovin (TZV). Small cell clusters and single cells were transferred to a new coated 6 well plate containing stem cell medium supplemented with 2 µM TZV. After overnight cultivation (~ 24 hours later), the medium was removed and replaced by stem cell medium without supplementation of TZV. Human iPSCs between the passages 15 to 40 were used for cardiac differentiation in this study.

2.2.1.3 Directed differentiation of hiPSCs into hiPSC-CMs

The direct differentiation of hiPSCs into hiPSC-CMs was initiated by modulation of the WNT signaling pathway according to Cyganek et al. (2018). Two wells of a 80-90 % confluent 6 well plate with hiPSCs were washed twice with Versene and incubated for 3 to 4 min with Versene. Detached cells were resuspended in stem cell medium supplemented with 2 µM TZV and transferred to a 15 ml falcon. Subsequently, 3 ml of stem cell medium were added to the cell suspension, the cell number was determined using a counting chamber or CASY (as described in 2.2.1.6) and the counted cells were plated in three different cell numbers (200.000, 230.000, 260.000 cells per well of a 6 well plate) on a Matrigel coated 6 well plate containing stem cell medium supplemented with 2 µM TZV. After 24 hours the TZV was removed by media change to stem cell media without TZV. Human iPSCs were further cultivated for two to three days to reach the required confluence of 80-90 % per well prior to directed differentiation.

In order to induce mesodermal differentiation, hiPSCs were incubated in Cardio Differentiation medium supplemented with 4 µM CHIR99021 (day0-day2), a glycogen-synthase-kinase-3 inhibitor inducing the WNT pathway. After 48 hours, the medium was changed to Cardio Differentiation medium supplemented with 5 µM IWP2, a WNT pathway inhibitor inducing cardiac differentiation. The medium was changed on day 4 to Cardio Differentiation medium. On day 8 the medium was changed to Cardio Culture medium. The first spontaneous contraction was observed around day 8 to 10.

Alternatively, the direct differentiation was started with Cardio Differentiation medium containing 6 µM CHIR99021. After 24 hours, the medium was changed to Cardio Differentiation medium. On day 3, 5 µM IWP2 was supplemented to the Cardio

Differentiation medium. Medium was changed to Cardio Differentiation medium on day 5 and to Cardio Culture medium on day 8-10. The first spontaneous contractions were observed around day 10.

To achieve lower cell densities, digestion of hiPSC-CMs was performed with Collagenase B (400 U/ml in RPMI1640) and 0.25 % Trypsin- Ethylenediaminetetraacetic acid (EDTA) or Cardio Digestion Mix. Afterwards, cardiomyocytes were metabolically selected with lactate, obtaining a highly purified population of cardiomyocytes (Tohyama et al. 2013).

Around day 12-14 wells with spontaneous beating hiPSC-CMs (> 30 % contracting areas in one well) were washed once with Versene and incubated for 1 to 2 hours with 37°C prewarmed Collagenase B. Detached cells were carefully transferred to a 15 ml falcon and centrifuged at 100 x g for 10 min. Supernatant was discarded and the remaining cell pellet was resuspended in prewarmed 0.25 % Trypsin-EDTA or Cardio Digestion Mix and incubated at 37°C for 10 min in a water bath. Every 2 to 3 min the tube was flicked by hand to singularize the cells. Digestion was terminated by adding the double volume of Cardio Digestion medium and centrifugation at 100 x g for 10 min. Supernatant was discarded, and the remaining cell pellet was resuspended in a small volume of Cardio Digestion medium. Dependent on the pellet size, cells were replated on 6 to 15 wells of a Matrigel coated 6 well plates containing Cardio Digestion medium.

To purify the cardiomyocyte population, medium was changed to Cardio Selection medium containing lactate instead of glucose 48 hours after digestion and reseeding. The Cardio Selection medium was changed every second day and again changed to Cardio Culture medium after 5 to 7 days of selection depending on the cell density. For maturation, cardiomyocytes were cultured to an age of 60 days in Cardio Culture medium. Cardiomyocyte purification and quality was observed by visual estimation of contracting areas. In this study, cardiomyocyte populations with contracting areas greater than 90 % were used for further experiments.

2.2.1.4 Freezing and thawing of cultivated cells

Cryopreservation of hiPSCs was performed according to the splitting protocol (see 2.2.1.2). Detached cells were resuspended with stem cell medium supplemented with 4 µM TZV and 20 % DMSO. Subsequently, the cell suspension was carefully transferred in a cryo-tube, stored at -80°C for at least 2 hours in a freezing container filled with

isopropanol (to enable approximated freezing at -1°C per min) and finally transferred into -150°C.

Cardiomyocytes were digested with Trypsin-EDTA 0.25 % for 10 min. The digestion reaction was stopped with an equal volume of fetal bovine serum (FBS). Human iPSC-CMs were transferred into a 15 ml Falcon and centrifuged at 100 x g for 10 min. The supernatant was discarded and the remaining pellet was resuspended in a small volume of FBS. Cells were counted with counting chamber or CASY (see 2.2.1.6), a defined cell amount was diluted in Cardio Cryopreservation medium and transferred into a cryo-tube. The cryopreservation process was performed with a controlled rate freezer (KRYO 560-16, Planer), allowing a controlled freezing rate of -1°C per min down to -90°C. Long term storage of cardiomyocytes and hiPSC was implemented at -150 °C.

For recovery, cryo-tubes were thawed at 37°C, transferred in 10ml medium (Cardio Culture medium or stem cell medium) and centrifuged at 200 x g for 5 min. Human iPSCs were resuspended in 2 ml stem cell medium supplemented with 2 µM TZV and transferred to a Matrigel coated 6 well plate. CMs were resuspended in a small volume Cardio Digestion medium and plated in a Matrigel coated 6 well plate (1:120 dilution). After 30 min, 2ml Cardio Digestion medium was added carefully to the CMs.

2.2.1.5 Harvesting of cells for pellets

Human iPSCs were harvested by washing twice with DPBS followed by a 3 min incubation with prewarmed Versene. Cells were washed off the plate with DPBS, collected in a 1.5 ml safe lock tube and centrifuged at 12,000 x g for 1 min. Supernatant was discarded and the cells were snap-frozen in liquid nitrogen. Long term storage was performed at -80°C.

Cardiomyocytes were harvested as pellet by washing twice with DPBS and cell scraping. Cells were collected in a 1.5 ml safe lock tube and centrifuged at 12.000 x g for 1 min. Subsequent steps were performed according to the hiPSC harvesting protocol.

2.2.1.6 Cell counting

A counting chamber was used for cell counting of HEK293T, hiPSCs and hiPSC-CMs. Therefore, approximately 20 µl of the cell suspension was added in two fields of the counting chamber. In 4x4 quadrants of a field, vital cells were counted by observation

using a light microscope. The cell count was calculated by the mean value of the cell count from each 4x4 quadrant/64*10^6.

The CASY Cell Counter was used for cell counting of hiPSCs and hiPSC-CMs. Therefore, 10 ml CALCIUM SPARKSY Ton was transferred in a CASY cup and 20 µl of the cell suspension was added. The CASY cup was secured with a lid and the content was mixed by inverting the cup three times. The measurement of the sample was performed according to the manufacturer's instructions of "measuring samples and displaying size distributions".

2.2.2 Molecular biological analysis

2.2.2.1 Genomic DNA isolation for DNA sequencing

The QIAamp DNA Mini kit was used for genomic DNA (gDNA) isolation. According to the manufacturer's instructions, cells were incubated at 50°C for 10 min with Proteinase K to lyse the cells. Equal volume of ethanol was transferred to the cell lysate and the gDNA was purified through a spin column. The elution was performed with 50-100 µl nuclease-free water and gDNA concentration of the eluate was measured with a NanoDrop 2000/2000c at 260 nm and 280 nm.

2.2.2.2 Total RNA isolation from hiPSC and hiPSC-CMs

Cells were harvested as pellets as described in 2.2.1.5. For total RNA isolation the SV Total RNA isolation and purification kit was used. The snap frozen cell pellet was resuspended in 400-800 µl of RNA lysis buffer depending on the cell pellet size. Total RNA isolation and purification was performed according to the manufacturer's instructions without the heating step in RNA dilution buffer. The RNA was eluted with 30-50 µl nuclease-free water and the RNA concentration was measured with a NanoDrop One at 260 nm and 280 nm. The purified RNA was immediately used for complementary DNA (cDNA) synthesis or stored at -80°C.

First strand cDNA synthesis was performed with the RT^2 First strand Kit according to the manufacturer's instructions.

2.2.2.3 Polymerase chain reaction for KO clone sequencing

Polymerase chain reaction (PCR) of the gene of interest SFRP5 was done according to the pipetting instructions (table 17) and the 3-step cycling protocol (table 18) below.

Table 17: Pipetting instructions for SFRP5^{KO} clone screening on genomic level.

Component	20 µl reaction volume
gDNA (100 ng/µl)	1 µl
nuclease-free water	Up to 20 µl
5x Phusion Green GC Buffer	4 µl
DMSO (8 %)	1.6 µl
10 mM dNTPs	0.5 µl
sense primer (10 µM)	1 µl
antisense primer (10 µM)	1 µl
Phusion Hot Start II High-Fidelity DNA polymerase	0.2 µl

Table 18: Cycling protocol for SFRP5^{KO} clone screening on genomic level.

Cycle Step	Temperature	Time	Cycles
Initial denaturation	95°C	5 min	1
Denaturation	98°C	5 min	40 n
Annealing	62°C	30 sec	
Extension	72°C	50 sec	
Final extension	72°C	1 min	
	4°C	hold	1

2.2.2.4 Quantitative PCR

For quantitative gene expression analysis qPCR was performed with the CFX96 Real-Time Detection System (BioRad) using the RT^2 SYBR Green qPCR Mastermix (Qiagen). Samples were prepared according to table 19 below. Negative control, reference genes (18S and GAPDH) and the genes of interest were amplified independently on the same 96 well plate using triplicates for each sample. The cycling program is listed in table 20. The results were analyzed with the BioRad CFX Maestro Software followed by the Excel-based ddC(t) analysis method in which the gene of interest is normalized to the reference gene. GraphPad Prism 7 graphs was used to visualize the results and perform statistics. Primer sequences for qPCR are listed in table 5.

Table 19: Pipetting instructions for qPCR using RT² SYBR Green qPCR Mastermix.

Component	25µl reaction volume
Nuclease free water	10.5 µl
Sense + antisense Primer (10µM)	1 µl
RT² SYBR Green qPCR Mastermix	12.5 µl
cDNA	1 µl

Table 20: Cycling protocol for qPCR using RT² SYBR Green qPCR Mastermix.

Cycle Step	Temperature	Time	Cycles
Initial denaturation	95°C	15 sec	1
Denaturation	95°C	15 sec	50 n
Extension	60°C	60 sec	
melt curve	55-95°C	6°C/step	
	4°C	hold	1

2.2.2.5 Agarose gel electrophoresis

For PCR product analysis, the electrophoretic separation and detection of the PCR products within an agarose gel was used. Therefore, 1.5 % agarose was dissolved in 1x TBE buffer and heated in a microwave until the mixture was transparent. Midori Green Advance (0.04 µl/ml) was added to visualize the amplified PCR product. GeneRuler 100 bp Plus DNA Ladder was used for estimation of the PCR product length. The gel was run for 30 min at 120 V or for sequencing 45 min at 100 V. BioDoc Analyze (Biometra) was used for documentation.

2.2.2.6 Gel extraction and DNA Sequencing

DNA or RNA products for sequencing were excised from the agarose gel using a clean scalpel. According to the manufacturer's instructions of the QUIAquick Gel extraction kit, the DNA or RNA was isolated through a spin column system and finally eluted with 30 µl nuclease-free water. DNA or RNA concentration was measured with a NanoDrop one at 260 nm and 280 nm.

The DNA or RNA was subsequently sequenced by a commercial sequencing lab (SeqLab, Göttingen). 10 to 45 ng/µl extracted DNA was mixed with 3 µl sequencing primer (primer concentration 10 µM) and nuclease-free water to a final volume of 12 µl. The sequencing results were analyzed using online tool NCBI nucleotide alignment tool (Blast.ncbi.nlm.gov) and ChromasPro2.

2.2.2.7 Heat shock transformation of chemo-competent E. coli and plasmid purification

The amplification of the CRISPR/Cas9 plasmids, ordered as a Sigma all-in-one-plasmid, and the AAV-overexpression plasmids was performed with NEB10-beta competent E. coli according to the high efficiency transformation protocol (NEB 2019). Cells were thawed on ice and mixed with 100 ng plasmid-DNA. The E. coli-DNA-mixture was incubated on ice for 30 min and afterwards a heat shock was performed for exactly 30 sec at 42°C. Afterwards the mixture was placed onto the ice again, and following 5 min of incubation, 950 µl SOC outgrowth medium was added to the mixture. The cell suspension was vigorously shaken at 250 rpm for 1 hour. Afterwards, cells were plated on a lysogeny broth(LB)-agar plate supplemented with kanamycin sulfate 50 mg/ml (ampicillin sodium salt 100mg/ml for AAV-plasmids) and incubated overnight at 37°C. Three plasmid-harboring E. coli colonies were chosen and manually transferred in 4 ml LB-medium containing 50 mg/ml kanamycin sulfate (100 mg/ml ampicillin sodium salt). These chosen E. coli clones were cultivated in a shaker (250 rpm) at 37°C overnight.

The plasmid purification was performed according to the manufacturer's instructions of the NucleoSpin Plasmid EasyPure mini kit. Harvested E. coli cultures from 2.2.2.7 were lysed and cellular compartments were spun down. The clarified lysate was transferred to a NucleoSpin Plasmid EasyPure column, binding the plasmid-DNA. After washing the silica membrane, the plasmid-DNA was eluted in 30 µl nuclease free water. The concentration of the plasmid-DNA was measured with the Nanodrop 2000/2000c at 260 nm and 280 nm.

2.2.3   Protein expression analysis

2.2.3.1 Immunofluorescence analysis

To analyze cardiac specific proteins, iPSC derived WT-CMs, KO-CMs and AAV-threatened CMs of healthy donors were digested on glass coverslips with low density for Immunofluorescence analysis.

CMs were fixated with Roti-Histofix 4 % (incubation for 20 min at room temperature (RT)). After three washing steps with DPBS hiPSC-CMs were stored in DPBS containing 1 % bovine serum albumin (BSA) at 4°C overnight for blocking unspecific binding sites. Immunostaining was performed with antibodies diluted in staining buffer. The glass

cover slips were placed on screw cups in a humidified chamber. The first antibody was diluted in 250 µl staining buffer and incubated overnight at 4°C. Subsequently, cells were washed three times with DPBS for 5 min in an uncoated 6 well plate. Glass cover slips were transferred back in the humidified chamber and incubated with the secondary antibody in 250 µl staining buffer for 1 hour at RT. The staining solution was discarded and cells were incubated with Hoechst for 10 min at RT protected from light. After 3x 5 min washing with DPBS in an untreated 6 well plate and a final wash cycle with distilled water, the coverslip was placed upside down on a microscope slide and mounted with Fluoromount-G.

Image recording was performed with the LSM 710 confocal microscopy system using Z-Stack acquisition mode (frame size 2048x2048; Bit depth: 12bit; pinhole: 1.8 Airy Units, Gain: 600-700).

2.2.3.2 Flow cytometry

Purification of hiPSC-CM cultures and AAV transduction efficiency was determined by flow cytometry. For fixation, cardiomyocytes were washed two times with DPBS and incubated for 10 min with 0.25 % Trypsin-EDTA. Digest was stopped using double amount of Cardio Digestion medium. Cells were transferred into a 15 ml falcon and centrifuged at 300 x g for 5 min. Supernatant was discarded, the remaining pellet was resuspended in 2 ml 4 % Roti-Histofix for 10 min at RT, incubated to fixate the cells, and subsequently washed twice with DPBS. Fixated hiPSC-CMs were subsequently incubated for 2 hours in blocking solution. For immunostaining with Anti-α-actinin, half of the fixated cell suspension was transferred to a separate tube for negative control stained only with Hoechst. The other half of the cells was centrifuged at 300 x g for 5 min at 4°C, blocking solution was discarded and cell pellet was resuspended in staining solution (1 % BSA with 0.1 % Triton) and incubated on ice for 10 min. Afterwards, hiPSC-CMs were centrifuged at 300 x g for 5 min at 4°C, resuspended with the primary antibody (Anti-α-actinin 1:1000 in 50 µl staining solution) and incubated overnight at 4°C. Primary antibody was washed-off with DPBS and the secondary antibody linked with the Alexa Fluor 488 fluorophore (donkey Anti-mouse, dilution 1:500) was incubated for 1 hour at RT. Finally, the cells were incubated with Hoechst for 10 min (dilution 1:10000). For flow

cytometry measurement hiPSC-CMs were resuspended in DPBS, strained through a 40 µm cell strainer, and transferred to a fluorescence activated cell sorting (FACS) tube.

For AAV transduction efficiency analysis the cells were resuspended in 100 µl DPBS after washing steps. To clear the cell suspension from clumps, cells were strained through a 40 µm cell strainer and transferred to a FACS tube.

GFP and α-actinin fluorescence was measured with a LSRII flow cytometer (BD Bioscience). At least 10,000 events per sample were recorded. Results were analyzed using the flowing software 2.

2.2.3.3 Western Blot Analysis

Human iPSC-CM pellets were harvested as described in 2.2.1.5 and stored at -80°C or directly used to lysate the pellet. Frozen cell pellets were incubated with RIPA lysis buffer (Life Technologies) for 10 min on ice and centrifuged at 5000 rpm for 5 min at 4°C. The supernatant was transferred to a new tube on ice. Protein concentration measurement was performed with Pierce bicinchonic acid assay kit, according to the manufacturer's instructions and measured with the Nanodrop One. The samples were stored at -80°C for further use or immediately used for sodium dodecyl sulfate-polyacrylamide gel electrophoresis (SDS-PAGE) preparation.

For protein fractionation due to the proteins' molecular weight, 30 µg Protein and 4x Laemmli Sample Buffer with dithiotreitol were mixed with distilled water to a final volume of 30 µl per sample. Prepared samples were denatured at 95°C for 5 min. SDS-PAGE gel (TGX StainFree FastCast Acrylamide Starter Kit; BioRad) was prepared according to the manufacturer's instructions. A pre-stained molecular weight marker (Precision Plus Protein All Blue Standard) and 25 µl of the prepared samples were loaded in the wells of the gel. Electrophoresis was performed in an electrophoresis chamber filled with 1x running buffer at constant 100 V for 2 hours.

The transfer of proteins from the gel into a membrane the semi-dry rapid blot system from BioRad was used. According to the manufacturer's instructions of the TransBlot Turbo kit (BioRad), the separated proteins were transferred from SDS-gel to a nitrocellulose-membrane using the Trans-Blot Turbo Transfer System (BioRad, 25 V, 2.5 A, 7 min). Free binding sites of the membrane were blocked in 5 % non-fat dry milk in Tris-buffered saline with Tween20 (TBS-T) or 5 % BSA in TBS-T for 1 hour at RT.

Subsequently the primary antibody, diluted in 3 % non-fat dry milk in TBS-T or 3 % BSA in TBS-T, was added to the membrane and incubated overnight at 4°C. The following day, the membrane was washed three times for 5 min with TBS-T. The HRP-conjugated secondary antibody (Anti-mouse NA931, Anti-rabbit NA934 dilution 1:10.000), diluted in 3 % non-fat dry milk in TBS-T or 3 % BSA in TBS-T, was incubated for 1 hour at RT. For imaging, the membrane was washed 3 times for 5 min each with TBST, removing soluble antibody-complexes. For chemiluminescence visualization of the immune reaction the SuperSignal West Femto Maximum Sensitivity Substrate (Thermo Fisher Scientific) and the chemiluminescence detection system (Bio-Rad, ChemiDoc XRS+) was used.

2.2.4   AAV-mediated overexpression of SFRP5

AAV transduction was performed with all three cell lines using AAV-Basic and AAV-SFRP5. At day 46, cardiomyocytes were directly exposed to AAV particles (multiplicity of infection (MOI) = 10^5) for 72 hours in 1.5 ml Cardio Culture medium supplemented with 10 µl/ml Penicillin-Streptomycin solution (Pen/Strep). For immunofluorescence or Calcium imaging analysis 50,000 cells per glass cover slip were used. At least 600,000 cells per 6 well were required for RNA and protein analysis. Cardiomyocytes were cultured with Cardio Culture medium supplemented with 10 µl/ml Pen/Strep for an additional 14 days. Via fluorescence microscopy (Zeiss, Axio Observer A1) reporter gene fluorescence was first detected on day 5 and lasted until pellet collection or fixation.

2.2.5   HEK293T cell transfection with overexpression plasmids

The validation of the overexpression plasmids was performed with HEK293T cells using PolyFect Transfection Reagent (Qiagen). The transfection was done according to the manufacturer's instructions ("protocol for transient transfection of 293T cells"). Fluorescence microscopy images were taken 12 hours after transfection and cell pellets were collected after 24 hours. Downstream analysis implied SFRP5 expression analysis on transcriptional and protein level.

2.2.6   Generation of KO-hiPSC clones by CRISPR/Cas9

For generation of the SFRP5^{KO} hiPSC clones, wild type hiPSCs were transfected with the CRISPR/Cas9 Sigma All-in-one plasmids using the Human Stem Cell Nucleofector Kit 2. One hour before transfection, hiPSCs with 80-90 % confluency were pre-treated with 2 µM TZV. The DNA-nucleofector solution consists of 82 µl human stem cell nucleofector solution (Kit 2), 18 µl supplement 1 and 1 µg of each CRISPR/Cas9 plasmid. Human iPSCs were detached (according to 2.2.1.2) and counted with CASY cell counter as described in 2.2.1.6. For nucleofection $2x10^6$ cells were transferred into a 15 ml Falcon and centrifuged 5 min at 200x g. The supernatant was discarded, and cells were resuspended in the DNA-nucleofection mix, transferred into nucleofection cuvette and placed in the nucleofector holder of an Amaxa Nucleofector II Device. The program B-016 was used for nucleofection of hiPSCs. Subsequently, nucleofected cells were reseeded in one well of a Matrigel coated 6 well plate containing stem cell medium, 2 µM TZV and 10 µl/ml Pen/Strep.

24 hours after transfection, plasmid-harboring hiPSC were sorted by the FACS facility of the UMG. For this purpose, transfected hiPSCs were washed once with Versene, detached by 2 min Versene incubation, and resuspended in FACS medium. The cell suspension was filtered through a cell strainer (40 µm) into a sterile FACS tube and immediately sorted from the FACS facility in GFP$^+$ and GFP$^-$ population, while the GFP$^+$ cells contained the CRISPR/Cas9 plasmid. Positive transfected cells (GFP$^+$ cells) were seeded on a 96 well plate containing mouse embryonic fibroblasts (MEF)-conditioned StemMACS medium, 10 µl/ml Pen/Strep, 2 µM TZV and 50 ng/µl bFGF. Medium containing MEF-conditioned StemMACS medium, 10 µl/ml Pen/Strep and 50 ng/µl bFGF was changed twice a week.

First colonies were detectable after 10-18 days. Slowly the TZV and bFGF was tapered and the MEF-conditioned StemMACS medium supplemented with 10 µl/ml Pen/Strep and 50 ng/µl bFGF was changed to StemMACS medium. Approximately after 2 weeks the first colonies are ready for splitting by short Versene incubation and transferred to a Matrigel coated 12 well plate containing StemMACS medium, 1x Pen/Strep and 2 µM TZV. With a confluence of 50 %, half of the clone was scraped with a cell scraper and the cell suspension medium was collected for DNA isolation as described in 2.2.2.1. The CRISPR/Cas9 targeted gene side was amplified via PCR. PCR products were loaded on an

agarose gel (see 2.2.2.3, 2.2.2.5) and DNA bands of interest were cut out of the agarose gel (see 2.2.2.6). The target DNA was purified using the Quiaquick Gelextraction kit and sequenced by SeqLab as described in 2.2.2.6.

The sequencing results demonstrated mixed clones or heterozygote clones. To obtain pure single cell clones of SFRP5[KO] hiPSC-clones were replated on a Matrigel coated 6 well plate in high dilution and cultured with StemFlex. Medium was changed every second day. After a few days single cell colonies were visible and manually transferred onto a new 6 well plate coated with Matrigel. New cell clones were expanded and analyzed on the genomic level via sequencing as described in 2.2.2.6.

After purification of the KO clones they were analyzed on the mRNA level to detect posttranscriptional changes induced by CRISPR/Cas9-mediated nucleotide alteration. SV Total RNA Isolation System (see 2.2.2.2) and RT2 First strand kit (Qiagen) were used to produce cDNA of the KO-hiPSC clones according to the manufacturer's instructions. The region of interest was expanded via PCR with GoTaq DNA polymerase. PCR products were loaded on agarose gel as described in 2.2.2.5. Target PCR bands were excised out of the gel and cDNA was extracted and sequenced by Seqlab (see 2.2.2.6).

Table 21: Pipetting instructions for GoTaq DNA polymerase

Component	25 µl reaction volume
cDNA (100 ng/µl)	2 µl
nuclease-free water	14.3 µl
5x Green GoTaq Reaction Buffer	5 µl
10 mM dNTPs	1.6 µl
sense primer (10 µM)	1 µl
antisense primer (10 µM)	1 µl
GoTaq DNA polymerase	0.1 µl

Table 22: Cycling protocol for GoTaq DNA polymerase

Cycle Step	Temperature	Time	Cycles
Initial denaturation	95°C	2 min	1
Denaturation	94°C	30 sec	40
Annealing	56°C	30 sec	
Extension	72°C	30 sec	
Final extension	72°C	5 min	1
	4°C	hold	1

2.2.7   mRNA-sequencing of treated hiPSC-CMs

The mRNA-seq was performed at the NGS-facility for Integrative Genomics, University Medical Center Göttingen as described in Khadjeh et al (2020). Differential expression analysis was conducted by Orr Shomroni (NGS-facility for Integrative Genomics, University Medical Center Göttingen).

Cytoscape and ClueGo were used for pathway analysis of significantly regulated genes (cut off log2FC > 0.095/ < - 0.095; adjusted p-value < 0.05) of the transcriptomes (Shannon et al. 2003; Bindea et al. 2009). Regulated pathways are visualized with modified KEGG maps: calcium signaling (hsa04260), apoptosis (hsa04210).

2.2.8   Calcium imaging

WT-hiPSC-CMs (iWT.D2.1-CM and iBM76.1.-CM) were digested in a low density to Matrigel coated glass cover slips (25.000 cells per well) three weeks before calcium recording. 14 days before recording cells were transduced with AAV-Basic and AAV-SFRP5 (MOI = 10^5). Cells were used for recording 12-14 days after virus transduction (age of 55 to 70 days). For calcium imaging, cells were washed once with Tyrode and incubated with 5 µM Rhod-2 AM fluorescent calcium indicator and 0.02 % [w/v] pluronic F-127 in Tyrode's solution for 30 min at 37°C. For recording, the cells were paced with a field stimulation of 0.25 Hz (18 V, 3 ms duration, 20-22°C) eliminating calcium kinetics aberrations depending on beating frequency. Recording was performed using a recording chamber with platin electrodes for glass cover slips (diameter 25 mm). For inotropic stimulation, cells were incubated for 10 min at 20-22°C with the β-sympathomimetic isoprenaline hydrochloride (100 nM) before recording. Cytosolic calcium recording was performed using line scan mode (512 pixels, 45 µm, 1057.7 Hz, 20,000 cycles; 63x1.4 NA oil objective and Zen 2009 software) of the LSM 70 confocal microscopy system (figure 4A). Cytosolic calcium measurements were recorded at 561 nm. Emission was collected at 566-646 nm. Each measured cell was imaged at 488 nm for GFP expression control.

Calcium transients were analyzed by plotting the mean signal intensity as a function of time using ImageJ (figure 4B). Raw data were polynomically smoothed (Savitzky-Golay filter, 20 neighbors) using Excel. For final analysis, smoothed data were transferred to LabChart Pro 8 (ADInstruments) using the PEAK Analysis Tool (Settings were adopted

from Cyganek et al. 2018). Results displayed the mean of four calcium transients per single cell recording (figure 4C).

Changes in spontaneous open variability of RYR2 leading to local increase of cytosolic calcium concentration, also known as Calcium sparks, were analyzed by ImageJ and Excel. Calcium sparks were analyzed in a defined plot in the last diastole of each recorded cell (1 sec, 40 µm) using ImageJ plugin "SparkMaster" (settings: 1057.7 lps, 0.088 µm, Fl. U. 0, citeria 3.3, intervals 3) (figure 4D) (Picht et al. 2007). For detailed analyzes, calcium sparks with a minimal amplitude of 0.1 ΔF/F0, minimal width of 1 µm and minimal duration of 5 ms were selected. Calcium sparks parameter full width at half maximum, full width, amplitude, full duration at half maximum, time to peak and full duration were graphically demonstrated in figure 4E. Calcium sparks size is the product of spark amplitude, full width and full duration. The calcium leak is defined as the sum of all spark sizes in 40 µm x 1 sec diastolic phase of line scan.
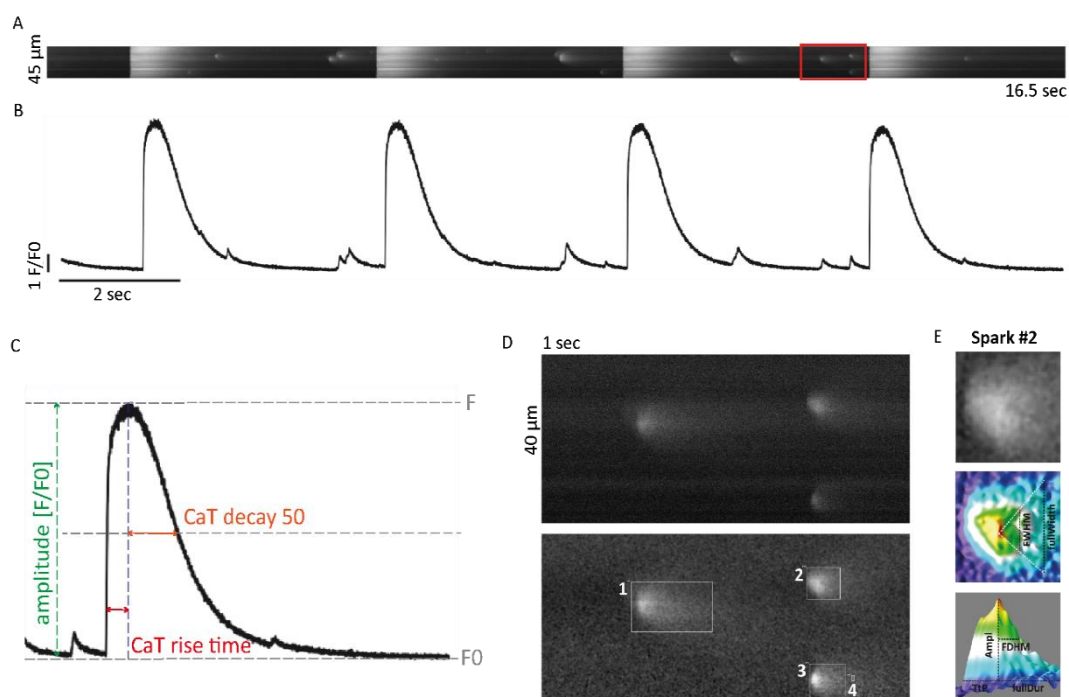

Figure 4: Analysis of calcium sparks and transients. Calcium cycling is crucial for cardiomyocyte contraction. Changes in calcium cycling of hiPSC-CMs were analyzed using confocal line scan mode **(A)**. A 45 µm line was drawn in the cytosol of a GFP⁺ hiPSC-CM. Four contractions were recorded during 16.5 sec and further analyzed with ImageJ by plotting signal intensity as a function of time **(B)**. With Excel polynomically smoothing and LabChart PEAK Analysis Tool the calcium transients parameter amplitude, time of calcium decay at 50 % of amplitude (calcium transients decay 50) and rise time were analyzed **(C)**. Spontaneous calcium release of ryanodine receptor 2, also known as calcium sparks, were analyzed in the diastole of cardiomyocyte contraction (framed in red in **A**). The chosen diastolic section (1 sec x 40 µm) is enlarged in **D** with corresponding image after analysis with ImageJ plugin "SparkMaster". Exemplary

calcium spark #2 was chosen for visualisation of calcium spark parameter full width at half maximum (FWHM), full width, spark amplitude (Ampl), full duration at half maximum (FDHM), full duration (full Dur) and time to peak (TtP). Adapted from Dr. Lukas Cyganek, Stem Cell Unit, UMG.

3   Results

3.1   Validation of successful differentiation of SFRP5^{WT} hiPSC-CMs

The modulation of WNT signaling enabled the differentiation of stem cells into contractile cardiomyocytes. According to the directed differentiation protocol, wild type hiPSCs (SFRP5^{WT} hiPSC) were differentiated and cultured up to 60 days for adequate maturation (figure 5) and further downstream analysis. Differentiation efficiency was examined by observation of contracting areas. In this study, only differentiated cultures with > 90 % contracting areas were used.
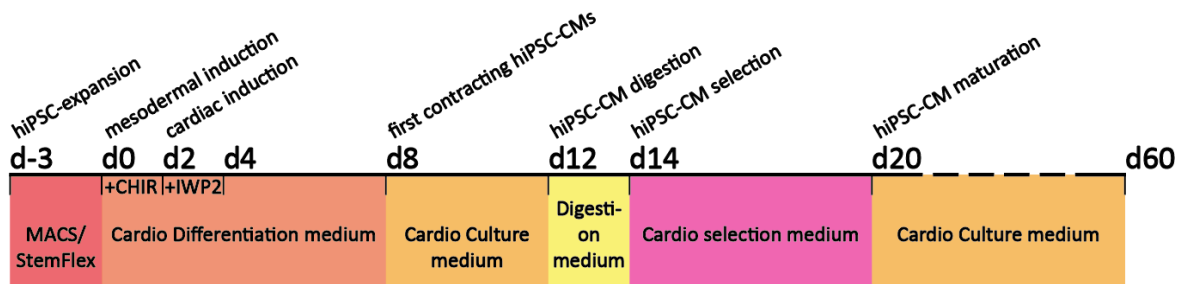

Figure 5: Steps and influences in the process of cardiac differentiation. Three days before differentiation initiation, hiPSCs were split and cultivated until they reached approximately 80-90 % confluency. Cardio Differentiation medium supplemented with WNT/β-catenin signaling activator CHIR (d0-d2) and WNT signaling inhibitor IWP2 (d2-d4) induced mesodermal and subsequently cardiac differentiation. Contracting cardiomyocytes were observed on day 8 and medium was changed to Cardio Culture medium. On day 12 contractile cells were digested and replated for metabolic selection with Cardio Selection medium (d14-d20). For adequate maturation hiPSC-CMs were cultured with Cardio Culture medium up to day 60.

Cardiac specific marker expression of SFRP5^{WT} hiPSC-CMs was validated via immunofluorescence imaging. The cardiac contraction filaments were stained with Anti-α-actinin antibody and Anti-RYR2 antibody. The expression of α-actinin and RYR2 is co-localized displaying regular cardiac sarcomere organization. Distinct cardiac specific cell-cell communication was displayed by cardiac specific gap junction protein connexin 43 (Cx43), competent for electric signal conduction between neighboring cells (figure 6).
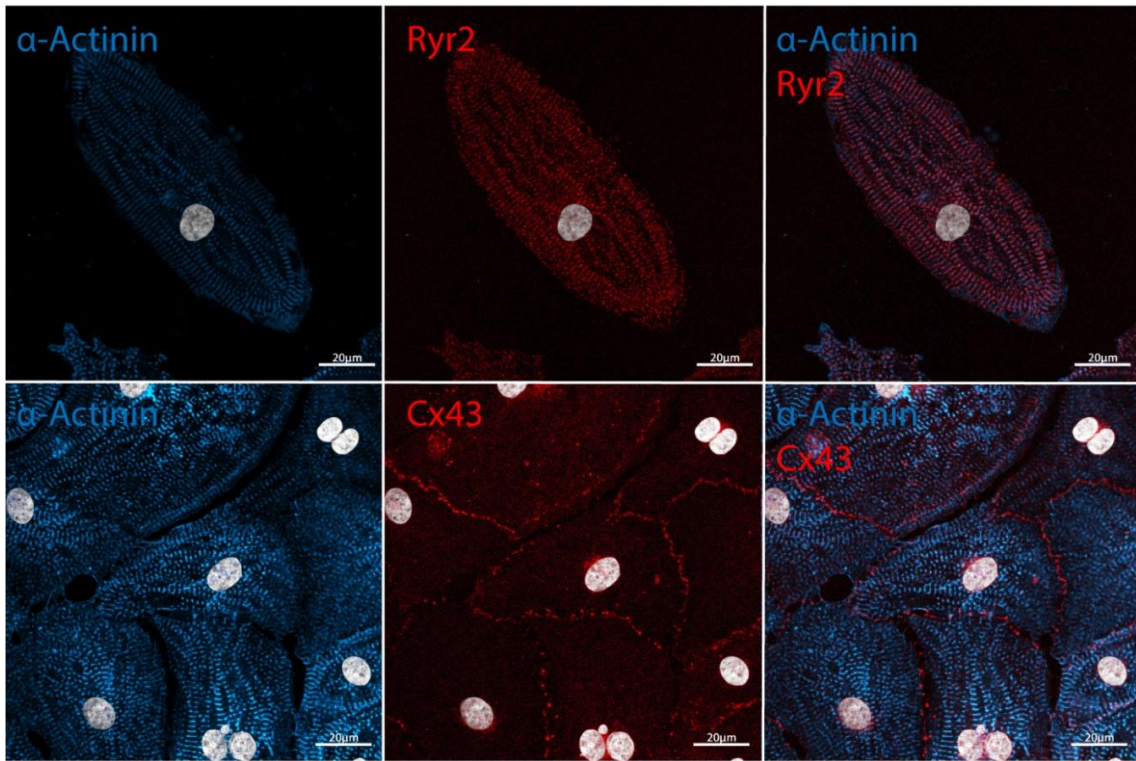
Figure 6: Cardiac marker expression in SFRP5^WT^-hiPSC-CMs. SFRP5^WT^-hiPSC-CMs were stained with Anti-α-actinin antibody (blue, 1:1000), Anti-Ryr2 antibody (red, 1:500) and Anti-Cx43 antibody (red, 1:1000), nuclei were stained with Hoechst (grey, 1:2000). Cell type specific expression of α-actinin and Ryr2 was validated displaying a regular sarcomere structure. Cardiac specific cell-cell communication was shown by Cx43 immunostaining. Scale bar 20 µm.

With the here applied directed differentiation protocol modulating the WNT pathway activity and the subsequent step of metabolic purification, highly enriched populations of functional cardiomyocytes were obtained. Differentiation efficiency and contractile function of SFRP5^KO^ hiPSC-CMs were comparable to SFRP5^WT^ hiPSC-CMs (data not shown).

3.2 AAV-mediated overexpression

3.2.1 Establishment of AAV6-mediated gene transfer: validation of overexpression via HEK293T transfection

In order to verify feasibility of the AAV6 overexpression system and to test whether gene transfer can be successfully accomplished using the plasmids obtained from Vector Biolabs, SFRP5 overexpression was validated initially in HEK293T cells. The GFP expression was detectable 12 hours after plasmid transfection in both pAAV-Basic (Control^pOE^) or pAAV-SFRP5 (SFRP5^pOE^) HEK293T cells (figure 7A).

To validate the overexpression of SFRP5, cell pellets were used for mRNA and protein expression analysis. SFRP5 expression changes were analyzed by qPCR displaying a significant upregulation of *SFRP5* in SFRP5[pOE] compared to Control[pOE] HEK293T cells (figure 7B). The expression of GFP and SFRP5 was further validated on the protein level by western blot. GFP protein expression was observed in SFRP5[OE] and Control[pOE] HEK293T cells. SFRP5[pOE] HEK293T cells showed a clearly detectable SFRP5 expression on the protein level. In contrast, untreated and Control[pOE] HEK293T cells showed no SFRP5 expression as expected (figure 7C).
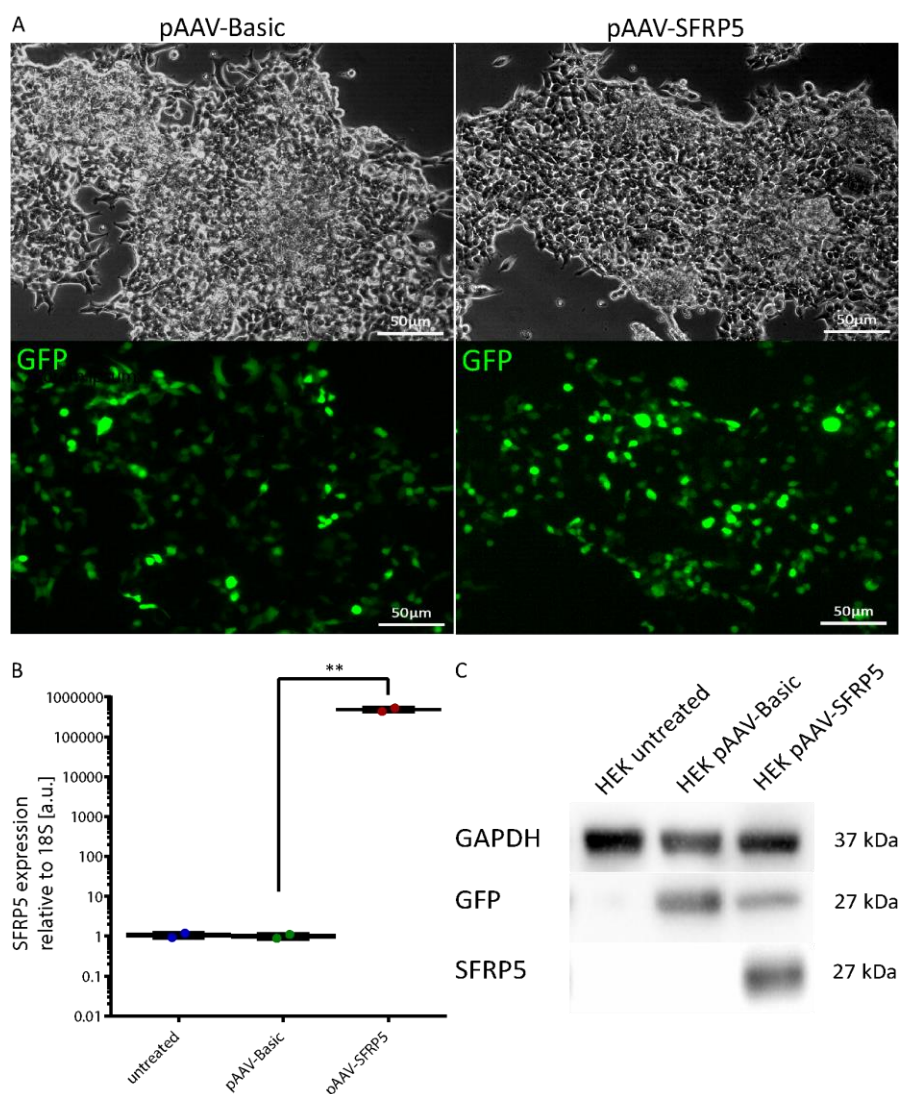
Figure 7: Validation of SFRP5 overexpression system in HEK293T cells. HEK293T cells were transfected with AAV-Basic and AAV-SFRP5 overexpression plasmids (pAAV) using the Polyfect transfection reagent. **(A)** Fluorescence images of living cells were taken 12 hours after transfection. Robust GFP expression was observed with pAAV-Basic and pAAV-SFRP5. Scale bar: 50 µm. **(B)** HEK 293T cells were pelleted 24 hours after transfection. SFRP5 expression was examined on the transcriptional level via qPCR. The results displayed a significant overexpression (485,000-fold, **) of SFRP5 in pAAV-SFRP5 compared to pAAV-Basic and the untreated control. 18S was used as housekeeping gene. Data represent means ± SEMs, **$P < 0.01$

unpaired, two-tailed t-test. **(C)** Western blot analysis was performed with HEK293T cells 24 hours after transfection. GFP (ab290, 1:1000), SFRP5 (ab198206, 1:100) and GAPDH (MAB374, 1:1000) antibodies combined with an HRP-conjugated second antibody were used for protein detection. GAPDH was detected in treated and untreated HEK293T cells. The pAAV treated HEK293T cells showed GFP expression, while SFRP5 expression was only detected in HEK293T cells transfected with pAAV-SFRP5.

These results demonstrate successful overexpression of GFP and SFRP5 on the transcriptional and protein level by plasmid transfection of HEK293T cells. Therefore, the overexpression system was applied to the hiPSC-CMs using AAV serotype 6.

3.2.2   Establishment of AAV6-mediated gene transfer: overexpression of candidate genes in hiPSC-CMs

After validation of the overexpression in HEK293T cells, the overexpression system was applied to hiPSC-CMs. In order to establish the AAV6 gene transfer protocol, hiPSC-CMs were incubated three times with AAV6 (MOI = 10^5) for 48 hours consecutively. However, after long-term virus treatment with AAV-Basic (Control^{OE}) and AAV-SFRP5 (SFRP5^{OE}) most of the cells lost their beating ability. Transcriptional expression analysis via qPCR displayed a lower expression of the cardiac marker cardiac troponin T (cTnT) in Control^{OE} and SFRP5^{OE} hiPSC-CMs compared to untreated hiPSC-CMs (figure A.1). This finding points towards a significant stress response of the hiPSC-CMs after extensive exposure to AAV6.

Therefore, the transduction times and direct virus exposure time was reduced to a single transduction with the same MOI of AAV6 (MOI = 10^5) for 72 hours. Under these conditions, cTnT expression of Control^{OE} and SFRP5^{OE} hiPSC-CMs was unchanged compared to the untreated hiPSC-CMs (figure A.2C, conducted by Dr. W. Tahir, Department of Cardiology and Pneumology, UMG). Via confocal microscopy the regular sarcomere structure was confirmed with α-actinin immunofluorescence staining (figure A.2A) indicating that the AAV transfection itself had no acute influence on cardiomyocyte quality. Consequently, viral transduction induced background effects, which might lead to misguided conclusions, can be reduced by single transduction.

The transduction efficiency of AAV-Basic was validated by flow cytometry. The direct cell fluorescence of the reporter gene GFP at 488 nm was used for detecting successfully transduced hiPSC-CMs in flow cytometry analysis. The results displayed a good transduction efficiency of approximately 99 % GFP$^+$ cells 14 days after AAV-Basic

transduction (figure 8A), indicating a robust and stable gene expression after virus treatment at least until day 14. Quantitative analysis of Anti-α-actinin immunostained hiPSC-CMs via flow cytometry (figure 8B) displayed a ≥ 99 % purity of cardiomyocyte culture. Because of the metabolic purification strategy, the culture contains ≥ 99 % cardiomyocytes. Thus, a ubiquitous CMV-promotor could be used for the AAV-mediated overexpression and consequently, resulting effects are most likely only cardiomyocyte related.
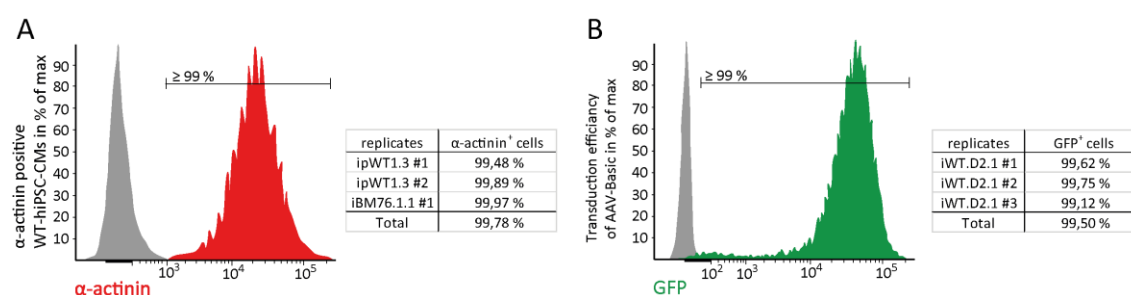

Figure 8: Transduction efficiency of AAV-Basic treated hiPSC-CMs. To quantify the transduction efficiency of AAV6, FACS analysis of AAV-Basic transduced hiPSC-CMs was performed and compared to untreated hiPSC-CMs. A FACS graph example of analyzed GFP⁺ and α-actinin⁺-hiPSC-CM is shown in the figure, respectively. **(A)** To validate cardiomyocyte quality, hiPSC-CMs were fixed and immunostained with Hoechst 1:1000 and Anti-α-actinin 1:1000 (secondary antibody Alexa Fluor 488 Anti-mouse 1:500). Negative control (grey) was incubated only with Hoechst. Flow cytometric analysis displayed a mean of over 99 % α-actinin positive cells (red) in two different hiPSC-CM lines (n = 2). **(B)** Cells were fixed and prepared for FACS analysis as described in 2.2.3.2. At day 14 after transduction, over 99 % of hiPSC-CMs transfected with AAV-Basic were positive for GFP (green).

To confirm and quantify the SFRP5 overexpression, SFRP5^{OE} and Control^{OE} hiPSC-CMs were analyzed on transcriptional and protein level. SFRP5 expression was highly increased (approximately 40,000-fold) in SFRP5^{OE} hiPSC-CMs compared to Control^{OE} hiPSC-CMs (validated via qPCR and western blot, figure 9). In addition, the GFP expression was validated on the protein level showing a higher protein abundance in Control^{OE} compared to SFRP5^{OE} hiPSC-CMs.
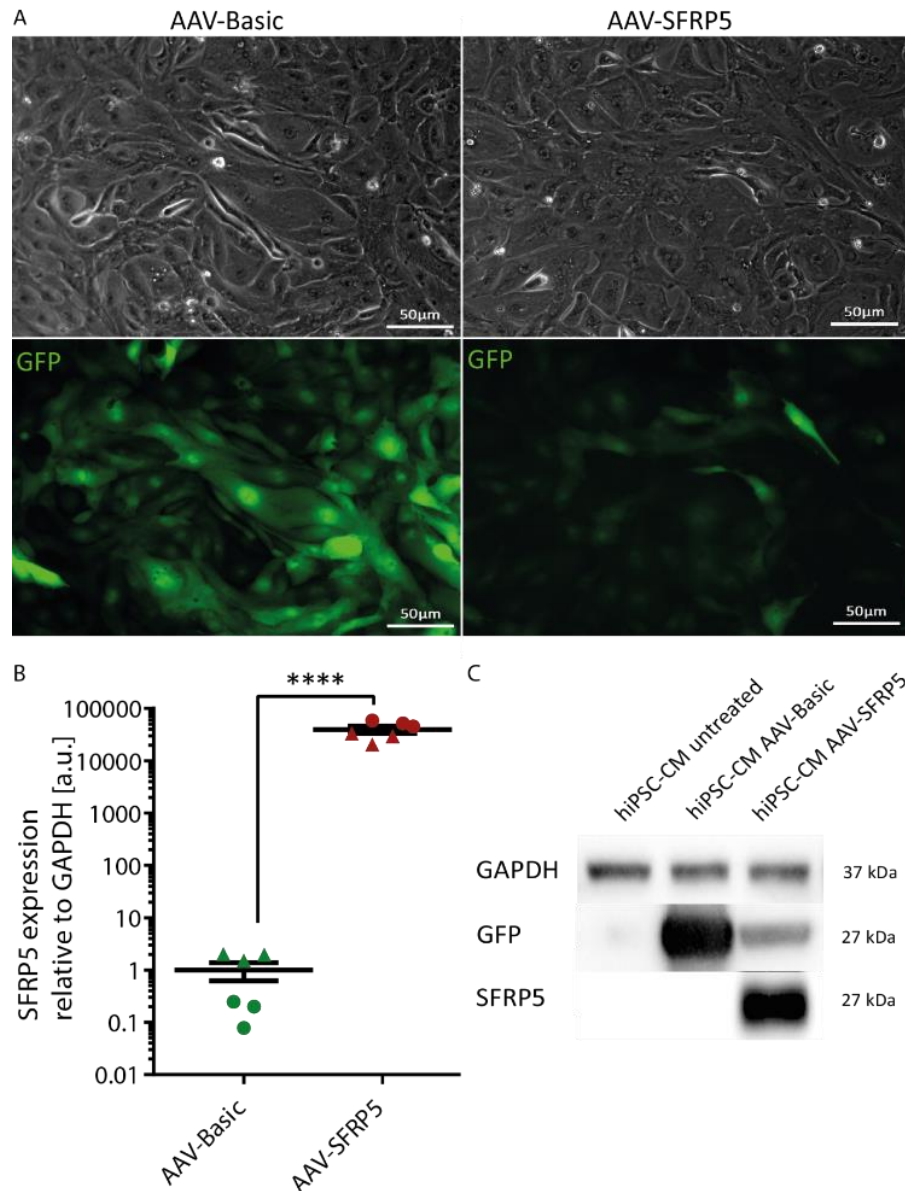
Figure 9: SFRP5 overexpression in hiPSC-CMs. hiPSC-CMs were transduced with AAV-Basic and AAV-SFRP5 (MOI = 10^5) as described in 2.2.4. 14 days after transduction, cells were pelleted for analysis on transcriptional and protein level. **(A)** Fluorescence images detecting GFP expression were taken 10 days after transduction. Control[OE] hiPSC-CMs showed a stronger GFP fluorescence compared to SFRP5[OE] hiPSC-CMs. **(B)** On the transcriptional level SFRP5 overexpression was determined by qPCR showing a significant overexpression (approximately 40,000-fold) of SFRP5[OE] hiPSC-CMs compared to Control[OE] (housekeeping gene GAPDH). Data are presented as mean ± SEM. ****P < 0.0001 unpaired, two-tailed t-test. **(C)** On the protein level GFP and SFRP5 expression was examined in untreated, Control[OE] and SFRP5[OE] hiPSC-CMs. GFP protein expression (Anti-GFP, ab290) was detected in both Control[OE] and SFRP5[OE] hiPSC-CMs, whereas Control[OE] hiPSC-CMs show a higher GFP protein amount compared to SFRP5[OE] hiPSC-CMs. SFRP5 (Anti-SFRP5, sc-374397) was only detected in SFRP5[OE] hiPSC-CMs.

To confirm cardiomyocyte quality, two-month-old hiPSC-CMs were treated with AAV-Basic or AAV-SFRP5 according to the transduction protocol established before (see 2.2.4). After two weeks additional culturing, cells were stained with Anti-α-actinin and

Anti-GFP antibodies to examine the sarcomere structure of transduced hiPSC-CMs. Confocal images confirmed a regular sarcomere structure of Control[OE] and SFRP5[OE] hiPSC-CMs (figure 10).
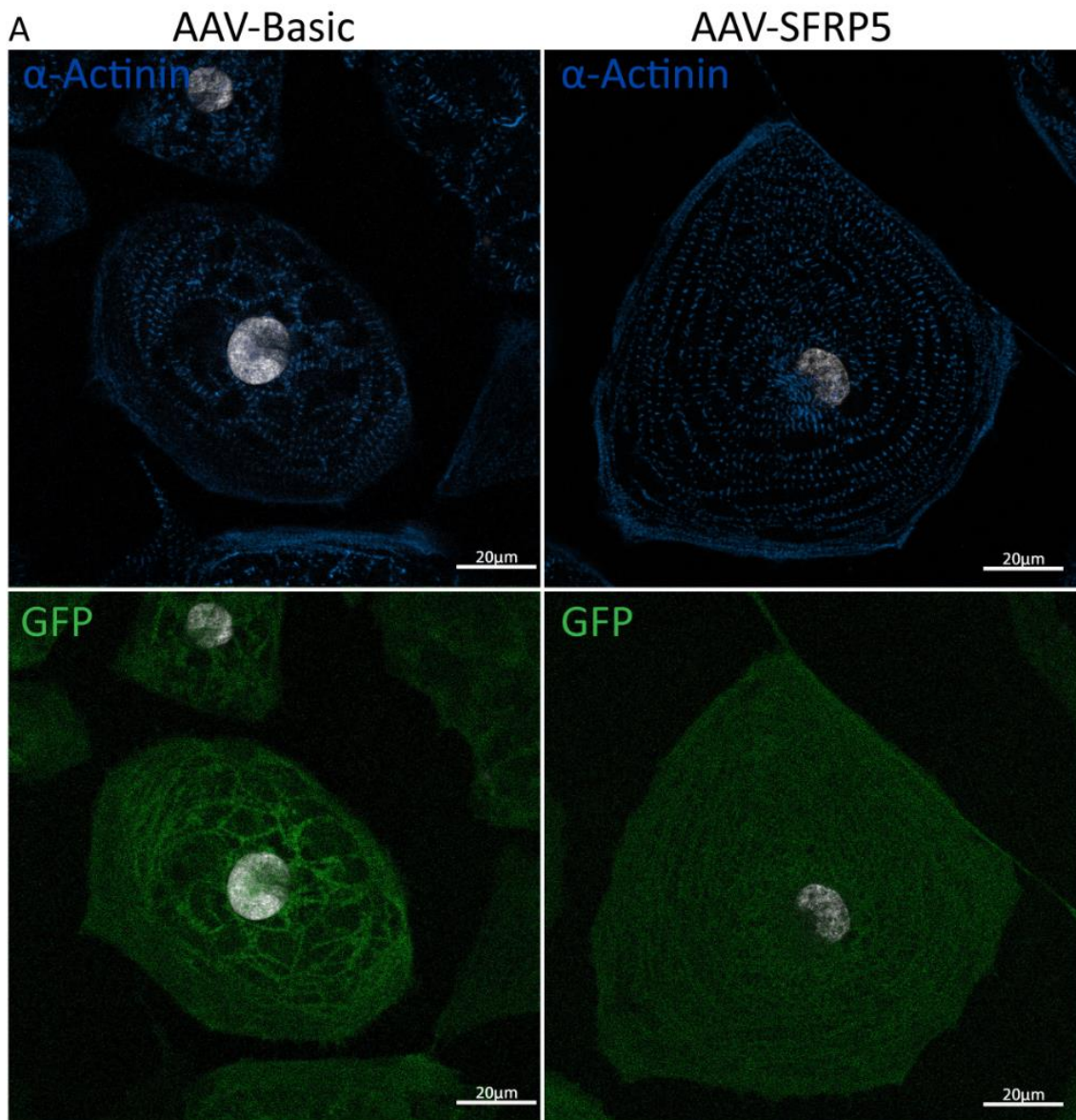
Figure 10: Fluorescence images of Control[OE] and SFRP5[OE] hiPSC-CMs. Two-month-old hiPSC-CMs were treated with AAV-Basic or AAV-SFRP5 according to transduction protocol in 2.2.4 and subsequently fixed and stained with Anti-α-actinin (1:1000) and Anti-GFP (1:1000), displaying organized sarcomere structure.

In summary, the AAV6 overexpression system was successfully applied to hiPSC-CMs, allowing to investigate the molecular and functional consequences of SFRP5 overexpression in human CMs.

3.2.3   Next generation sequencing of SFRP5 overexpressing hiPSC-CMs

To analyze the function of SFRP5 in human cardiomyocytes, mRNA-seq of SFRP5[OE] and Control[OE] hiPSC-CMs were performed in cooperation with NGS-facility for Integrative Genomics, University Medical Center Göttingen. An RNA sequencing screen led to the identification of downstream effects, affected pathways, and networks altered due to the AAV-mediated SFRP5 overexpression in hiPSC-CMs.

Gene expression variability between SFRP5[OE] (indicated as "treatment") and Control[OE] (indicated as "control") hiPSC-CM samples are represented in a principal component analysis (PCA)-plot (figure 11). As replicates of treatment and control demonstrate low variation within their groups, highly differential gene expression is displayed between control and treatment groups. The differential expression analysis identified 2722 genes (adjusted p-value < 0.05, log2 fold change > 0.95/ < - 0.95). From these differentially expressed genes, 1220 genes were significantly upregulated, while 1502 genes were significantly downregulated. Among the most significantly regulated genes, SFRP5 was identified as the most significant and highest upregulated candidate, as expected due to successful AAV-mediated overexpression.

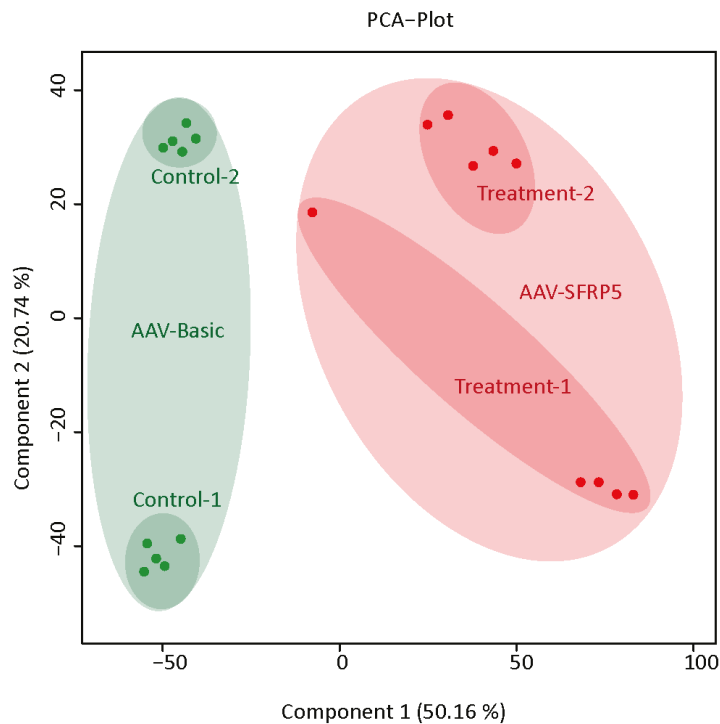**Figure 11: PCA-plot and heat map of the mRNA-seq screen.** WT-hiPSC-CM lines iBM76.1 (group-1) and iWT.D2 (group-2) with five technical replicates per cell line were used for this analysis. AAV-transduction was performed according to the protocol in 2.2.4. Control[OE] is indicated as "control" and SFRP5[OE] hiPSC-CMs are indicated as "treatment". **(A)** The PCA-plot of component 1 (50.16 %) versus component 2 (20.74

%), illustrates differential gene expression between control replicates at -50 of component 1 and treatment replicates clustering at approximately 0-100 of component 1. Low expression variabilities were observed between replicates within the respective groups. Analysis was done by Orr Shomroni and illustration was created by Dr. Sara Klas, Department of Cardiology and Pneumology, UMG.

In order to identify the underlying pathways affected upon SFRP5 expression, a network enrichment analysis of the 2722 significantly differentially expressed genes was performed using Cytoscape2.2.7 (figure 12A). Network enrichment analysis displayed significant regulation of calcium handling pathways, cardiac contraction, and apoptosis (figure 12A). In a second network enrichment analysis, up- and downregulated pathways were separated into single clusters, demonstrating downregulation of "muscle contraction" pathways and upregulation of apoptosis and ER stress (figure 12B). Therefore, we focused our further analysis on cardiac contraction regulation and intrinsic apoptotic signaling pathways in response to ER stress by ClueGO and the KEGG database.
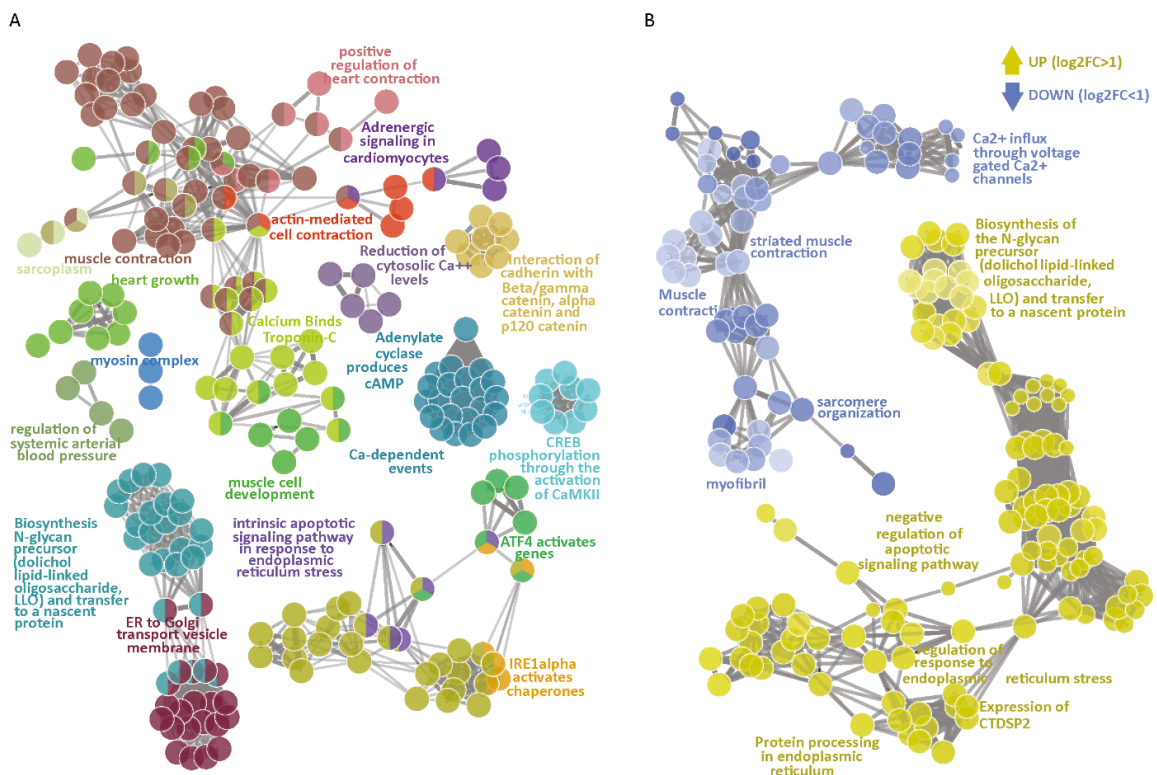
Figure 12: Network enrichment analysis of the mRNA-seq screen. The mRNA-seq screen identified 2722 differentially expressed genes (log2 fold change > 0.95 and adjusted p-value < 0.05) clustered in a network enrichment analysis. Single node colors in **(A)** represent the pathways grouped in one specific cluster. The node size indicates the significance of the pathways (% of associated genes regulated in the single pathways and their interactions). The network of up- and downregulated genes are displayed in **(A)**, identifying regulated pathway networks in heart contraction, apoptosis, and vesicle transport. **(B)** Separated networks of up- or downregulated genes (log2 fold change > 0.95 and adjusted p-value < 0.05)

highlight expression tendencies of affected pathways. Upregulated genes are involved in negative regulation of apoptosis, regulation of response to ER stress and protein processing in the ER. Downregulated pathways include calcium (Ca) influx through voltage gated calcium channels, muscle contraction and sarcomere organization. Illustration and analysis were performed by Dr. Sara Klas, Department of Cardiology and Pneumology, UMG.

The cardiac contraction pathway is significantly downregulated in SFRP5^{OE} hiPSC-CMs. Subunits of LTCC regulating calcium influx and pore formation (associated genes: *CACNA1c*, *CACNA1b*, *CACNB2*) were downregulated, while the LTCC subunit γ4 (associated gene: *CACNG4*) was upregulated. Additionaly, *RYR2* was downregulated as well as the crossbridging proteins cTnT (associated gene: *TNNT2*), actinin (associated gene: *ACTC1*) and Myosin (associated genes: *MYH6/7*, *MYL4*). Further regulated genes identified in the screen are the downregulated *STRIP2* and upregulated PKCε (associated gene: *PRKCE)*.

The WNT inhibitor SFRP5 and DKK (associated gene: *DKK1, DKK4*) were upregulated in this screen. In contrast, *WNT5A* and its downstream targets PLC (associated gene: *PLCB2*), CAMKII (associated gene: *CAMK2A*) and calmodulin (associated gene: *CAML3*) were downregulated. Furthermore, sodium-protone exchanger, NKA α-subunit's catalytic domain (associated genes: *ATP1A2*, *ATP1A4*) and a part of plasma membrane bound β-subunit (associated gene: *ATP1B4*) were upregulated, whereas *ATP1B2* and *FXYD2* were downregulated.
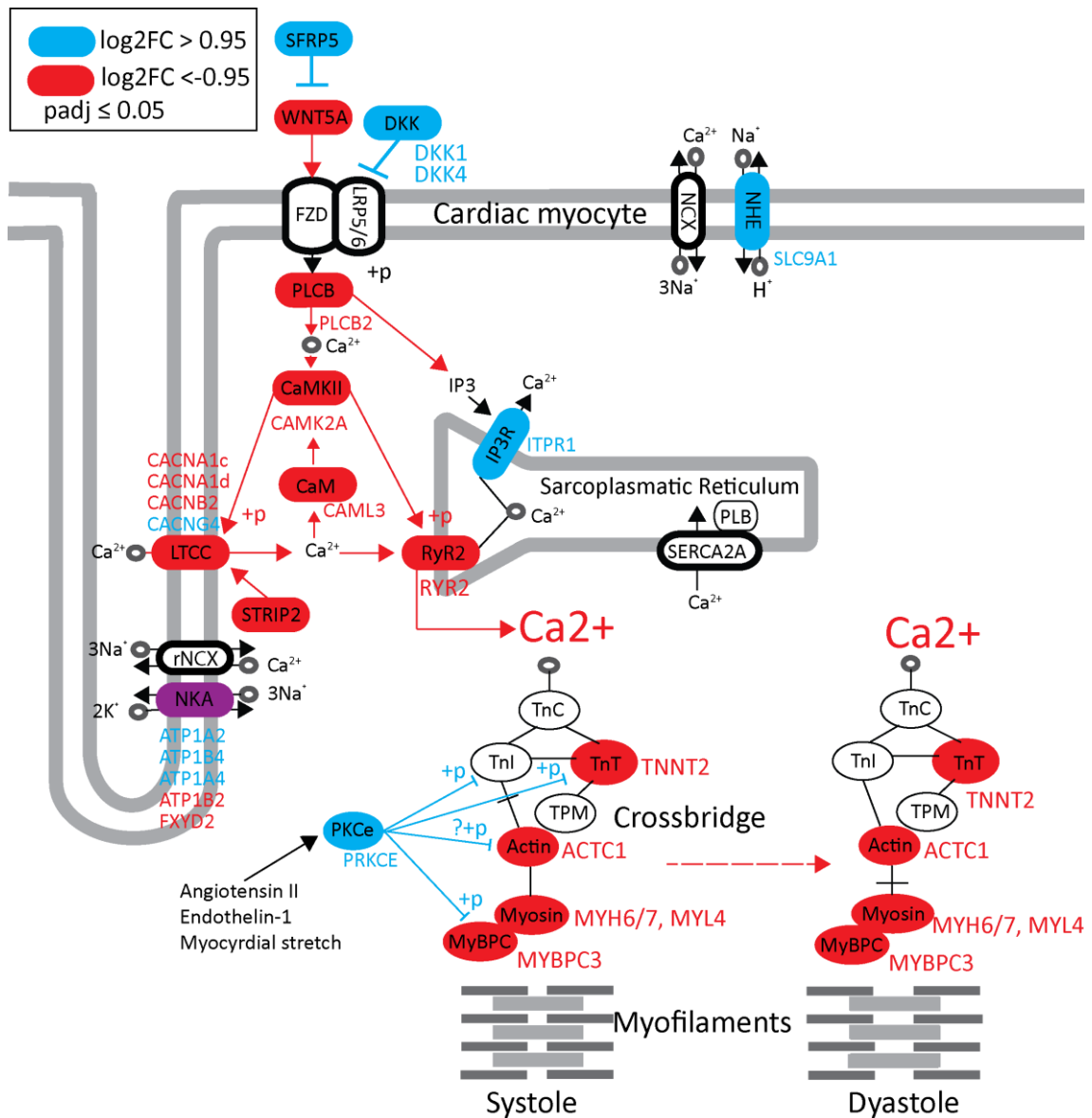
Figure 13: Analysis of cardiac contraction and its connection to WNT signaling pathway changes. Calcium channels, contractile filaments and ATP dependent calcium pumps are involved in cardiomyocyte contraction. Upregulated genes (adjusted p-value < 0.05, Log2 fold change > 0.95) are indicated in red, downregulated genes adjusted p-value < 0.05, Log2 fold change < - 0.95) are indicated in blue. SFRP5[OE] hiPSC-CMs displayed significant downregulation of calcium channel LTCC (associated genes: *CACNA1c*, *CACNA1d*, *CACNB2*), *STRIP2*, *RYR2* as well as contraction filaments actinin (associated gene: *ACTC1*), Myosin (associated genes: *MYH6/7*, *MYL4*), TnT (associated gene: *TNNT2*) and additionally PRKCε (associated gene: *PRKCE*). ATP dependent calcium pump *SERCA2A* and *NCX* were not regulated. *SFRP5* and DKK (associated gene: *DKK1*, *DKK4*) were upregulated. *WNT5A* and its downstream targets phospholipase C (PLC; associated gene: *PLCB2*), CAMKII (associated gene: *CAMK2A*) and calmodulin (CaM; associated gene: *CAML3*) were downregulated. Furthermore, sodium-potassium ATPase α-catalytic domain (associated genes: *ATP1A2* and *4*) and the *ATP1B4* gene of the membrane-bound β-domain were upregulated, whereas *ATP1B2* and *FXYD2* were downregulated. The sodium-protone exchanger (NHE) and IP3R (associated gene: *ITPR1*) expression were elevated (associted gene: *SLC9A1*).

The significant upregulation of *SFRP5* in the mRNA-seq screening was confirmed by qPCR analysis (figure 14A-B). Furthermore, promising downstream candidates identified in the mRNA-seq were further validated by qPCR. *WNT5A* is a known direct target of SFRP5 which was downregulated in the mRNA-seq, as expected from the literature. Additionally, differentially regulated genes involved in calcium handling like *CACNB2*, coding for LTCC, and *RYR2* were transcriptionally validated by qPCR analysis. In line with the mRNA-seq data, qPCR analysis verified the significantly downregulated expression of *WNT5A, RYR2* and *CACNB2* in SFRP5[OE] hiPSC-CMs compared to the Control[OE] (figure 14C-H).
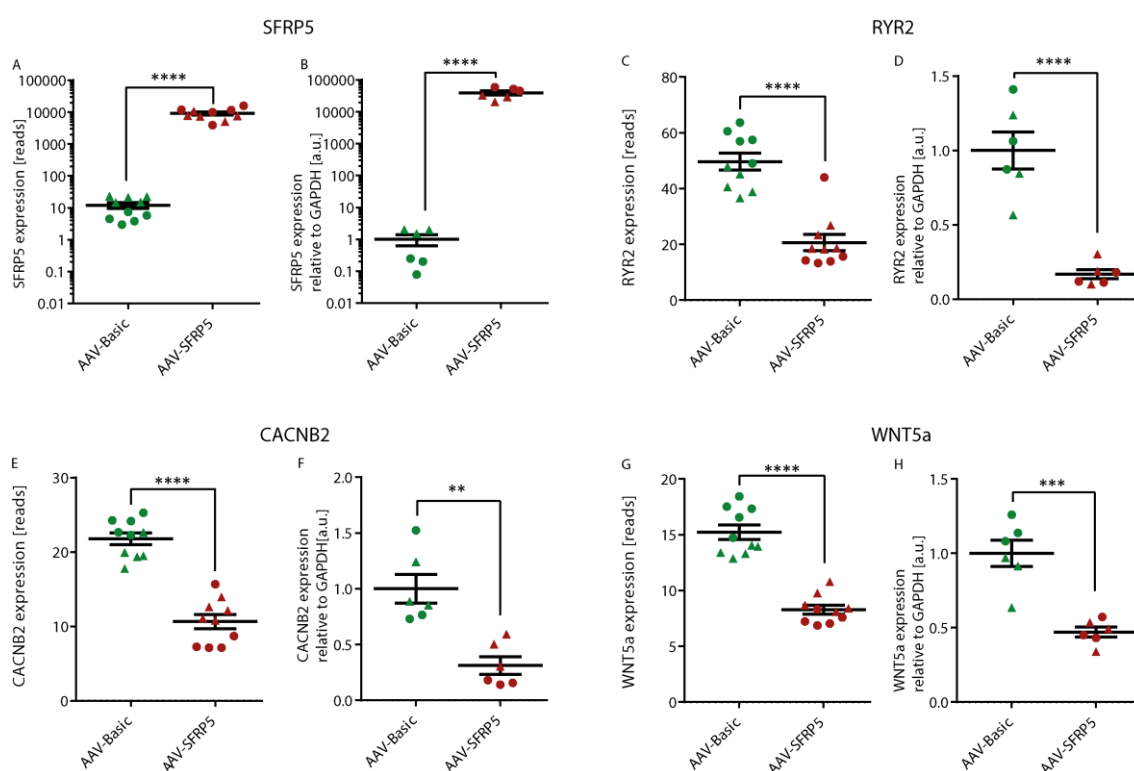
Figure 14: Promising functional downstream candidates identified in the mRNA-seq were further validated by qPCR. *SFRP5* was significantly upregulated in the mRNA-seq data set and by qPCR analysis in SFRP5[OE] hiPSC-CMs compared to Control[OE]. *WNT5A*, *RYR2* and *CACNB2* were significantly downregulated in the mRNA-seq screen of SFRP5[OE] hiPSC-CMs, which was confirmed by qPCR. Data represent means ± SEMs, ***P < 0.001 and ****P < 0.0001 was determined by unpaired, two-tailed t-test.

Besides pathways involved in cardiac contraction, pro- and anti-apoptotic pathways were also regulated in the mRNA-seq data set of SFRP5[OE] hiPSC-CMs. Pro-apoptotic genes involved in ER stress response, TNF- and canonical WNT pathway were upregulated, whereas also anti-apoptotic protein transcription was elevated. In detail, genes involved in ER stress response were significantly upregulated: IRE1α (associated

gene: *ERN1*), *FOS*, BIM (associated gene: *BCL2L11*), PERK (associated gene: *EIF2AK3*), *ATF-4*, CHOP (associated gene: *DDIT3*). Moreover, the transcription of the pro-apoptotic TNF-pathway members *TRADD*, CREB (associated genes: *CREB3L1*, *CREB3L4*, *ATF4*) and c/EBPβ (associated gene:*CEBP*) was elevated. Additionaly, the canonical pro-apoptic WNT-pathway was upregulated in the mRNA-seq screen, in detail via *WNT16*, TCF/LEF (asscociated gene: *LEF1*), *c-Myc* and caspase 8 (CASP8) transcriptional upregulation, together with Idax (associated gene: *CXXC4*) and c-FLIP (associated gene: *CFLAR*) downregulation. The expression of anti-apoptotic BCL-2 (associated gene: *BCL2*), BCL-XL (associated gene: *BCL2L11*), *HAX1* and *ATF-5* was also upregulated. Less pro-apoptotic stimulus was driven due to cathepsin (associated gene: *CTSS*) and JNK (associated gene: *MAPK10*) downregulation. The common distal pathway of apoptosis by cytochrome c (CytC), APAF-1, pro-caspase 9 (ProCASP9) forming the apoptosome activating the effector caspase 9 (CASP9), 6 and 7 (CASP6/7) were not regulated in this screen.

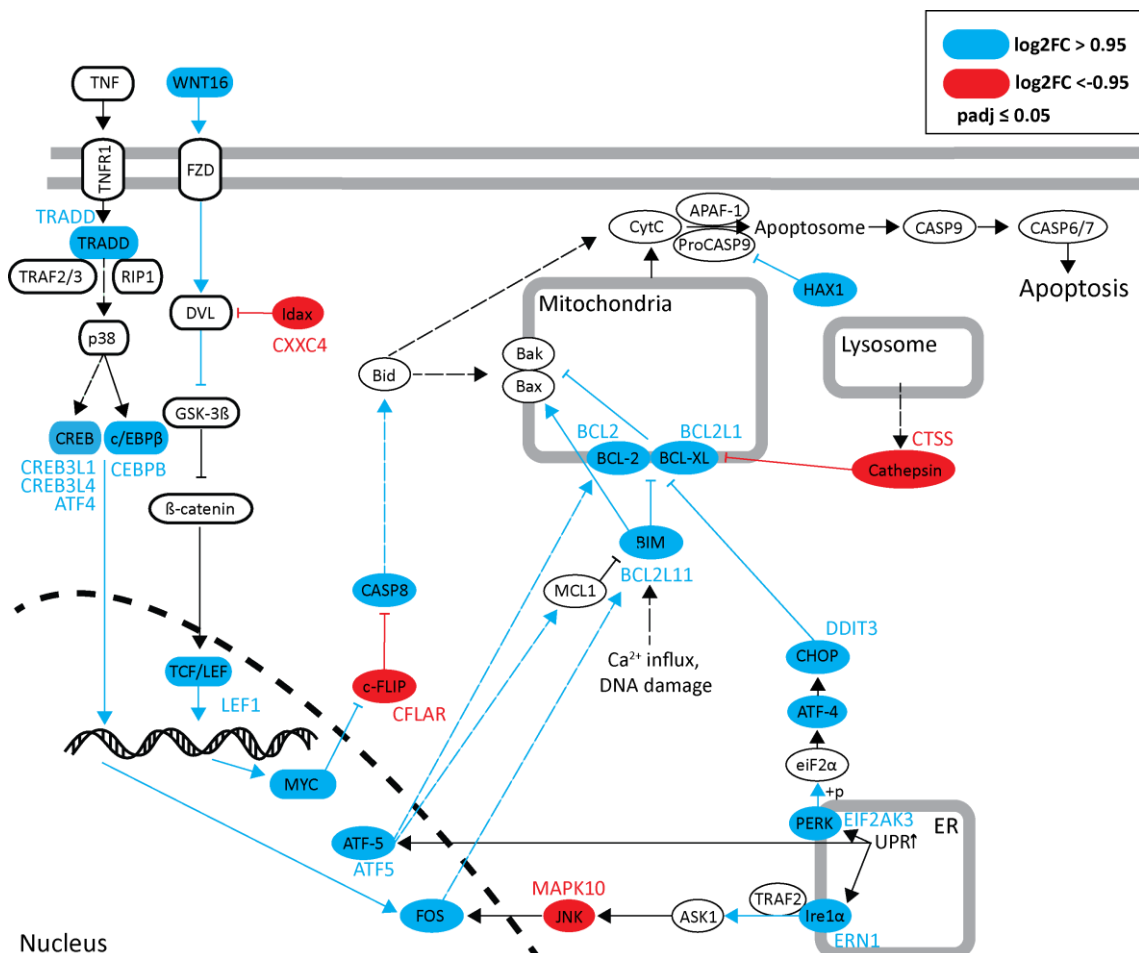**Figure 15: Analysis of intrinsic apoptotic pathway regulation in the mRNA-seq screen.** Differentially expressed genes in SFRP5[OE] hiPSC-CMs are involved in the apoptosis pathway. Upregulated genes (adjusted p-value < 0.05, Log2 fold change > 0.95) are indicated in red, downregulated genes (adjusted p-value < 0.05, Log2 fold change <-0.95) are indicated in blue. Pro-apoptotic ER stress response and TNF

pathway members IRE1α (associated gene: *ERN1*), *FOS*, *TRADD*, CREB (associated genes: *CREB3L1*, *CREB3L4*, *ATF4*), c/EBPβ (associated gene: *CEBPB*) and BIM (associated gene *BCL2L11*) together with PERK (associated gene: *EIF2AK3*), ATF-4 and CHOP (associated gene: *DDIT3*) were upregulated whereas cathepsin (associated gene: *CTSS*) was downregulated. Canonical WNT pathway members *WNT16*, TCF/LEF (associated gene *LEF1*), MYC and pro-apoptotic CASP 8 (associated gene: *CASP8*) were upregulated, together with Idax (associated gene: *CXXC4*), and c-FLIP (associated gene: *CFLAR*) downregulation. mRNA expression of anti-apoptotic *ATF5*, BCL-2 (associated gene: *BCL2*), BCL-XL (associated gene: *BCL2L11*) and *HAX1* were elevated. The common distal pathway of apoptosis by cytochrome C (CytC), APAF-1, pro-caspase 9 (ProCASP9) forming apoptosome and activating effector caspase 9 (CASP9), caspase 6 and 7 (CASP6/7) was not regulated in the screen.

In conclusion, mRNA-seq of SRFP5^{OE} hiPSC-CMs revealed a downregulation of cardiac calcium channels, contractile filaments and WNT5A-mediated signaling. Moreover apoptosis related genes were differentially expressed in SFRP5^{OE} hiPSC-CMs compared to the Control^{OE}.

3.2.4   Functional analysis: Calcium imaging

Calcium handling is a crucial component for proper cardiomyocyte function. The mRNA-seq of SFRP5^{OE} hiPSC-CMs revealed differentially regulated genes involved in cardiomyocyte contraction and calcium handling. Consequently, fluorescence based confocal calcium imaging of SFRP5^{OE} and Control^{OE} hiPSC-CMs was performed to investigate the role of SFRP5 on calcium cycling in more detail.

For recording SFRP5^{OE} and Control^{OE}, hiPSC-CMs were loaded with calcium indicator Rhod-2 AM to display cytosolic calcium cycling changes during cardiac contraction. The intensity of calcium indicator Rhod-2 AM was recorded as a function of time. Calcium cycling during cardiomyocyte contraction was displayed as calcium transient, and local calcium accumulation by spontaneous opening of RYR2 was analyzed as calcium sparks. Cells were field stimulated with 0.25 Hz in order to eliminate calcium kinetic aberrations depending on beating frequency. In calcium transient analysis the subsequent parameters were analyzed: the time for calcium upstroke (described as rise time), the intensity of maximum calcium concentration in the cytosol (described as amplitude) and the calcium decrease until 50% of the amplitude, either due to SR reuptake or efflux to extracellular space (described as decay 50). Calcium sparks were recorded and analyzed during diastole. Spark parameter were analyzed focusing on calcium spark frequency, spark size (sum of full width, full duration, and amplitude) and calcium leak (the sum of

all spark sizes). Furthermore, β-adrenergic stimulation via isoprenaline hydrochloride (iso, 100 nM) was used for stress induction in hiPSC-CMs after measurements at basal condition.

SFRP5^{OE} hiPSC-CMs revealed a significant reduction in calcium transients' amplitude, a faster rise time, and a faster calcium decay 50 under basal condition. After inotropic stimulation with iso, SFRP5^{OE+iso} compared to Control^{OE+iso} hiPSC-CMs revealed equal parameter changes as observed unter basal conditions. A significant reduction in all three parameters was also observed in SFRP5^{OE+iso} compared to SFRP5^{OE} hiPSC-CMs, whereas only calcium transient rise time and decay 50 were reduced between Control^{OE+iso} and Control^{OE} hiPSC-CMs (figure 16A-C). Exemplary recorded calcium transients are demonstrated in figure 16D which outlines the reduced amplitude, the faster rise time and the shorter calcium decay 50 in SFRP5^{OE} compared to Control^{OE} hiPSC-CMs under basal conditions.
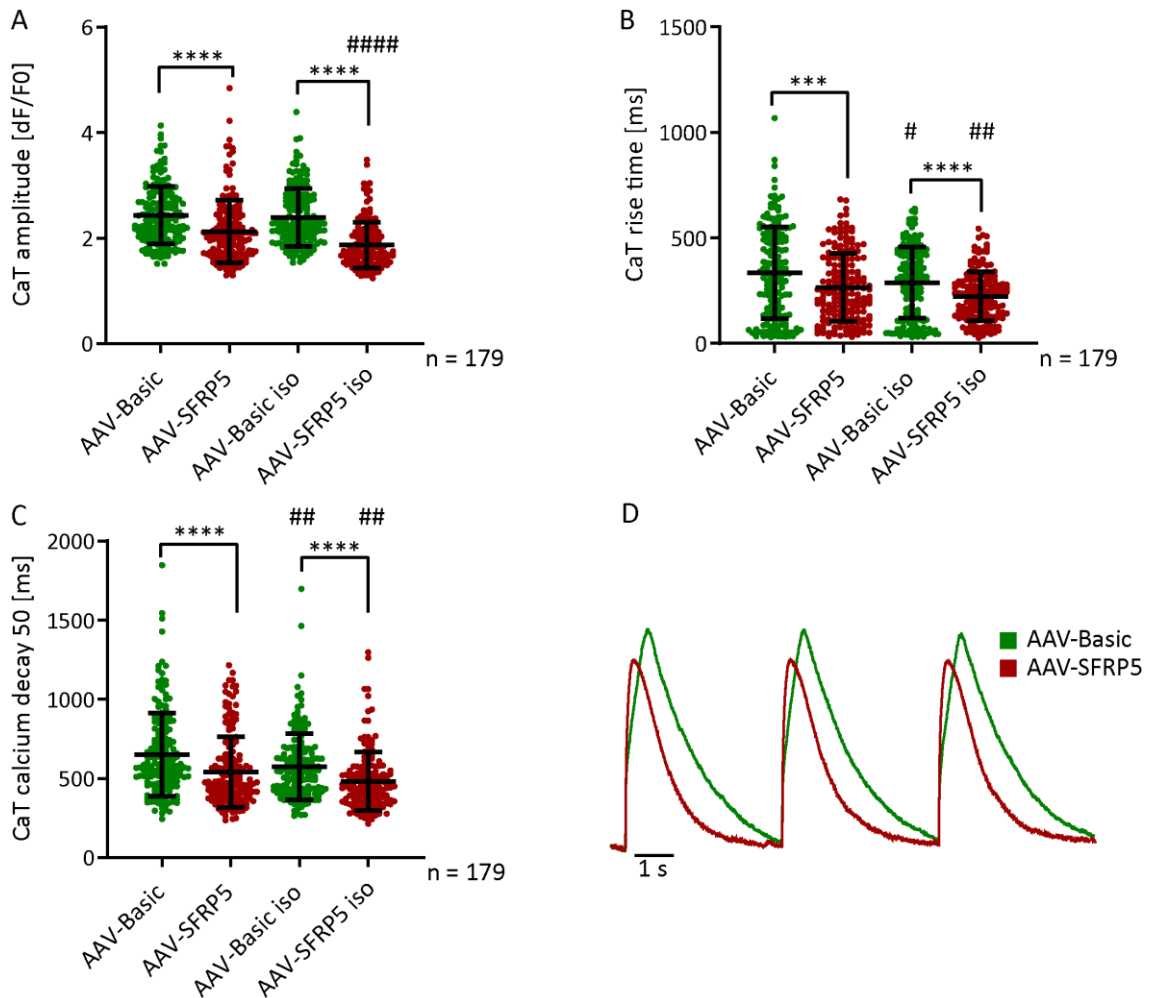
Figure 16: Calcium transient analysis of AAV-treated hiPSC-CMs. Cytosolic calcium cycling during cardiomyocyte contraction of SFRP5[OE] and Control[OE] hiPSC-CMs was recorded by confocal line scan mode. Human iPSC-CMs were loaded with Rhod-2 AM and paced at 0.25 Hz. Incubation with isoprenaline hydrochloride (iso, 100 nM) was used for positive inotropic stimulation. Calcium transients were analyzed using ImageJ by plotting the mean signal intensity as a function of time (2.2.8). **(A, B)** Quantitative analysis of calcium transients displayed lower amplitude **(A)** and faster rise time **(B)** of SFRP5[OE] hiPSC-CMs under basal condition and after iso incubation. **(C)** Time for calcium decay at 50 % of the amplitude is significantly reduced in SFRP5[OE] hiPSC-CMs under all conditions. Exemplary calcium transients under basal conditions are shown in **D**. Data are presented as mean ± SD. #$P < 0.05$, ##$P < 0.01$, ###$P < 0.001$, ****/####$P < 0.0001$ determined by unpaired, two-tailed t-test. * compared to AAV-Basic, # compared to basal condition.

Besides significant alterations in the calcium transients of SFRP5[OE] hiPSC-CMs, only small changes in calcium sparks were observed. An exemplary record of calcium sparks and their 3D surface plot of Control[OE] and SFRP5[OE] hiPSC-CMs is shown in figure 17A and B. Although, slight differences in various calcium spark parameters (frequency, full duration, full width, time to peak shown in figure 17C, F, G, I) were observed between the groups, the overall calcium leak (figure 17E), as the sum auf all sparks, was not significantly changed between SFRP5[OE] and Control[OE] under basal conditions. However,

in iso stimulated cells, a reduction in the calcium leak was observed in SFRP5[OE+iso] compared to Control[OE+iso] hiPSC-CMs.

Figure 17: Calcium spark analysis of AAV-treated hiPSC-CMs. Spontaneous calcium release of RYR2, also known as calcium sparks, were recorded in the diastole of cardiomyocyte contraction. SFRP5[OE] and

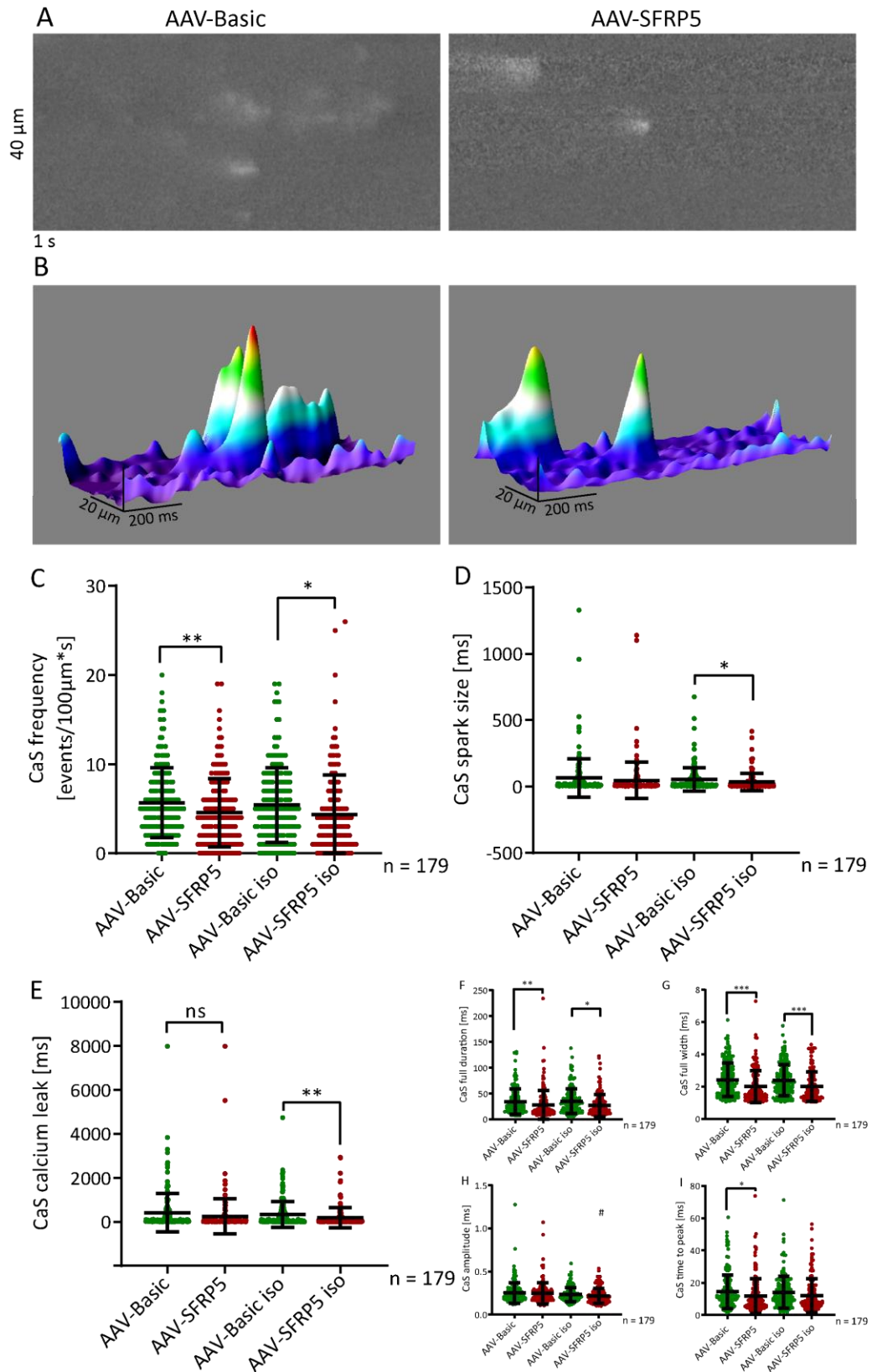Control^{OE} hiPSC-CMs were seeded on glass cover slips and analyzed 12-14 days after transduction. For cytosolic calcium imaging hiPSC-CMs were loaded with Rhod-2 AM, paced at 0.25 Hz and analyzed using confocal line scan mode. Three independent differentiations of two SFRP5^{WT} hiPSC lines (iBM76.1 and iWT.D2.1) with n = 179 cells were used for this analysis. To induce positive inotropic stress hiPSC-CMs were incubated with isoprenaline hydrochloride (iso, 100 nM) for 10 min before recording. Calcium spark recordings of SFRP5^{OE} and Control^{OE} hiPSC-CMs are exemplary presented in **(A)** with a corresponding 3D surface plot in **(B)**. Calcium spark recordings were analyzed using the ImageJ plugin "SparkMaster". **(C-G)** Quantitative analysis of calcium spark parameters are shown in **(C-I)**. **(C)** Calcium spark frequency was significantly reduced in SFRP5^{OE} and SFRP5^{OE+iso} hiPSC-CMS. **(D, E)** The spark size and calcium leak were not reduced under basal conditions but after iso stimulation. **(F, G, H)** Furthermore, spark size parameter full duration and full width were significantly reduced in SFRP5^{OE} and SFRP5^{OE+iso}, whereas spark amplitude was not regulated. **(I)** Calcium spark parameter time to peak was only reduced in SFRP5^{OE} compared to Control^{OE} hiPSC-CMs. There were rarely alterations between the SFRP5^{OE+iso}/SFRP5^{OE} or Control^{OE+iso}/Control^{OE} hiPSC-CMs. Data are presented as mean ± SD. *P < 0.05, **P < 0.01, ***P < 0.001, ****P < 0.0001 and ns > 0.05 were determined by unpaired, two-tailed t-test (C-G). * compared to AAV-Basic, # compared to basal condition.

Concluding, calcium transients analysis revealed a shorter rise time, reduced amplitude and faster calcium reuptake in SFRP5^{OE} and SFRP5^{OE+iso} hiPSC-CMs. The calcium spark frequency was reduced in SFRP5^{OE} and SFRP5^{OE+iso} hiPSC-CMs as well as the calcium leak in SFRP5^{OE+iso} compared to Control^{OE+iso} hiPSC-CMs, whereas other calcium spark parameters were hardly influenced.

3.3 Genome editing by CRISPR/Cas9

Furthermore, the function of SFRP5 was examined in hiPSC-CMs by stably knocking out (KO) these two genes individually using the CRISPR/Cas9 technology. The KO experiments were performed with two different plasmids (table 3) containing two different gRNAs for each candidate gene.

3.3.1 Generation of CRISPR/Cas9-targeted SFRP5^{KO}-hiPSC line

SFRP5^{WT} hiPSC were transfected with the respective CRISPR/Cas9 plasmids via nucleofection. Upon electroporation only a very small amount of the cells became GFP^{+} (figure 18B). Nucleofected cells were sorted by FACS for GFP expression (co-expressed in CRISPR/Cas9 plasmids) and 5-50 GFP^{+} cells were transferred into a 96 well plate 24 hours after nucleofection. Cells were cultured for several days before expansion and cryopreservation. A few hiPSC clones showed an atypical morphology and impaired colony formation indicating loss of their pluripotent state. Therefore, only clones with

stem cell like-morphology were further analyzed on the genomic level for CRISPR/Cas9-mediated editing through PCR-amplifying the region of interest and subsequent Sanger sequencing (SeqLab Göttingen).

Sequencing analysis revealed multiple heterozygously edited as well as mixed clones, most likely due to plating 5-50 cells per well. Since definite discrimination between heterozygous or mixed clones was not possible, the clones were singularized a second time in a new six well plate by limited dilution. Individual clones were picked, expanded, and analyzed on the genomic level. The singularization step was repeated 2-3 times to assure pure colonies. In the end, a successfully purified clone with a complete KO of SFRP5 (SFRP5^{KO}) was chosen for further analysis.
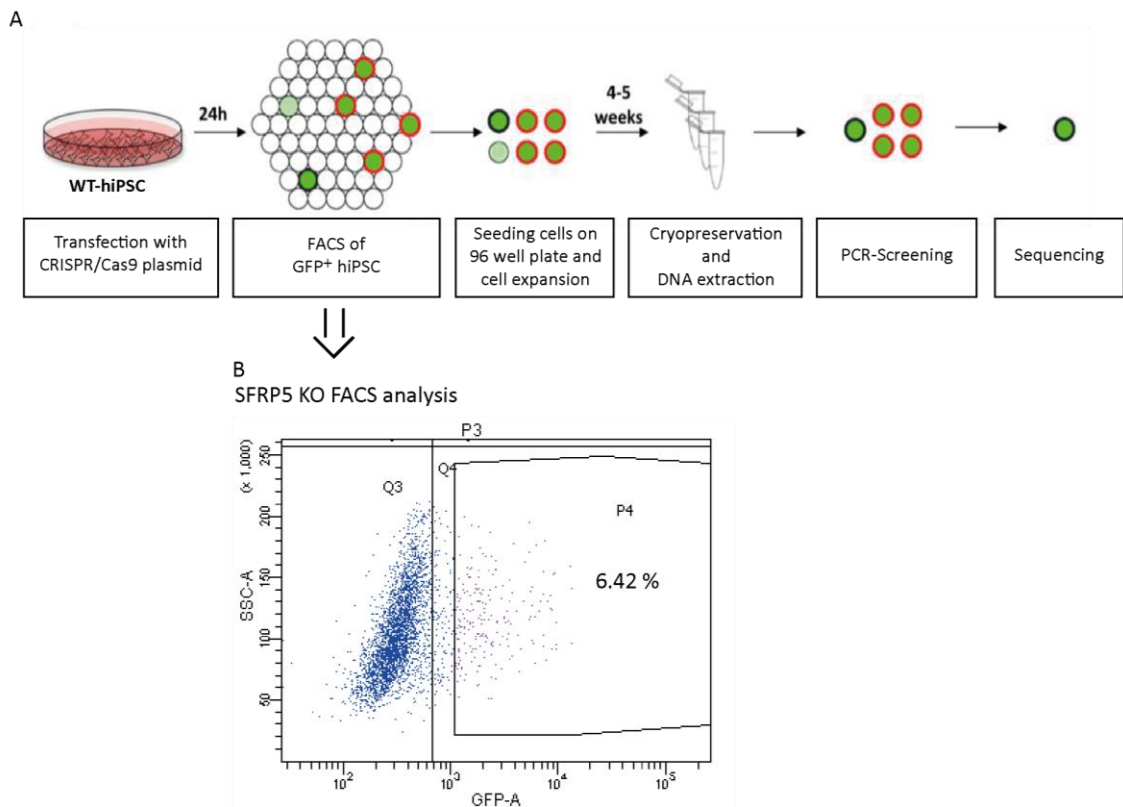
Figure 18: Strategy for genome editing in hiPSCs with clonal derivation. (A) 2x 10^6 SFRP5^{WT} hiPSCs were transfected via electroporation with 2 µg of CRISPR/Cas9 plasmids containing two different gRNAs for the candidate. FACS sorting followed 24 hours after cell transfection and 5-50 GFP$^+$ cells were plated in each well of a 96 well plate using MEF-conditioned StemMACS medium with 1x Pen/Strep, 2 µM TZV and 50 ng/µl bFGF. For cell expansion, cells with stem cell-like morphology were transferred to one well of a Matrigel coated 24 well plate. Cryopreservation and DNA extraction was performed with a confluent well from a 12 well plate. Clones were screened for insertions/deletions on the genomic level via PCR and sequencing of the targeted site. Positive KO clones were selected for further analysis (adapted from Henze 2016). **(B)** FACS sorting was performed in the FACS facility of the UMG. Exemplary FACS dot plot for SFRP5 with 6.42 % transfection efficiency is displayed.

3.3.2 Analysis of SFRP5^{KO} hiPSC and SFRP5^{KO} hiPSC-CMs

The human SFRP5 gene consists of three exons located on chromosome 10. The gRNA target sites are both located in the first exon with 350 bp distance between each other. 33 transfected clones were screened for the potential CRISPR/Cas9-mediated gene KO. Seven of these clones displayed changes in the genomic sequence. For further downstream analysis, one homozygous SFRP5^{KO} clone was determined and used for the further experiments.

The SFRP5^{KO} clone 21 displayed a deletion of 8 bps on both alleles of the genome leading to a frameshift in the mRNA sequence, which generated a premature stop codon at amino acid position 51 of the transcribed protein (figure 19). The complete genomic DNA, mRNA, and protein sequence of SFRP5^{WT} and SFRP5^{KO} is displayed in figure A.3. The purity of the SFRP5^{KO} clone was re-evaluated on the genomic level every four weeks.
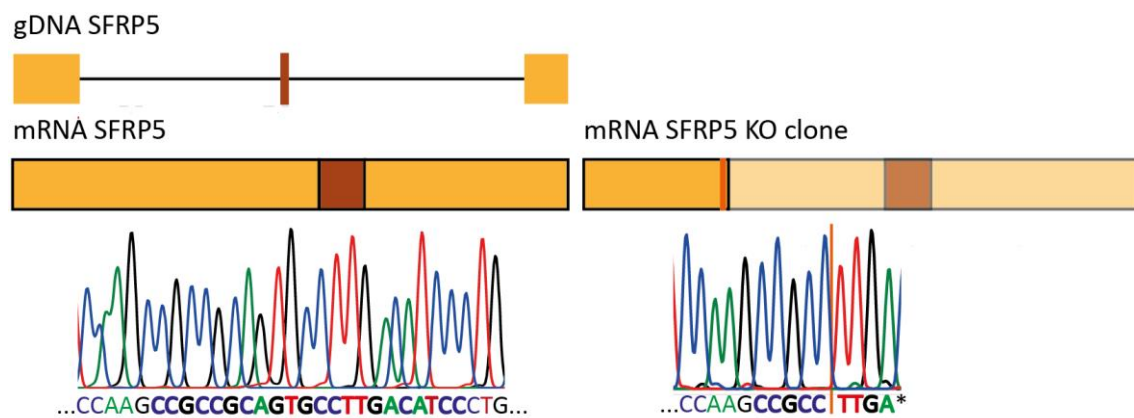
Figure 19: Genomic structure of SFRP5 locus in the SFRP5^{KO} clone 21 around the targeted site. The SFRP5^{WT} gene consists of three exons and is located on chromosome 10. The targeted sequence is shown in bold. A fragment of 8 bps (GCAGTGCC, underlined in the chromatogram of mRNA SFRP5) was deleted in CRISPR targeted site (position is marked with orange line). This leads to a frameshift and a predicted premature stop codon (TGA) in the following coding sequence.

As SFRP5 is not expressed in undifferentiated stem cells, the resulting mRNA sequence of the SFRP5^{KO} clone can only be validated with mRNA isolated from differentiated SFRP5^{KO} hiPSC-CMs. The cardiac differentiation was performed according to the directed differentiation protocol described in 2.2.1.3. The SFRP5^{KO} hiPSC-CMs displayed a comparable differentiation efficiency and contractile properties compared to SFRP5^{WT} hiPSC-CMs. No obvious differences in the organization of sarcomeres were detected in SFRP5^{KO} hiPSC-CMs (figure 20).
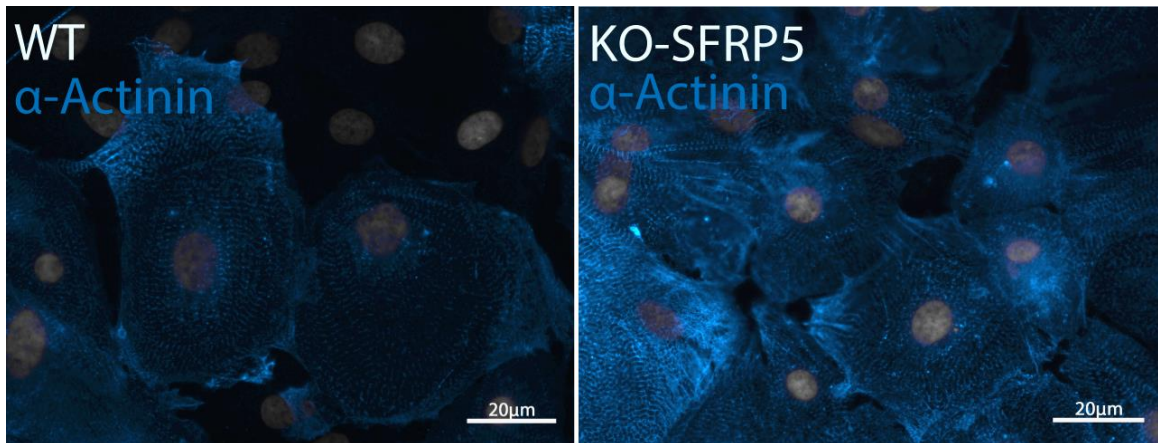
Figure 20: Sarcomere structure of hiPSC-CMs from the SFRP5^{KO} clone 21. SFRP5^{WT} and SFRP5^{KO} hiPSC-CMs were cultured for 60 days and subsequently stained with Hoechst and Anti-α-actinin (blue, 1:1000) revealing an organized sarcomere structure. Images were taken with a fluorescence microscope (Zeiss Axio Imager M2), scale bar: 20 μm.

The SFRP5 KO in the clone 21 was additionally validated on the mRNA level by qPCR. Differentiated SFRP5^{KO} hiPSC-CMs showed a significant reduction of the SFRP5 mRNA expression compared to SFRP5^{WT} hiPSC-CMs (figure 21A). Furthermore, the successful SFRP5 KO was also examined on protein level. Given the low protein expression in SFRP5^{WT} hiPSC-CM, SFRP5 could not be detected by western blot neither in SFRP5^{WT} nor in SFRP5^{KO} hiPSC-CMs. Moreover, SFRP5^{KO} hiPSC-CMs were analyzed for the expression of candidate genes previously identified in RNA sequencing of SFRP5^{OE} hiPSC-CMs. However, CACNB2 (coding for LTCC), RYR2 and WNT5A expression in SFRP5^{KO} hiPSC-CMs showed no significant differences compared to SFRP5^{WT} hiPSC-CMs (figure 21).
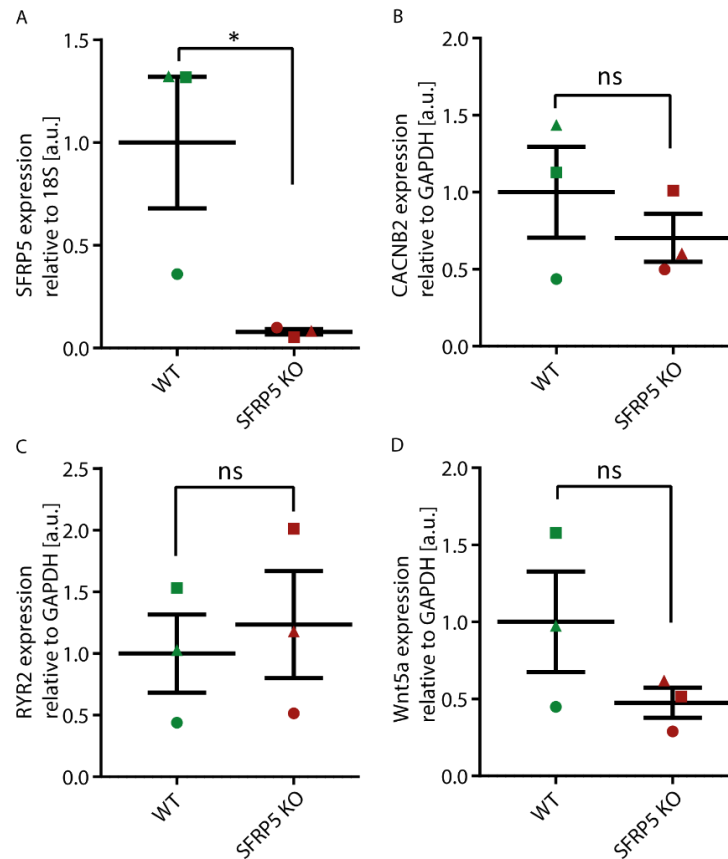
Figure 21: Gene expression analysis in SFRP5KO hiPSC-CMs compared to SFRP5WT hiPSCs-CMs. (A) SFRP5 expression was significantly downregulated in SFRP5[KO] hiPSC-CMs compared to SFRP5[WT] hiPSC-CMs (normalized gene expression to 18S). **(B-D)** CACNB2, RYR2 and Wnt5a expression was not significantly altered in SFRP5[KO] hiPSC-CMs (relative to GAPDH). Three independent differentiations including three technical replicates for the qPCR were analyzed. Triangle, square and circle represent technical replicates. Data are presented as mean ± SEM (**A-D**). [#]P < 0.05 and ns > 0.05 determined by unpaired, two-tailed t-test.

In conclusion, the SFRP5 KO was successfully generated in hiPSC, validated on the genomic level, and further validated in SFRP5[KO] hiPSC-CMs at the transcriptional level by qPCR. The candidate genes from the overexpression data set, found to be differentially expressed in the mRNA-seq screen of SFRP5[OE] hiPSC-CMs, showed no significantly altered expression in the SFRP5[KO] hiPSC-CMs when compared to the SFRP5[WT] hiPSC-CMs. Further analysis could involve calcium imaging at basal level and after stress induction via isoprenaline or angiotensin II, which may reveal opposite changes in calcium handling compared to SFRP5[OE] hiPSC-CMs.

4   Discussion

The differentially regulated candidate SFRP5 was identified in the RNA-seq of aortic stenosis patients in the process of cardiac remodeling. SFRP5 was expressed in healthy donor hearts, then decreased towards CH and was re-expressed in HF. The role of WNT-inhibitor SFRP5 in human cardiomyocytes was examined in two model systems in this thesis: AAV-mediated SFRP5^{OE} and CRISPR/Cas9-mediated SFRP5^{KO} in hiPSC-CMs. mRNA-seq of SFRP5^{OE} hiPSC-CMs identified differentially regulated genes in calcium handling and apoptosis. To validate calcium handling changes in SFRP5^{OE} hiPSC-CMs, functional analysis of calcium transients and calcium sparks was performed, displaying significant alterations in calcium transients, and slight changes in calcium sparks. SFRP5^{KO} hiPSCs were successfully differentiated into SFRP5^{KO} hiPSC-CMs and were further analyzed for differentially expressed candidate genes detected in SFRP5^{OE} hiPSC-CMs beforehand.

4.1   hiPSC-CMs as a human model system

Human iPSC-CMs, obtained by the directed differentiation from hiPSCs, provide a human cardiomyocyte model to study disease mechanisms and protein function *in vitro*.

The cardiac differentiation was performed according to Cyganek et al. (2018). Despite their great advantage of differentiation capacity, hiPSC-CMs represent a heterogeneous cell population of ventricular, atrial and nodal cells, which inherit immature morphological, molecular, structural, metabolic and functional aspects compared to adult rodent ventricular myocytes *in vitro* (reviewed in Yang et al. 2014).

The usage of metabolic selection during cardiac differentiation, first described in Tohyama et al. (2013), enabled an optimization of the protocol yielding in > 99 % of cardiomyocytes in the here applied differentiation, which was quantified via flow cytometry. Further immunostainings with RYR2, α-actinin and Cx43 displayed organized cross-striations, regular sarcomere structures, and cardiac specific cell communication through gap junctions in the here differentiated hiPSC-CMs. Thus, our protocol successfully produced hiPSC-CMs with a very good yield.

4.2   SFRP5 gain of function

As identified in the RNA-seq screen of aortic stenosis patients, SFRP5 is a potentially promising candidate to therapeutically target the transition to HF. Until now, little is known about the function of SFRP5 in human cardiomyocytes. Therefore, a gain of function model via AAV6-mediated SFRP5 overexpression and a loss of function model via CRISPR/Cas9 technique was established to examine its function in hiPSC-CMs. Initially, the overexpression system was successfully evaluated in HEK293T cells using plasmid lipofection. Subsequently it was successfully adapted for the hiPSC-CMs using AAV6 transduction. In hiPSC-CMs an AAV6-mediated transduction was required because plasmid transfection of postmitotic cells, like hiPSC-CMs, is inefficient. Downstream analysis identified differentially regulated apoptosis and calcium handling pathways and uncovered dysregulation of calcium handling in SFRP5^{OE} hiPSC-CMs via mRNA-seq and confocal calcium imaging.

4.2.1   Successful SFRP5 overexpression in HEK293T and hiPSC-CMs

HEK293T cells are a robust and well characterized cell line, which is easily accessible for plasmid transfection by lipofection. In our study HEK293T cells were used to validate a successful overexpression from the vector system at the mRNA and protein level. In HEK293T cells, a transfection efficiency of 50-60 % was observed in cells transfected with either Control^{pOE} or SFRP5^{pOE}. The GFP expression and fluorescence was slightly higher in Control^{pOE} HEK293T cells as shown by fluorescence microscopy and on the protein level by Western blot. These changes might result in a decreased protein expression due to the usage of multi-gene expression system as well as the often described phenomena of negative correlation between transfection efficiency and plasmid size (Kreiss et al. 1999; Hurh et al. 2013). However, SFRP5^{pOE} HEK293T cells displayed adequate GFP luminescence for the validation of the SFRP5 overexpression system. The negligible SFRP5 expression in HEK293T cells described in literature (NCBI 2020) was validated on the mRNA and protein level. Thereby, the measured SFRP5 overexpression appeared to be massive compared to the control.

For hiPSC-CMs, lipofection with plasmids is not efficient, so that the overexpression system must be adapted to hiPSC-CMs. Therefore, a viral mediated system able to transduce these postmitotic cells was established through application of AAV6 viral

particles. Although Rapti et al. (2015) reported the lack of pathogenicity of AAV6-mediated transduction in hiPSC-CMs, in our study we observed a significant downregulation of cTnT, a quality marker for cardiomyocytes, after long term virus treatment (3x MOI = 10^5). After reduction of the initially used triple incubation time to only a single one (1x MOI = 10^5), stable cTnT-expression was observed in Control^{OE} hiPSC-CMs compared to untreated control CMs (figure A.1). This indicates that the optimized AAV transduction condition had no apparent effects on cardiomyocyte quality. Furthermore, the transduction efficiency in Control^{OE} and SFRP5^{OE} hiPSC-CMs differed significantly. Via flow cytometry analysis the transduction efficiency of AAV-Basic was determined as 99 % in hiPSC-CMs, whereas AAV-SFRP5 displayed a lower transduction efficiency and dimmer GFP fluorescence as indicated during visual inspection. These effects may occur due to the multi-gene-transcript and that the AAV6-mediated viral transduction might be lower when the plasmid size increases (Kreiss et al. 1999; Hurh et al. 2013). Furthermore, the overexpression virus itself may has a lower transduction efficiency compared to the control virus. To verify this hypothesis the transfection efficiency of the AAV-SFRP5 virus must be quantified by flow cytometry using the same conditions as applied for the control.

SFRP5 overexpression was quantified 14 days after viral transduction by qPCR demonstrating a stable overexpression of ~40,000 fold compared to Control^{OE} hiPSC-CMs. Low SFRP5 expression in the control intensifies the effect of its overexpression. In the mRNA-seq screen the quantity of *SFRP5* mRNA in treated cardiomyocytes was comparable to the mRNA quantity of *TNNT2* in control cardiomyocytes. The successful AAV-SFRP5 treatment was further validated at the protein level via Western blotting, confirming the SFRP5 overexpression. In Control^{OE} hiPSC-CMs, SFRP5 was not detectable at the protein level because its basal expression seems to be significantly lower than in the OE cells. The successful SFRP5 overexpression is sufficient for the first analysis of its function in human cardiomyocytes. Due to the extensive overexpression of the protein affected pathways identified could be linked to SFRP5.

4.2.2 mRNA-seq analysis of SFRP5^OE hiPSC-CMs compared to Control^OE hiPSC-CMs

4.2.2.1 Regulation of pro- and anti-apoptotic pathways in SFRP5^OE hiPSC-CMs

Network enrichment and detailed pathway analysis displayed apoptosis activation via the intrinsic pathway due to UPR, as well as extrinsic pathway activation via TNFα and canonical Wnt pathway upon SFRP5 overexpression (figure 15). Besides upregulation of pro-apoptotic pathways, anti-apoptotic protein expression was also increased in SFRP5^OE hiPSC-CMs.

Upregulation of pro-apoptotic *BIM* and *CHOP* is mediated by intrinsic pathway activation due to the UPR, *IRE1α* and *PERK* (reviewed in Schröder and Kaufman 2006). Additionally, the upregulation of extrinsic apoptosis-inducing pathways via TNFα and canonical WNT signaling was demonstrated in the SFRP5^OE hiPSC-CMs. Interestingly, anti-apoptotic *BCL2* and *BCL-XL* were also upregulated in the mRNA-seq data set. The common termination pathway of apoptosis via cytochrome C, *APAF-1* and pro-caspase 9 forming the apoptosome to activate the effector caspases 6 and 7 was not regulated in the screen. Only the anti-apoptotic *HAX1* was upregulated in the common termination pathway, known to repress autocleavage of pro-caspase 9 (Han et al. 2006). Thus, our analysis at the transcriptome level indicates that SFRP5 is affecting pro- and anti-apoptotic pathways, which may support SFRP5's role in tissue homeostasis regulation, which was already displayed in several cancer types (Zhao et al. 2009; Peng et al. 2014; Gutiérrez-Vidal et al. 2015).

Furthermore, the influences on apoptosis induction of the applied AAV virus itself and the extensive overexpression of the secretory protein SFRP5 is a matter of discussion. Balakrishnan et al. (2013) discovered that UPR is modesty activated by transduction with AAV6 vectors inducing pro-apoptotic stimulation via IRE1a, PERK, and ATF6. To eliminate signals that are produced by a potential induction of the UPR due to virus capsids, the Control^OE hiPSC-CMs were included as control. However, the UPR and ER stress found in our pathway analysis could also be a result of the ~40,000 fold overexpression of the secreted protein SFRP5. Physiologically, secretory proteins are translated in the ER, where chaperones guide their folding. Vesicle transport mediates the secretory proteins from the ER to the Golgi and finally to the plasma membrane, where they are released by exocytosis. Extensive overexpression of a secretory protein like SFRP5 increases the

proteinbiosynthesis and folding rate beyond its capacities, which may also cause ER-stress and increase the UPR. To exclude the phenomenom of extensive overexpression inducing apoptosis, AAV-mediated overexpression of a well known secretory protein without involvement in apoptosis pathways could be examined, whether similar apoptosis regulation would be observed as in SFRP5^{OE} hiPSC-CMs. As of now we have not found an adequate secretory candidate, that meets all criteria.

In literature, the role of SFRP5 in apoptosis regulation was examined in different cell models, whereby pro- and anti-apoptotic stimulus was reported. SFRP5 has been shown to diminish cardiac inflammation of Wnt5a-positive macrophages after ischemia/reperfusion injury, thereby inhibiting murine cardiomyocyte apoptosis (Nakamura et al. 2016). Moreover, the anti-apoptotic role of SFRP5 through decrease of *BAX* was reported in human endothelial cells during oxidative stress conditions (Wang et al. 2017). The mRNA-seq data of SFRP5^{OE} hiPSC-CMs without induced oxidative stress did not confirm a downregulation of *BAX* as described by the publication mentioned above, probably due to cell type differences varying in the response to the same stimulus. Additionally, Jin et al. (2015) reported a repression of the TNFα-mediated apoptotic pathway upon Sfrp5 addition to the culture medium of neonatal rat ventricular cardiomyocytes, whereas our data showed an upregulation of the TNFα-mediated pathway. The discrepancy to the literature may occur due to the different origin of the cells and maturation status. Though, besides the reported anti-apoptotic role of SFRP5 mentioned above, our candidate was identified as a pro-apoptotic tumor suppressor gene in melanoma cell cancer, kidney cancer, breast cancer and further cancer types (Veeck et al. 2008; Kawakami et al. 2011; Chen et al. 2018). Similarly, apoptosis induction in cardiac fibroblasts treated with SFRP5 was reported by Bie et al. (2016). Furthermore, SFRP family members SFRP3 and SFRP4 were associated with increased apoptosis in failing ventricular tissue (Schumann et al. 2000). Consistent with our mRNA-seq screen, upregulation of the TNFα-mediated pro-apoptotic pathway is published to facilitate cardiac remodeling leading to HF, whereas the role of cardiomyocyte death in cardiac remodeling and heart failure is only poorly understood (Sun et al. 2007; Kim and Kang 2010). Thus it can be concluded that the role of SFRP5 for apoptosis may depend on the cell type or tissue and the respective apoptosis stimulus.

SFRP5 is a known soluble inhibitor of canonical and non-canonical WNT signaling which are also known to be involved in apoptosis induction (Suzuki et al. 2004; Li et al. 2008). Stabilized β-catenin of activated canonical WNT signaling pathway results in an induction of TCF/LEF transcription factor facilitating c-MYC expression and apoptosis pathway activation (Hu and Rosenblum 2004; Järvinen et al. 2011; Yang et al. 2014). In the RNA-seq of aortic stenosis induced HF, the canonical WNT target gene TCF/LEF (associated gene: *LEF1*) was upregulated indicating apoptosis induction in HF, which was also confirmed in tissue staining of failing cardiac biopsies (Khadjeh et al. 2020). TCF/LEF (associated gene: *LEF1*) and c-Myc overexpression was also observed in SFRP5[OE] hiPSC-CMs supporting its pro-apoptotic role. The upregulation of canonical WNT pathway in SFRP5[OE] hiPSC-CMs is in contradiction with SFRP5's known function to repress both the canonical and non-canonical WNT pathway (Li et al. 2008). These might occur by upregulation of *WNT16* in SFRP5[OE] hiPSC-CMs. Alternatively, the activation/inhibition of canonical WNT pathway by SFRP5 is tissue dependent: In trunk formation of mice and gastrointestinal tissues, SFRP5 was described as an inhibitor of canonical WNT signaling (Li et al. 2008; Satoh et al. 2008), whereas Holly et al. (2014) described canonical WNT signaling activation by SFRP5 in retinal development. In conclusion, SFRP5 overexpression may activate the canonical WNT signaling pathway through WNT16 overexpression or through an ambivalent role of SFRP5, which may promote apoptosis induction by TCF/LEF and c-MYC.

To further investigate the role of SFRP5 in apoptosis, SFRP5[OE] and Control[OE] hiPSC-CMs could be stimulated with cardiac stressor angiotensin II and apoposis inductors doxorubicin or hydrogen-peroxide. For cardiac stress induction angiotensin II-treatment, known to facilitate cardiac hypertrophy (reviewed in Schirone et al. 2017), could be used to mimic cardiac remodeling in hiPSC-CMs. These stressed cardiomyocytes may reveal apoptosis induction as observed in human aortic endothelial cells by Wang et al. (2017), which could be differentially regulated between SFRP5[OE] and Control[OE] hiPSC-CMs. Examining angiotensin II treated SFRP5[OE] hiPSC-CMs may help to further understand the role of SFRP5 in cardiac apoptosis regulation. To verify either pro- or anti-apoptotic stimulus of SFRP5, apoptosis induction with doxorubicin and hydrogen-peroxide could be performed in SFRP5[OE] and Control[OE] hiPSC-CMs.

As tumor suppressor gene, SFRP5 is known to be fundamental for tissue homeostasis as described above (Zhao et al. 2009; Peng et al. 2014). Published data and our mRNA-seq data revealed, that the role of SFRP5 in apoptosis is cell-type specific and stimulus-dependent, whereas also bias of extensive overexpression of secretory protein should be considered. Without pro-apoptotic treatment, SFRP5^{OE} hiPSC-CMs display regulation of pro-and anti-apoptotic pathways, whereas further analysis in differentially treated SFRP5^{OE} and Control^{OE} hiPSC-CMs (e.g. with angiotensin II-,Doxorubicin- and hydrogen-peroxide-treatment) may outline a predominant pro- or anti-apoptotic tendency of SFRP5 treatment. With regard to cardiac remodeling and end-stage HF, the role of cardiomyocyte apoptosis and other types of cell death is still controversely discussed.

4.2.2.2 Reduction of calcium channels and cardiac excitation-contraction-coupling proteins

In the mRNA-seq network enrichment analysis of SFRP5^{OE} hiPSC-CMs pathways involved in calcium cycling and cardiac contraction were significantly downregulated. Cardiac contraction, initiated by membrane depolarization of voltage gated sodium channels leading to CICR, is crucial for proper cardiomyocyte function, whereas its dysfunction is often associated with HF (Gómez et al. 1997). Thus, we performed pathway analysis for proteins involved in excitation-contraction-coupling.

The non-canonical WNT signaling pathway plays a crucial role in the regulation of calcium handling and the development of CH (Hagenmueller et al. 2014). Exemplary, the activation of Wnt5a-mediated non-canonical Wnt signaling pathway induces CH in mice (Hagenmueller et al. 2014). Additionally, Wnt5a-mediated neutrophil recruitment in the early phase of pressure-overload after TAC surgery in mice and consequently macrophage migration and cytokine and chemokine expression were reported to be an obligatory stimulus for cardiac hypertrophy and cardiac dysfunction (Wang et al. 2019). WNT5A is further known to be repressed by SFRP5, which additionally supports SFRP5's suggested anti-hypertrophic role first described in Jin et al (2015). The *WNT5A* downregulation by SFRP5 overexpression was also confirmed in our screen. Further downstream targets of the non-canonical WNT signaling pathway, PLCB (associated gene: *PLCB2*) and CAMKII (associated gene: *CAMK2A*) were downregulated in our mRNA-seq screen, confirming non-canonical pathway repression in SFRP5^{OE} hiPSC-CMs. CAMKII is known to phosphorylate cardiac calcium channels improving their

conductance ability (reviewed in Anderson et al. 2011). The hypothetically decreased cytosolic calcium influx due to less conductive and downregulated calcium channels may lead to the downregulation of calmodulin (associated gene: *CAML3*). Calcium-calmodulin complex activates CAMKII, thus hypothetical less cytosolic calcium and downregulated calmodulin result in less active CAMKII, which could further contribute transcriptional downregulation of CAMKII. In conclusion, our study demonstrated the non-canonical WNT signalig pathway to be transcriptionally repressed by SFRP5 overexpression in human cardiomyocytes, which might also impair calcium handling via CAMKII (figure 22).
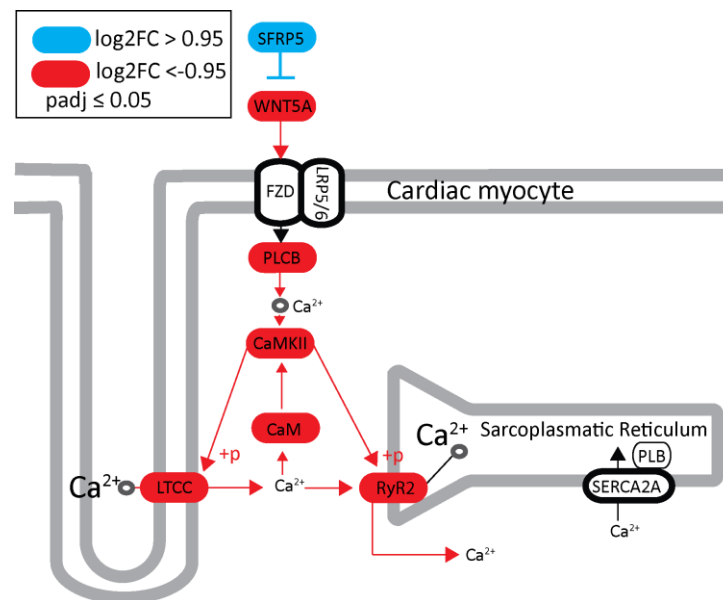
Figure 22: Non-canonical WNT signaling repression in SFRP5^{OE} hiPSC-CMs. The mRNA-seq of SFRP5^{OE} hiPSC-CMs revealed the repression of non-canonical WNT signaling pathway via downregulation of WNT5A. Upregulated genes (adjusted p-value < 0.05, Log2 fold change > 0.95) are indicated in red, downregulated genes (adjusted p-value < 0.05, Log2 fold change < - 0.95) are indicated in blue. The reduced expression of downstream target CAMKII may also lead to diminished posttranslational phosphorylation of calcium channels LTCC and RYR2 resulting in transcriptional downregulation. Due to the downregulation of calcium channels, reduced calcium influx occures during systole, thereby CAMKII activation complex formation of calcium-calmodulin (CaM) is attenuated leading to further repression of CAMKII function.

CICR is initiated by voltage-gated LTCC opening resulting in a local increase of cytosolic calcium concentration. The "trigger"-calcium leads to synchronized opening of RYR2 and calcium efflux of the sarcoplasmic reticulum initiating sarcomere contraction (reviewed in Eisner et al. 2017). LTCC subunit α and β (associated genes: *CACNA1c, CACNA1d, CACNB2*) were found to be significantly downregulated in our study, whereas subunit γ4 (associated gene: *CACNG4*) was upregulated. The γ4-subunit upregulation, which is

known to stabilize LTCC in an inactivated and closed state (Yang et al. 2011), points towards less channel conductance and thereby delayed CICR. Furthermore, SR calcium channel RYR2, crucial for contraction initiation, was significantly downregulated upon SFRP5 overexpression. RYR2 activation is regulated by several proteins like CAMKII, PKA, PP1, PP2a and FKBP12.6 (reviewed in Luo and Anderson 2013). Only CAMK2A gene expression was regulated in our screen pointing towards less phosphorylation and reduced conductance of RYR2, whereas the not cardiac specific δ-isoform of CAMKII (Edman and Schulman 1994) was regulated here upon SFRP5 overexpression. In accordance with the literature, downregulation of *RYR2* is compensated by an upregulation of the IP3-receptor, which represents a structurally and functionally similar SR calcium channel activated by IP3 (Go et al. 1995). In comparison with RYR2, IP3R mediates small calcium currents downstream of GPCR that are known to play a crucial role in promoting cardiac hypertrophy probably via calcineurin-NFAT pathway activation (Nakayama et al. 2010). Whereas calcineurin-NFAT pathway was not transcriptionally regulated in SFRP5[OE] hiPSC-CMs. In conclusion, decreased LTCC and RYR2 expression points towards reduced calcium conductance resulting in a repressed CICR in SFRP5[OE] hiPSC-CMs, which may diminish cardiomyocyte function.

Furthermore, downregulation of contractile filaments like *ACTC1* (actin associated gene)*, MYH6/7, MYL4* (myosin associated genes), *MYBPC3 (*myosin binding protein associated gene) and *TNNT2* (cTnT associated gene) indicate less contractile force in the SFRP5[OE] hiPSC-CMs. This could occur due to the regulation of sarcomere proteins by PKCε. The cardiac specific PKCε can be induced by angiotensin II, endothelin-1 and increased mechanical force during contraction rhythm (Clerk et al. 1994; Paul et al. 1997; Vincent et al. 2006). In our screen this PKC isoform is significantly upregulated in the SFRP5[OE] hiPSC-CMs. Since PKCε can phosphorylate and inactivate proteins involved in sarcomere function like cTnT, actinin, myosin and myosin-binding protein (Ping et al. 2001; Kooij et al. 2010), this might explain their transcriptional downregulation observed in our mRNA-seq screen. Furthermore, it was shown that upregulated PKCε desensitize contractile calcium handling and induces overall depression of the contractile function in human cardiomyocytes (Kooij et al. 2010). Mice overexpressing a constitutively active PKCε developed concentric hypertrophy decompensating in eccentric HF, which additionally outlines its role in the process of cardiac remodeling (Takeishi et al. 2000;

Goldspink et al. 2004; Montgomery et al. 2005). Thus, upregulated PKCε may repress cardiac contractile function by inactivation of sarcomere proteins in the SFRP5[OE] hiPSC-CMs.

Further proteins involved in calcium and cell homeostasis are differentially regulated in SFRP5[OE] hiPSC-CMs. NKA α-catalytic and membrane-bound β-domain (associated genes: *ATP1A2/4, ATP1B4*) were upregulated, whereas the genes of another β- and modulatory γ-subunit (associated genes: *ATP1B2* and *FXYD2*) were downregulated. Physiologically the sodium-potassium ATPase is responsible for the general and localised sodium homeostasis in the cell. Especially its upregulated isoform α2 (*ATP1A2)* is known to be co-localised and functionally coupled with NCX via ankyrin B underlining its role in cardiac calcium handling (Su et al. 1998; Mohler et al. 2005). This functional complex may regulate cardiac contractility via microdomain sodium currents in the junctional T-tubules of cardiomyocytes (Despa et al. 2012). Moreover, the modulatory subunit of NKA, especially FXYD subunit family repressing NKA ion transport (Pavlović et al. 2007), is downregulated in our mRNA-seq propably leading to a higher active NKA due to less inhibition. These may result in lower sodium concentrations in the dyade and may activate NCX calcium sequestration similar as described earlier and further resulting in reduced SR calcium stores (Despa et al. 2012). In contrast, voltage-gated sodium channel, SERCA, phospholamban and NCX were not regulated in our screen. The molecular changes and predicted influence on the calcium homeostasis are illustrated in figure 23. In conclusion, cardiac contractility may also be regulated via microdomain sodium through NKA and NCX leading to cytosolic calcium sequestration and consequently reduced SR calcium stores, whereas only NKA is transcriptionally regulated.
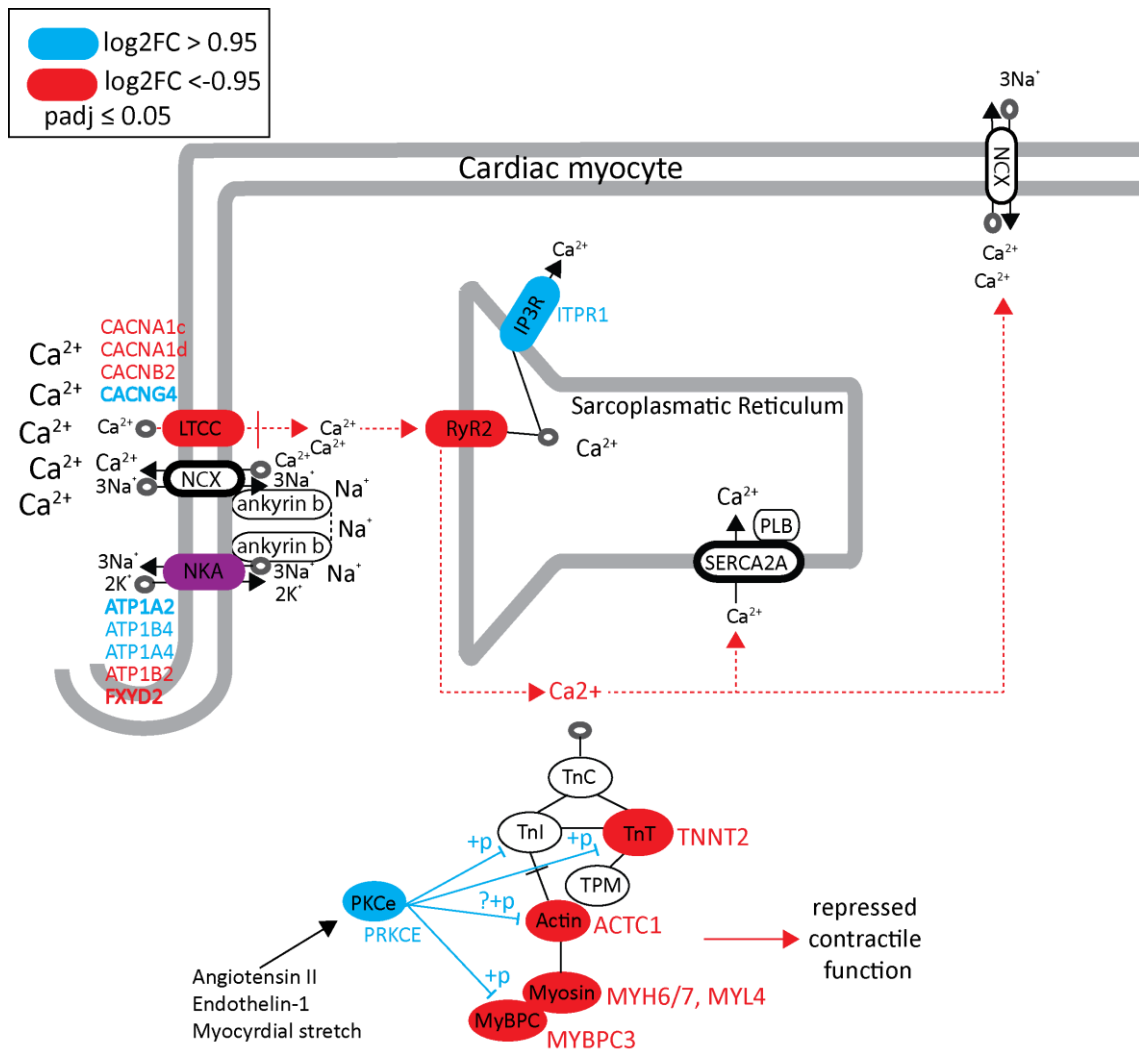
Figure 23: Cardiac handling in SFRP5[OE] hiPSC-CMs. The transcriptional changes of cardiac contraction proteins in SFRP5[OE] hiPSC-CMs displayed an overall repression of calcium cycling and contraction. Upregulated genes (adjusted p-value < 0.05, Log2 fold change > 0.95) are indicated in red, downregulated genes (adjusted p-value < 0.05, Log2 fold change < - 0.95) are indicated in blue. The downregulation of LTCC and the upregulation of its repressor gene *CACNG4* significantly attenuate the calcium channel activity. Furthermore, sodium and calcium microdomain homeostasis may induce cytosolic calcium sequestration via NCX. The more active NKA, due to α- and β-subunit overexpression and modulatory γ-subunit downregulation, is functionally coupled with NCX via ankyrin b. Sequestrated cytosolic sodium consequently results in cytosolic calcium sequestration for sodium influx via NCX promoting reduced calcium concentration in the dyad. Because of the predicted predominant calcium sequestration via NCX of reduced cytosolic calcium levels, smaller amounts of calcium can be sequestrated by SERCA resulting in reduced SR calcium stores. In turn, reduced SR calcium stores lead to reduced SR calcium outflow attenuating cardiomyocyte force development. Furthermore, upregulated PKCε phosphorylates and thereby attenuates sarcomere proteins, e.g. TnT, myosin, and myosin binding protein (MyBPC), resulting in repressed contractile function in addition to reduced cytosolic calcium levels during systole.

Downregulation of the non-canonical WNT pathway, calcium channels and proteins involved in excitation-contraction-coupling upon SFRP5 overexpression may identify

SFRP5 as a novel regulator of calcium handling in hiPSC-CMs. Transcriptional alterations and phosphorylation status of candidate genes should further be verified on the protein level to generate a strong statement out of these initial data sets. It should be noted that the 40,000 fold overexpression of a single secreted protein, here SFRP5, may interfere with normal processes of the protein biosynthesis machinery, probably affecting the synthesis of other proteins under this artifical condition. Nevertheless, the detected effects point towards a reduced CICR and attenuated contractile force due to the SFRP5 overexpression in hiPSC-CMs, therefore cardiomyocyte calcium handling was further examined via confocal calcium imaging.

4.2.3   Confocal calcium imaging of SFRP5 overexpressing hiPSC-CMs

Molecular changes in calcium handling were further validated using confocal calcium imaging. Functional analysis of calcium transients and sparks revealed significant alterations in SFRP5^{OE} hiPSC-CMs. They showed a decrease in calcium transient amplitude, faster calcium transient upstroke, faster calcium transient decay and a reduction of calcium spark frequency as well as a reduced calcium leak under isoprenaline conditions.

The calcium transient amplitude is meditated by the expression and/or activity of calcium handling proteins by regulating the SR calcium stores (Piacentino et al. 2003; reviewed in Roderick et al. 2007). Relating to alterations in the expression of calcium channels and proteins involved in excitation-contraction-coupling, the downregulation of LTCC and RYR2 may cause the decrease of calcium transient amplitude. Such a decreased calcium transient amplitude is associated with impaired excitation-contraction-coupling and reduced SR calcium content in failing cardiomyocytes (Gómez et al. 1997; Lindner et al. 1998; Pieske et al. 1999; Piacentino et al. 2003). Additionally, decreased calcium transient amplitude in SFRP5^{OE} hiPSC-CMs may occur due to the downregulation of STRIP2, which is known to be involved in calcium handling regulation. Interestingly, in STRIP2-KO-mice calcium transient amplitude was also reduced and these mice develop an early HF with reduced contractile function, whereas STRIP2 overexpression could rescue the failing phenotype (Eden et al. 2016). The downregulation of STRIP2 in our mRNA-seq screen and the predicted reduced contractile function substantiate the data of Eden et al. (2016). Moreover,

transcriptionally regulated NKA may also contribute to the reduced calcium transient amplitude found in SFRP5^{OE} hiPSC-CMs. Hypothetically, the transcriptional upregulation of *ATP1A2* forming NKA α2-isoform and the decrease of the inhibitory FXYD family member *FXYD2* may lead to reduced sodium concentrations in the junctional part of T-tubules. NCX sequestrate calcium for sodium influx, thus leading to reduced SR calcium stores and impaired contractility. This hypothesis is supported by findings from Yamamoto et al. (2005), where an upregulation of the α2-isoform caused by an α1-isoform KO in mice leads to a reduced calcium transient amplitude and NCX currents, thereby leading to reduced cardiac contractility (Su et al. 1998; Moseley et al. 2004; Yamamoto et al. 2005). Inversely, Su et al. (2001) reported that NKA short-term blockage with increased local cytosolic sodium leads to a significant increase in calcium transients mediated by reversed NCX currents sequestrating sodium for calcium influx into the cytosol. Our mRNA-seq screen substantiate these data because the reduced calcium transient amplitude in SFRP5^{OE} hiPSC-CMs might be caused by the downregulation of LTCC, RYR2, STRIP2 and an upregulated, higher active NKA, which points towards less circulating cytosolic calcium.

Higher conductance ability of calcium channels may facilitate the observed faster calcium transient upstroke in SFRP5^{OE} hiPSC-CMs. Posttranscriptional phosphorylation of LTCC and RYR2 is mediated by CAMKII, which leads to an improved conductance (Anderson et al. 2011). Even though CAMKII α-isoform is downregulated, the faster calcium transient upstroke points towards an improved conductance ability of the respective calcium channels. This detected effect might be explained by the fact that the predominant cardiac CAMKII isoform (the CAMKII δ-isoform) was not regulated in SFRP5^{OE} hiPSC-CMs. In summary, faster calcium upstroke can not be correlated to the mRNA-seq data and may occur due to posttranscriptional changes of calcium release channels.

Calcium reuptake indicated by calcium transients decay is mediated by NCX, SERCA and its inhibitor phospholamban (reviewed in Bers 2002). SFRP5^{OE} hiPSC-CMs displayed a faster calcium reuptake, without detectable changes at transcriptional level of the calcium sequestration proteins. Hypothetically, due to the unchanged expression of calcium reuptake proteins and the lower cytosolic calcium concentration during the systole, each single calcium channel, SERCA or NCX, has to pump less calcium to achieve

the diastolic cytosolic calcium concentration, which consequently results in a shorter time for the calcium decay. This hypothesis must be verified in further experiments, for example by measuring the cytosolic calcium concentration in real-time during a particular time period. In conclusion, there is no transcriptional explanation for the faster calcium decay, but it can be assumed that the faster calcium reuptake occurs due to a lower cytosolic calcium concentration during the systole and an unchanged calcium efflux pump activity.
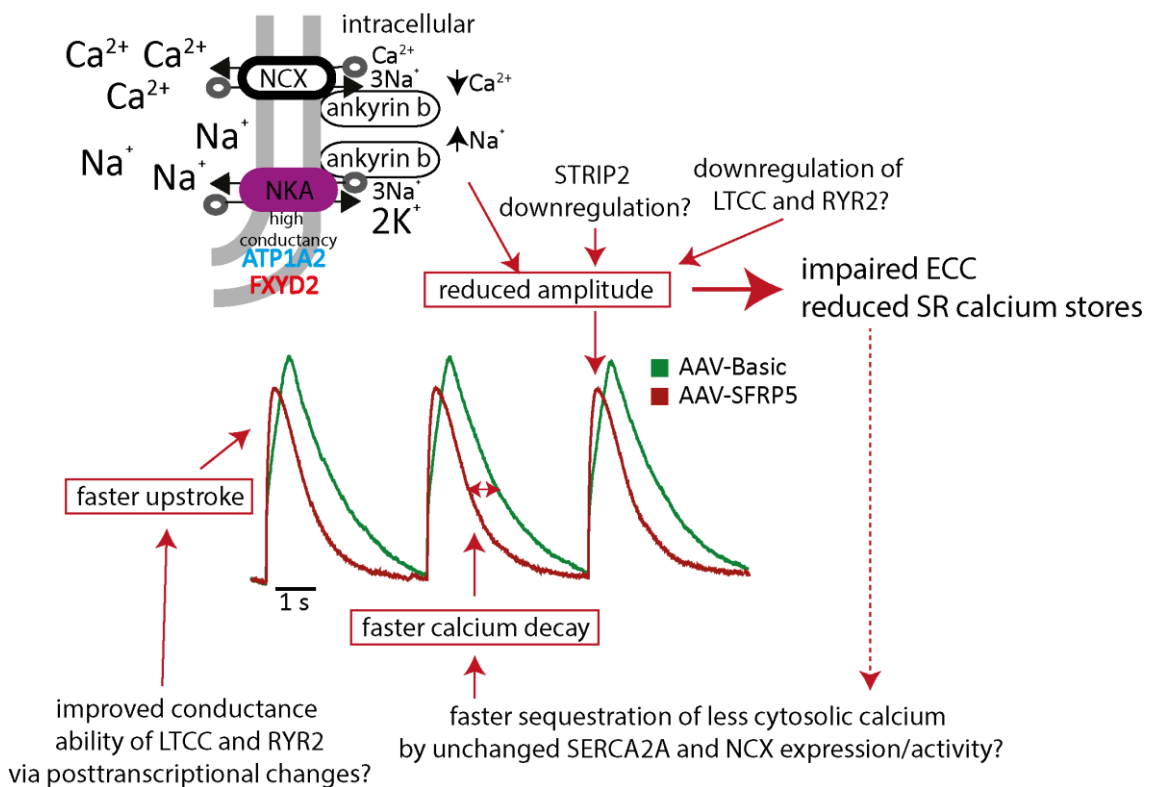
Figure 24: Overview of influences on calcium transients of SFRP5^{OE} hiPSC-CMs. Calcium transients of SFRP5^{OE} hiPSC-CMs displayed an increased amplitude, faster transient upstroke, and a faster calcium decay. The reduced amplitude may occur by the downregulation of calcium channels, especially LTCC and RYR2. Additionally, STRIP2 downregulation is associated with lower calcium transient amplitude. Furthermore, microdomain sodium and calcium homeostasis is reduced due to the functional coupling of NKA and NCX sequestrating cytosolic calcium. The reduced calcium transient amplitude leads to impaired ECC and reduced SR calcium stores. This further results in reduced cytosolic calcium during the systole, which may be faster sequestrated by unchanged SERCA and NCX expression/ activity leading to faster calcium decay of calcium transients. Faster calcium transient upstroke could not be correlated to the mRNA-seq data, whereas posttranscriptional changes may mediate this effect in SFRP5^{OE} hiPSC-CMs.

The spontaneous diastolic releases of the calcium from the SR, so called calcium sparks, were reduced in their frequency and the calcium leak was diminished during isoprenaline stimulation, possibly due to the downregulation of RYR2. However, calcium leak under basal conditions and the sum of all sparks were not significantly altered in

SFRP5[OE] hiPSC-CMs. In conclusion, calcium sparks are not significantly altered in SFRP5[OE] hiPSC-CMs.

Isoprenaline, a positive ionotropic substance, is an agonist of the β-adrenergic receptor in the heart activating PKA and CAMKII inducing cardiac stress response. Downstream of β-adrenergic signaling LTCC and RYR2 are phosphorylated, which increases their conductance ability and the phosphorylation of phospholamban resulting in reduced inhibition of SERCA2A (reviewed in Grimm and Brown 2010). In confocal calcium imaging we expected an increase in calcium transient amplitude and a decrease in calcium transient decay during isoprenaline stimulation (Curran et al. 2007). The predicted increase in diastolic calcium leak would depend on CAMKII and not PKA mediated β-adrenergic stimulation (Li et al. 2002; Curran et al. 2007). However, the stimulation with isoprenaline did not reveal the expected alterations in calcium handling in Control[OE] cardiomyocytes as described in the literature. The retrospective analysis of these experiments suggests that the chosen isoprenaline concentration was most likely too low. Consequently, calcium transients and calcium sparks in SFRP5[OE] hiPSC-CMs should be reanalyzed with higher isoprenaline concentrations.

In summary, calcium handling changes observed in SFRP5[OE] hiPSC-CMs can be partially explained by the transcriptional changes of the calcium channel proteins LTCC, RYR2 and NKA. Changes in calcium upstroke and decay could not be correlated to our mRNA-seq screening, but unknown posttranscriptional modifications of respective calcium channels may elucidate calcium handling alteration in SFRP5[OE] hiPSC-CMs. Therefore, transcriptional alterations should be verified on the protein level as well as on their protein phosphorylation state. To examine the expected reduced circulating calcium levels in SFRP5[OE] hiPSC-CMs, calcium indicator-based measurements should further evaluate the cytosolic calcium concentration during systole and diastole.

4.2.4   The role of SFRP5 in cardiac remodeling

Preliminary RNA-seq data sets from patients with aortic stenosis and TAC mice displayed a significant reduction of the SFRP5 expression from control to CH and the SFRP5 re-expression in HF. To analyze the role of SFRP5 in cardiac remodelling, we performed transcriptional and functional analysis, which confirmed its role as WNT pathway regulator and additionally identified SFRP5 as novel calcium cycling regulator in

cardiomyocytes. Therefore, we hypothesized that SFRP5s' anti-hypertrophic role, first described by Jin et al. (2015) in rat cardiomyocytes, may depend on calcium handling aberrations and WNT pathway regulation.

In functional analysis of calcium transients, SFRP5[OE] hiPSC-CMs displayed a decreased amplitude and a faster calcium reuptake. Regarding the calcium handling changes in hypertrophic cardiomyocytes, Berridge (2006) reviewed an increased calcium transient amplitude and a delayed calcium reuptake. The concordant relation between increased calcium transient amplitude and SR calcium content was described by Ke et al (2019) in TAC-operated hypertrophied, non-failing guinea-pigs compared to the sham-operated group. Therefore, we hypothesize that the reduced calcium transient amplitude in SFRP5[OE] hiPSC-CMs may be related to reduced calcium stores. The prolongation of calcium reuptake was reported in pressure-overload hypertrophy animal models of rats, felines and guinea pigs (Bailey and Houser 1992; Naqvi and Macleod 1994; Primessnig et al. 2016), which may be based on transcriptional regulation of calcium reuptake proteins. The SERCA inhibitor phospholamban is significantly upregulated in CH of aortic stenosis patients (Khadjeh et al. 2020), which may reduce calcium affinity of SERCA2A leading to slower calcium reuptake in the SR (Pattison et al. 2008). Faster calcium reuptake was detected in In SFRP5[OE] hiPSC-CMs, whereas no transcriptional alterations in *SERCA2A* or its inhibitor phospholamban could be found in the mRNA-seq analysis. We hypothesized these changes within the scope of posttranscriptional modifications.

Additionally, we focused on known WNT pathway regulation in cardiac remodeling. In SFRP5[OE] hiPSC-CMs, the activation of canonical WNT pathway occurred likely via upregulation of *WNT16,* and *LEF1* and the repression of non-canonical pathway via downregulation of *WNT5A*. Similar transcriptional regulation of canonical and non-canonical WNT pathway was also described in Sfrp1-deficient mice, which resulted in increased cardiac size, mild hypertrophy, left ventricular dilation and consequently impaired cardiac function (Sklepkiewicz et al. 2015). Whereas, Wnt5a-mediated activation of non-canonical WNT pathway was reported to induce murine cardiac hypertrophy (Hagenmueller et al. 2014). Canonical WNT signaling pathway activation in HF is known to be associated with improved cardiomyocyte function (Haq et al. 2003; Hirotani et al. 2007), whereas after angiotensin II induced CH in mice, activation of canonical WNT pathway leads to cardiac dysfunction (Baurand et al. 2007). The

differences in the functional outcome due to distinct stimuli outlines the complex role of the WNT signaling pathway in cardiac remodeling.

In conclusion, we identified SFRP5 as a novel regulator of calcium handling in human cardiomyocytes, which may also reveal anti-hypertrophic effects in the process of cardiac remodeling. The predicted reduction of intracellular calcium stores and reduced circulating calcium in SFRP5^{OE} hiPSC-CMs may protect the cell against calcium overload in hypertrophied cardiomyocytes, which could also lead to impaired cardiomyocyte function. The complex regulation of WNT signaling and its functional outcome in cardiomyocytes due to SFRP5 overexpression has to be evaluated in further experiments.

4.3 SFRP5 loss of function: Generation of SFRP5^{KO} hiPSC line and their differentiation into SFRP5^{KO} hiPSC-CMs

Gene editing in hiPSCs is known to be more difficult and inefficient compared to stable cell lines (Mali et al. 2013). Low transfection rates (1-6%) may occur due to large CRISPR/Cas9 plasmids and the low survival rate of transfected hiPSCs. Furthermore, harsh conditions during cell sorting harm the hiPSCs, therefore the generation of KO-hiPSC lines is challenging. Some of the transfected and GFP$^+$ sorted hiPSCs additionally lost their pluripotency during cultivation as indicated by their altered cell morphology pointing towards their spontaneous differentiation into other cell types. These effects could be minimized by the usage of the high nutrient stem-cell medium StemFlex resulting in higher survival rates, faster recovery after nucleofection and preservation of pluripotency. Alternative delivery techniques like mRNA transfection or ribonucleoprotein complexes could also provide several advantages including higher transfection efficiencies and more gentle sorting conditions for experiments in the future (reviewed in Lino et al. 2018).

A small amount of GFP+ hiPSCs inherited homogenous NHEJ-mediated indels, inversions or deletions resulting in a KO of the gene of interest. Predesigned gRNAs in Sigma All-in-one plasmids are described to have very low numbers of potential off-target sites which favors their application for our purpose. The high guanine and cytosine amount in the seed sequence adjacent to protospacer adjacent motif in the predesigned gRNAs further

contributed to the potentially high on-target specification (Ren et al. 2014). To identify off-target cleavage of Cas9 Digenome-seq is the gold standard, detecting off-target mutagenesis frequencies of < 0.1 % (Kim et al. 2015).

Our careful selection of the targeted position within the coding sequence of the gene of interest should avoid the generation of alternative start codons or truncated proteins with partial functionalities. Despite partial deletion of the targeted sequence, alternative splicing can reconstruct parts of the mRNA. This can result in the expression of a truncated protein from the targeted gene of interest that potentially still harbors sites with partial functionality. Off-target mutations were not examined with the limits of the performed analysis in this thesis. Finally, one stable and purified hiPSC line of the targeted gene of interest was generated and used for further analysis.

The final SFRP5^{KO} hiPSC line was used for the analysis of the functional and molecular impact of SFRP5 during the differentiation into hiPSC-CMs because it was shown that *Sfrp5* is expressed in murine cardiac progenitor cells (Fujii et al. 2017). Furthermore, cardiac specification after mesoderm induction is initiated by DKK1, an inhibitor of the non-canonical signaling WNT pathway similar to SFRP5 (Ueno et al. 2007). Thus, it can be assumed that SFRP5 might play a role in cardiomyocyte differentiation.

In this study, hiPSCs harboring the SFRP5 depletion could be efficiently differentiated into SFRP5^{KO} hiPSC-CMs comparable to the differentiation of isogenic SFRP5^{WT} hiPSCs. The targeted SFRP5 mRNA degradation was successfully validated in SFRP5^{KO} hiPSC-CMs by qPCR excluding the expression of a protein with partial SFRP5 functionality. The analysis via light- and fluorescence microscopy revealed no severe functional alterations for the contractility via visual inspection or sarcomere organization compared to SFRP5^{WT} hiPSC-CMs. Furthermore, the predicted target genes from the SFRP5 overexpression study *CACNB2, RYR2* and *WNT5A* were additionally examined at the transcriptional level in SFRP5^{KO} hiPSC-CMs by qPCR without significant alterations. Consequently, a potential role of SFRP5 for the differentiation of pluripotent cells into cardiomyocytes could not be validated within the limitations of this study.

Since SFRP5 expression in healthy CMs is rather low, this might explain that no obvious differences could be observed at basal level. In contrast, there might be significant functional changes after cardiac stress induction. This hypothesis is supported by SFRP5-

KO mice of Nakamura et al. (2016). Although Sfrp5^{KO} mice exhibited no detectable phenotype when compared with SFRP5^{WT} mice at baseline, they displayed larger infarct sizes, enhanced cardiac myocyte apoptosis, and diminished cardiac function following ischemia/reperfusion injury. Furthermore, these SFRP5^{KO} mice did not exhibit alteration in heart development, which was also observed in SFRP5^{KO} hiPSC-CMs (Nakamura et al. 2016).

Further functional experiments of calcium handling, contractile force measurements and apoptosis are required to comparatively analyze the functional role of SFRP5 for cardiac differentiation and CMs.

4.4 Outlook

Future research to investigate the detailed role of SFRP5 should focus on analyzing apoptosis signaling, calcium handling and contractile force.

To further analyze the functions of SFRP5 in hiPSC-CMs a treatment with synthesized and purified soluble SFRP5 protein should be established to mimic its overexpression more physiologically as soluble secreted protein. With soluble proteins or different MOI's of AAV's, gradients of overexpression could be analyzed to reduce artificial overexpression of secreted protein. To further validate the predicted role of SFRP5 in cardiac remodeling, a disease model of cardiac hypertrophy is needed, which could be established via angiotensin II-treatment of hiPSC-CMs. To examine the role of SFRP5 in cardiomyocyte apoptosis e.g. a doxorubicin induced apoptosis assays could be applied. These experiments should be performed with SFRP5^{OE} hiPSC-CMs as well as with SFRP5^{KO} hiPSC-CMs at basal level and after angiotensin II-treatment. Additionally, the transduction efficiency of AAV-SFRP5 must be determined for each experiment by flow cytometry. Further experiments are also required to examine and interpret the calcium handling changes in more detail. Calcium imaging should be performed with untreated SFRP5^{KO} hiPSC-CMs and after angiotensin II or isoprenaline treatment. The isoprenaline concentration should be increased compared to the here applied concentration to induce more reproducible and stable positive inotropic effects in hiPSC-CMs. Moreover, calcium imaging should be performed with synthetic SFRP5 or reduced MOI of AAV's in order to reproduce calcium transient alterations with physiological increase of protein

expression. To validate the predicted reduced cytosolic calcium concentration during systole, Fura2 measurement techniques should be established and performed additionally. Moreover, the determination of the cell size is suggested as an additional read out, in order to determine a potential hypertrophy induction due to SFRP5 depletion or overexpression. To validate transcriptional alterations at the protein level western blots for analyzing e.g. the phosphorylation state should be performed to confirm the predicted posttranslational modifications in calcium handling proteins.

Additionally, off-target mutation sites should be analyzed in established SFRP5^{KO} hiPSC-CMs. This should be performed ideally on the whole genome level by e.g. Digenome-seq identifying off-target mutagenesis frequencies of < 0.1%.

Engineered heart muscle tissues can be used to analyze interactions of CMs with cardiac fibroblasts and the resulting alterations of their response to different stimuli. One interesting measurement would be the assessment of the contractile force from SFRP5^{OE}, SFRP5^{KO} and angiotensin II treated engineered heart muscles compared with other models. Furthermore, engineered heart muscles with hiPSC-CMs would allow analyzing the effects of an SFRP5 overexpression or deletion in a more "natural, heart-like" context compared to the hiPSC-CM monoculture analyzed in this thesis. With such a complex model, effects of a physiological overexpression via synthetic proteins, artificial overexpression via AAV-SFRP5 and SFRP5 depletion can be examined to elucidate potential effects of SFRP5 additionally or exclusively on the cardiac fibroblasts.

5   Conclusion

The mRNA sequencing screen of aortic stenosis patients with preserved and reduced ejection fraction were compared to corresponding mouse model of transverse aortic constriction identifying the differentially regulated candidate SFRP5 significantly decreasing from control to compensated hypertrophy and re-expressing in patients with heart failure. Until today little is known about the function of SFRP5 in human cardiomyocytes.

Using SFRP5 gain of function in hiPSC-CMs via AAV-mediated overexpression, mRNA sequencing screen was performed identifying the differentially regulated apoptosis and calcium handling pathways. Expression of pro- and anti-apoptotic genes was regulated in SFRP5^{OE} hiPSC-CMs, especially intrinsic and extrinsic apoptosis induction as well as increased expression of anti-apoptotic proteins. Furthermore, reduced calcium channel and sarcomere protein expression together with differential microdomain sodium and calcium homeostasis regulation indicates reduced calcium circulation and sarcoplasmic calcium stores due to increased calcium sequestration. These results were further validated in functional analysis of SFRP5^{OE} hiPSC-CMs using confocal calcium imaging. Calcium transients were significantly altered due to SFRP5 overexpression indicating reduced ECC and smaller SR calcium stores, thereby confirming transcriptional alterations of calcium handling proteins. The calcium handling regulation by SFRP5 overexpression may result in protecting the cell against calcium overload and/or reduce contractile force. The functional outcome of SFRP5s anti-hypertrophic effects in calcium handling and WNT pathway regulation can only be hypothesized and have to be examined in further experiments.

CRISPR/Cas9-mediated SFRP5^{KO} hiPSC lines were efficiently differentiated into SFRP5^{KO} hiPSC-CMs, indicating no potential role of the non-canonical WNT signaling inhibitor SFRP5 for cardiomyocyte differentiation. Furthermore, SFRP5^{KO} hiPSC-CMs did not reveal alterations in sarcomere structure, contractility, or expression changes of predicted SFRP5 target genes identified in the mRNA-sequencing study, probably due to low expression levels of SFRP5 in hiPSC-CMs.

The thesis identified SFRP5 as novel calcium handling modulator in hiPSC-CM. Functional and transcriptional analysis displayed contrary calcium handling of SFRP5^{OE} hiPSC-CMs

compared to hypertrophied CMs, supporting its predicted anti-hypertrophic role. However, further investigations are required to identify the detailed underlying mechanisms and their impact on cardiac contractility as well as on the potential therapeutic opportunities.
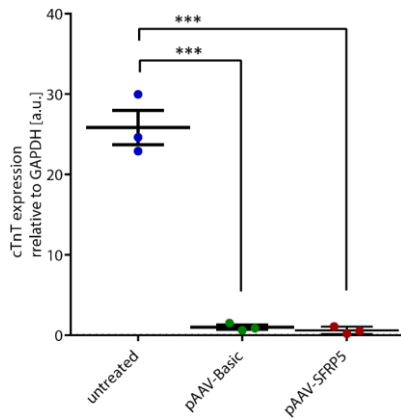
6   Appendix

Figure A.1: cTnT expression in AAV-treated hiPSC-CMs. Human iPSC-CM were treated with AAV-Basic and AAV-SFRP5 (MOI = 10^5) three times for 48 hours and cultured up to day 14. Cardiac TnT expression was examined via qPCR displaying a significant reduction in AAV-Basic and AAV-SFRP5, indicating a significant reduction of cardiomyocyte quality due to extensive AAV-treatment. GAPDH was used as housekeeping gene. Data are presented as mean ± SEM in a dot plot diagram (n = 3). ***$P < 0.001$ was determined by unpaired, two-tailed t-test.
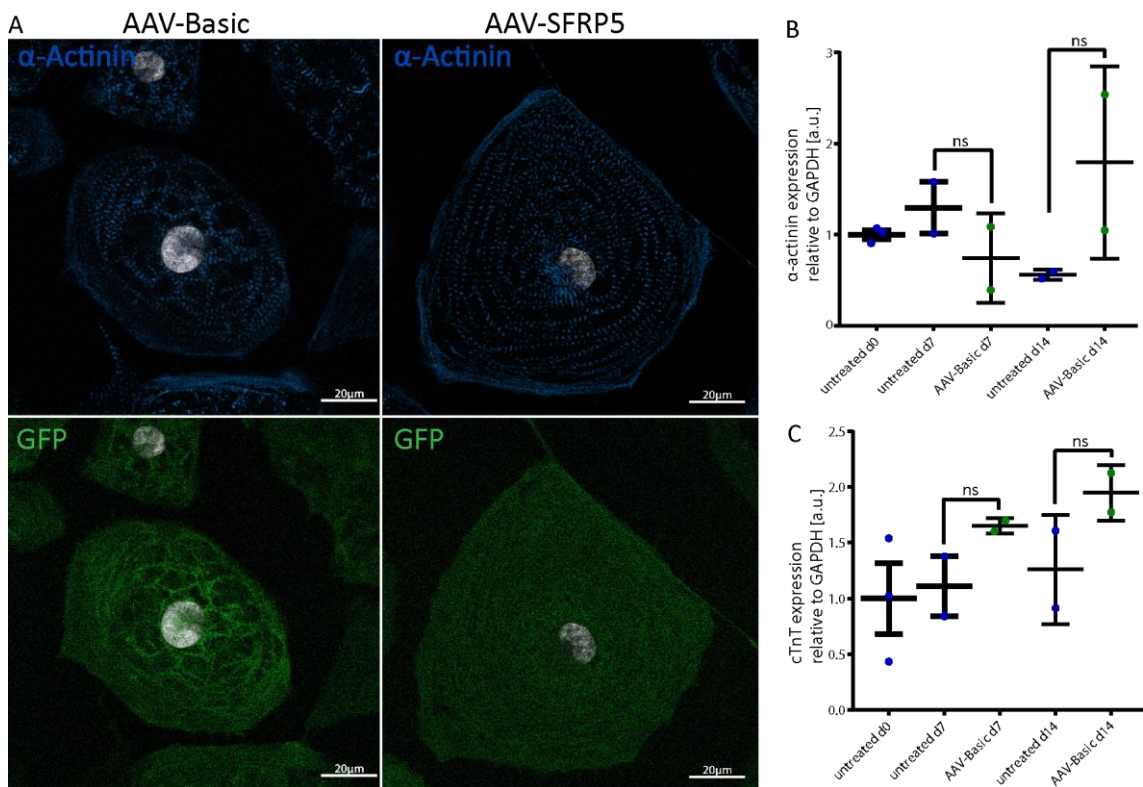
Figure A.2: Validation of cardiomyocyte quality after AAV-treatment. Human iPSC-CMs were cultured to day 46 and subsequently infected with AAV-Basic and AAV-SFRP5 (MOI = 10^5) one time for 72 hours and cultured up to day 14 after transduction. Cell pellets were collected at day 7 and 14 after transduction. **(A)** 14 days after virus treatment hiPSC-CMs were fixed and immunostained with Anti-GFP antibody and Anti-α-actinin antibody. GFP+ hiPSC-CMs displayed a regular sarcomere structure indicated by α-actinin staining. **(B, C)** α-actinin and cTNT was used to validate cardiomyocyte quality after AAV-treatment, showing no significant transcriptional differences at different time points (d7 and d14). Data are resented as mean ± SEM in a dot plot diagram (n = 2). Ns > 0.05 was determined by unpaired, two-tailed t-test.

A   SFRP5 gDNA Exon 1

WT   ATGCGGGCGGCGGCGGCGGCGGGGGGCGTGCGGACGGCCGCGCTGGCGCTGCTGCTGGGGGGCGCTGCACTGG
KO   ATGCGGGCGGCGGCGGCGGCGGGGGGCGTGCGGACGGCCGCGCTGGCGCTGCTGCTGGGGGGCGCTGCACTGG

WT   GCGCCGGCGCGCTGCGAGGAGTACGACTACTATGGCTGGCAGGCCGAGCCGCTGCACGGCCGCTCCTACTCCAA
KO   GCGCCGGCGCGCTGCGAGGAGTACGACTACTATGGCTGGCAGGCCGAGCCGCTGCACGGCCGCTCCTACTCCAA

WT   G**CCGCCGCAGTGCCTTGACATCCC**TGCCGACCTGCCGCTCTGCCACACGGTGGGCTACAAGCGCATGCGGCTGCC
KO   G**CCGCC -------- TTGACATCCC**TGCCGACCTGCCGCTCTGCCACACGGTGGGCTACAAGCGCATGCGGCTGCC

WT   CAACCTGCTGGAGCACGAGAGCCTGGCCGAAGTGAAGCAGCAGGCGAGCAGCTGGCTGCCGCTGCTGGCCAAG
KO   CAACCTGCTGGAGCACGAGAGCCTGGCCGAAGTGAAGCAGCAGGCGAGCAGCTGGCTGCCGCTGCTGGCCAAG

WT   CGCTGCCACTCGGATACGCAGGTCTTCCTGTGCTCGCTCTTTGCGCCCGTCTGTCTCGACCGGCCCATCTACCCGT
KO   CGCTGCCACTCGGATACGCAGGTCTTCCTGTGCTCGCTCTTTGCGCCCGTCTGTCTCGACCGGCCCATCTACCCGT

WT   GCCGCTCGCTGTGCGAGGCCGTGCGCGCCGGCTGCGCGCCGCTCATGGAGGCCTACGGCTTCCCCTGGCCTGAG
KO   GCCGCTCGCTGTGCGAGGCCGTGCGCGCCGGCTGCGCGCCGCTCATGGAGGCCTACGGCTTCCCCTGGCCTGAG

WT   ATGCTGCACTGCCACAAGTTCCCCCTGGACAACGACCTCTGCATCGCCGTGCAGTTCGGGCACCTGCCCGCCACC
KO   ATGCTGCACTGCCACAAGTTCCCCCTGGACAACGACCTCTGCATCGCCGTGCAGTTCGGGCACCTGCCCGCCACC

WT   GCGCCTCCAG
KO   GCGCCTCCAG

B   SFRP5 mRNA

WT   AGTCGGGGCGCCCGCAGCGCAGGCTGCCACCCACCTGGGCGACCTCCGCGGCGGCGGCGGCGGCGGCGGCTGGG
KO   AGTCGGGGCGCCCGCAGCGCAGGCTGCCACCCACCTGGGCGACCTCCGCGGCGGCGGCGGCGGCGGCTGGG

WT   TAGAGTCAGGGCCGGGGGCGCACGCCGGAACACCTGGGCCGCCGGGCACCGAGCGTCGGGGGGCTGCGCG
KO   TAGAGTCAGGGCCGGGGGCGCACGCCGGAACACCTGGGCCGCCGGGCACCGAGCGTCGGGGGGCTGCGCG

WT   GCGCGCACCTGGAGAGGGCGCAGCCATGCGGGCGGCGGCGGCGGCGGGGGGCGTGCGGACGGCCGCGCTG
KO   GCGCGCACCTGGAGAGGGCGCAGCCATGCGGGCGGCGGCGGCGGCGGGGGGCGTGCGGACGGCCGCGCTG

WT   GCGCTGCTGCTGGGGGGCGCTGCACTGGGCGCCGGCGCGCTGCGAGGAGTACGACTACTATGGCTGGCAGGC
KO   GCGCTGCTGCTGGGGGGCGCTGCACTGGGCGCCGGCGCGCTGCGAGGAGTACGACTACTATGGCTGGCAGGC

WT   CGAGCCGCTGCACGGCCGCTCCTACTCCAAG**CCGCCGCAGTGCCTTGACATCCC**TGCCGACCTGCCGCTCTGCC
KO   CGAGCCGCTGCACGGCCGCTCCTACTCCAAG**CCGCCTTGA***------------------------------------

WT   ACACGGTGGGCTACAAGCGCATGCGGCTGCCCAACCTGCTGGAGCACGAGAGCCTGGCCGAAGTGAAGCAG
WT   CAGGCGAGCAGCTGGCTGCCGCTGCTGGCCAAGCGCTGCCACTCGGATACGCAGGTCTTCCTGTGCTCGCTCT
WT   TTGCGCCCGTCTGTCTCGACCGGCCCATCTACCCGTGCCGCTCGCTGTGCGAGGCCGTGCGCGCCGGCTGCGCG
WT   GCCGCTCATGGAGGCCTACGGCTTCCCCTGGCCTGAGATGCTGCACTGCCACAAGTTCCCCCTGGACAACGAC
WT   CTCTGCATCGCCGTGCAGTTCGGGCACCTGCCCGCCACCGCGCCTCCAGTGACCAAGATCTGCGCCCAGTGTG
WT   AGATGGAGCACAGTGCTGACGGCCTCATGGAGCAGATGTGCTCCAGTGACTTTGTGGTCAAAATGCGCATCAA
WT   GGAGATCAAGATAGAGAATGGGGACCGGAAGCTGATTGGAGCCCAGAAAAAGAAGAAGCTGCTCAAGCCGG
WT   GCCCCCTGAAGCGCAAGGACACCAAGCGGCTGGTGCTGCACATGAAGAATGGCGCGGGCTGCCCCTGCCCAC
WT   AGCTGGACAGCCTGGCGGGCAGCTTCCTGGTCATGGGCCGCAAAGTGGATGGACAGCTGCTGCTCATGGCCG
WT   TCTACCGCTGGGACAAGAAGAATAAGGAGATGAAGTTTGCAGTCAAATTCATGTTCTCCTACCCCTGCTCCCTC
WT   TACTACCCTTTCTTCTACGGGGCGGCAGAGCCCCACTGAAGGGCACTCCTCCTTGCCCTGCCAGCTGTGCCTTG
WT   CTTGCCCTCTGGCCCCGCCCCAACTTCCAGGCTGACCCGGCCCTACTGGAGGGTGTTTTCACGAATGTTGTTAC
WT   TGGCACAAGGCCTAAGGGATGGGCACGGAGCCCAGGCTGTCCTTTTTGACCCAGGGGTCCTGGGGTCCCTGG
WT   GATGTTGGGCTTCCTCTCTCAGGAGCAGGGCTTCTTCATCTGGGTGAAGACCTCAGGGTCTCAGAAAGTAGGC
WT   AGGGGAGGAGAGGGTAAGGGAAAGGTGGAGGGGGCTCAGGGCACCCTGAGGCGGAGGTTTCAGAGTAGAA
WT   GGTGATGTCAGCTCCAGCTCCCCTCTGTCGGTGGTGGGGCCTCACCTTGAAGAGGGAAGTCTCAATATTAGGC
WT   TAAGCTATTTGGGAAAGTTCTCCCCACCGCCCCTGTACGCGTCATCCTAGCCCCCCTTAGGAAAGGAGTTAGGG
WT   TCTCAGTGCCTCCAGCCACACCCCCTGCCTTCCCCAGCTTGCCCATTTCCCTGCCCCAAGGCCCAGAGCTCCCCC
WT   CAGACTGGAGAGCAAGCCCAGCCCAGCCTCGGCATAGACCCCCTTCTGGTCCGCCCCGTGGCTCGATTCCCGGG
WT   ATTCATTCCTCAGCCTCTGCTTCTCCCTTTTATCCCAATAAGTTATTGCTACTGCTGTGAGGCCATAGGTACTAGA
WT   CAACCAATACATGCAGGGTTGGGTTTTCTAATTTTTTTTAACTTTTTTAATTAAATCAAAGAAAACAAAAAAAAAAA
WT   AAAAAA

C   SFRP5 protein sequence

WT   MRAAAAAGGGVRTAALALLLGALHWAPARCEEYDYYGWQAEPLHGRSYSKPPQCLDIPADLPLCHTVGYKRMRLP
KO   MRAAAAAGGGVRTAALALLLGALHWAPARCEEYDYYGWQAEPLHGRSYSKP*------------------------

WT   NLLEHESLAEVKQQASSWLPLLAKRCHSDTQVFLCSLFAPVCLDRPIYPCRSLCEAVRAGCAPLMEAYGFPWPEMLH
KO   --

WT   CHKFPLDNDLCIAVQFGHLPATAPP*
KO   -------------------------

Figure A.3: Molecular analysis of SFRP5^WT and SFRP5^KO hiPSC-CMs. (A) Genomic DNA sequence of Exon 1 in SFRP5^WT and SFRP5^KO hiPSC were compared. The SFRP5^KO displayed an 8 bp deletion in the targeted

CRISPR-site indicated in bold. The occurring frameshift in the mRNA of SFRP5^{KO} hiPSC-CMs **(B)** lead to an early stop codon 'TGA' in the targeted CRISPR-site resulting in a truncated mRNA. **(C)** The protein sequence of SFRP5^{KO} compared to SFRP5^{WT} further displayed a truncated protein.

7 References

Abraityte A, Vinge LE, Askevold ET, Lekva T, Michelsen AE, Ranheim T, Alfsnes K, Fiane A, Aakhus S, Lunde IG, et al. (2017): Wnt5a is elevated in heart failure and affects cardiac fibroblast function. J Mol Med Berl Ger 95, 767–777

Ai X, Curran JW, Shannon TR, Bers DM, Pogwizd SM (2005): Ca2+/calmodulin-dependent protein kinase modulates cardiac ryanodine receptor phosphorylation and sarcoplasmic reticulum Ca2+ leak in heart failure. Circ Res 97, 1314–1322

Akoumianakis I, Sanna F, Margaritis M, Badi I, Akawi N, Herdman L, Coutinho P, Fagan H, Antonopoulos AS, Oikonomou EK, et al. (2019): Adipose tissue-derived WNT5A regulates vascular redox signaling in obesity via USP17/RAC1-mediated activation of NADPH oxidases. Sci Transl Med 11, 5055

Anderson ME, Brown JH, Bers DM (2011): CaMKII in myocardial hypertrophy and heart failure. J Mol Cell Cardiol 51, 468–473

Arvanitis DA, Vafiadaki E, Sanoudou D, Kranias EG (2011): Histidine-rich calcium binding protein: the new regulator of sarcoplasmic reticulum calcium cycling. J Mol Cell Cardiol 50, 43–49

Ashpole NM, Herren AW, Ginsburg KS, Brogan JD, Johnson DE, Cummins TR, Bers DM, Hudmon A (2012): Ca2+/calmodulin-dependent protein kinase II (CaMKII) regulates cardiac sodium channel NaV1.5 gating by multiple phosphorylation sites. J Biol Chem 287, 19856–19869

Azevedo PS, Polegato BF, Minicucci MF, Paiva SAR, Zornoff LAM (2016): Cardiac remodeling: concepts, clinical impact, pathophysiological mechanisms and pharmacologic treatment. Arq Bras Cardiol 106, 62–69

Bailey BA, Houser SR (1992): Calcium transients in feline left ventricular myocytes with hypertrophy induced by slow progressive pressure overload. J Mol Cell Cardiol 24, 365–373

Baines CP, Song CX, Zheng YT, Wang GW, Zhang J, Wang OL, Guo Y, Bolli R, Cardwell EM, Ping P (2003): Protein kinase Cε interacts with and inhibits the permeability transition pore in cardiac mitochondria. Circ Res 92, 873–880

Balakrishnan B, Sen D, Hareendran S, Roshini V, David S, Srivastava A, Jayandharan GR (2013): Activation of the cellular unfolded protein response by recombinant adeno-associated virus vectors. PloS One 8, e53845

Balke C, Shorofsky SR (1998): Alterations in calcium handling in cardiac hypertrophy and heart failure. Cardiovasc Res 37, 290–299

Barandon L, Couffinhal T, Ezan J, Dufourcq P, Costet P, Alzieu P, Leroux L, Moreau C, Dare D, Duplàa C (2003): Reduction of infarct size and prevention of cardiac rupture in transgenic mice overexpressing FrzA. Circulation 108, 2282–2289

Baurand A, Zelarayan L, Betney R, Gehrke C, Dunger S, Noack C, Busjahn A, Huelsken J, Taketo MM, Birchmeier W, et al. (2007): β-catenin downregulation is required for adaptive cardiac remodeling. Circ Res 100, 1353–1362

Bergmann MW (2010): WNT signaling in adult cardiac hypertrophy and remodeling: lessons learned from cardiac development. Circ Res 107, 1198–1208

Berridge MJ (2006): Remodelling Ca2+ signalling systems and cardiac hypertrophy. Biochem Soc Trans 34, 228–231

Bers DM (2002): Cardiac excitation-contraction coupling. Nature 415, 198–205

Bie Zi dong, Sun Li ye, Geng Chuan liang, Meng Qing guo, Lin Xiao jing, Wang Yu feng, Wang Xue ban, Yang J (2016): MiR-125b regulates SFRP5 expression to promote growth and activation of cardiac fibroblasts. Cell Biol Int <u>40</u>, 1224–1234

Bindea G, Mlecnik B, Hackl H, Charoentong P, Tosolini M, Kirilovsky A, Fridman WH, Pagès F, Trajanoski Z, Galon J (2009): ClueGO: a Cytoscape plug-in to decipher functionally grouped gene ontology and pathway annotation networks. Bioinforma Oxf Engl <u>25</u>, 1091–1093

Bond J, Sedmera D, Jourdan J, Zhang Y, Eisenberg CA, Eisenberg LM, Gourdie RG (2003): Wnt11 and Wnt7a are up-regulated in association with differentiation of cardiac conduction cells in vitro and in vivo. Dev Dyn Off Publ Am Assoc Anat <u>227</u>, 536–543

Bretón-Romero R, Feng B, Holbrook M, Farb MG, Fetterman JL, Linder EA, Berk BD, Masaki N, Weisbrod RM, Inagaki E, et al. (2016): Endothelial dysfunction in human diabetes is mediated by Wnt5a-JNK signaling. Arterioscler Thromb Vasc Biol <u>36</u>, 561–569

Bryant D, Becker L, Richardson J, Shelton J, Franco F, Peshock R, Thompson M, Giroir B (1998): Cardiac failure in transgenic mice with myocardial expression of tumor necrosis factor-α. Circulation <u>97</u>, 1375–1381

Bundgaard H, Kjeldsen K (1996): Human myocardial Na,K-ATPase concentration in heart failure. Mol Cell Biochem <u>163–164</u>, 277–283

Burgoyne JR, Mongue-Din H, Eaton P, Shah AM (2012): Redox signaling in cardiac physiology and pathology. Circ Res <u>111</u>, 1091–1106

Calderone A, Thaik CM, Takahashi N, Chang DL, Colucci WS (1998): Nitric oxide, atrial natriuretic peptide, and cyclic GMP inhibit the growth-promoting effects of norepinephrine in cardiac myocytes and fibroblasts. J Clin Invest <u>101</u>, 812–818

Carvajal-Vergara X, Sevilla A, D'Souza SL, Ang YS, Schaniel C, Lee DF, Yang L, Kaplan AD, Adler ED, Rozov R, et al. (2010): Patient-specific induced pluripotent stem cell derived models of LEOPARD syndrome. Nature <u>465</u>, 808–812

Carvalho JL, de Carvalho PH, Gomes DA, Goes AM (2012): Characterization of decellularized heart matrices as biomaterials for regular and whole organ tissue engineering and initial in-vitro recellularization with ips cells. J Tissue Sci Eng <u>Suppl 11</u>, 002

Chang JT, Esumi N, Moore K, Li Y, Zhang S, Chew C, Goodman B, Rattner A, Moody S, Stetten G, et al. (1999): Cloning and characterization of a secreted frizzled-related protein that is expressed by the retinal pigment epithelium. Hum Mol Genet <u>8</u>, 575–583

Chen M, Zsengellér Z, Xiao CY, Szabó C (2004): Mitochondrial-to-nuclear translocation of apoptosis-inducing factor in cardiac myocytes during oxidant stress: potential role of poly(ADP-ribose) polymerase-1. Cardiovasc Res <u>63</u>, 682–688

Chen S, Guttridge DC, You Z, Zhang Z, Fribley A, Mayo MW, Kitajewski J, Wang CY (2001): Wnt-1 signaling inhibits apoptosis by activating beta-catenin/T cell factor-mediated transcription. J Cell Biol <u>152</u>, 87–96

Chen Y, Zou D, Wang N, Tan T, Liu Y, Zhao Q, Pu Y, Thapa RJ, Chen J (2018): SFRP5 inhibits the migration and invasion of melanoma cells through Wnt signaling pathway. OncoTargets Ther <u>11</u>, 8761–8772

Cho YK, Kang YM, Lee SE, Lee YL, Seol SM, Lee WJ, Park JY, Jung CH (2018): Effect of SFRP5 (Secreted Frizzled-Related Protein 5) on the WNT5A (wingless-type family member 5A)-induced endothelial dysfunction and its relevance with arterial stiffness in human subjects. Arterioscler Thromb Vasc Biol <u>38</u>, 1358–1367

Choudhury S, Bae S, Kumar SR, Ke Q, Yalamarti B, Choi JH, Kirshenbaum LA, Kang PM (2010): Role of AIF in cardiac apoptosis in hypertrophic cardiomyocytes from Dahl salt-sensitive rats. Cardiovasc Res 85, 28–37

Clerk A, Bogoyevitch MA, Anderson MB, Sugden PH (1994): Differential activation of protein kinase C isoforms by endothelin-1 and phenylephrine and subsequent stimulation of p42 and p44 mitogen-activated protein kinases in ventricular myocytes cultured from neonatal rat hearts. J Biol Chem 269, 32848–32857

Collins JF, Pawloski-Dahm C, Davis MG, Ball N, Dorn GW, Walsh RA (1996): The role of the cytoskeleton in left ventricular pressure overload hypertrophy and failure. J Mol Cell Cardiol 28, 1435–1443

Curran J, Hinton MJ, Ríos E, Bers DM, Shannon TR (2007): β-Adrenergic enhancement of sarcoplasmic reticulum calcium leak in cardiac myocytes is mediated by calcium/calmodulin-dependent protein kinase. Circ Res 100, 391–398

Cyganek L, Tiburcy M, Sekeres K, Gerstenberg K, Bohnenberger H, Lenz C, Henze S, Stauske M, Salinas G, Zimmermann WH, et al. (2018): Deep phenotyping of human induced pluripotent stem cell-derived atrial and ventricular cardiomyocytes. JCI Insight 3, e99941

Dai DF, Johnson SC, Villarin JJ, Chin MT, Nieves-Cintrón M, Chen T, Marcinek DJ, Dorn GW, Kang YJ, Prolla TA, et al. (2011): Mitochondrial oxidative stress mediates angiotensin II-induced cardiac hypertrophy and Gαq overexpression-induced heart failure. Circ Res 108, 837–846

Despa S, Lingrel JB, Bers DM (2012): Na+/K+-ATPase α2-isoform preferentially modulates Ca2+ transients and sarcoplasmic reticulum Ca2+ release in cardiac myocytes. Cardiovasc Res 95, 480–486

Devalla HD, Schwach V, Ford JW, Milnes JT, El-Haou S, Jackson C, Gkatzis K, Elliott DA, Chuva de Sousa Lopes SM, Mummery CL, et al. (2015): Atrial-like cardiomyocytes from human pluripotent stem cells are a robust preclinical model for assessing atrial-selective pharmacology. EMBO Mol Med 7, 394–410

Doyama K, Fujiwara H, Fukumoto M, Tanaka M, Fujiwara Y, Oda T, Inada T, Ohtani S, Hasegawa K, Fujiwara T, Sasayama S (1996): Tumour necrosis factor is expressed in cardiac tissues of patients with heart failure. Int J Cardiol 54, 217–225

Du Y, Zhao Y, Zhu Y, Hu C, Zhang J, Ji Q, Liu W, Han H, Yang L, Zhang D, et al. (2019): High serum secreted frizzled-related protein 5 levels associates with early improvement of cardiac function following ST-segment elevation myocardial infarction treated by primary percutaneous coronary intervention. J Atheroscler Thromb 26, 868–878

Eden M, Meder B, Völkers M, Poomvanicha M, Domes K, Branchereau M, Marck P, Will R, Bernt A, Rangrez A, et al. (2016): Myoscape controls cardiac calcium cycling and contractility via regulation of L-type calcium channel surface expression. Nat Commun 7, 11317

Edman CF, Schulman H (1994): Identification and characterization of δB-CaM kinase and δC-CaM kinase from rat heart, two new multifunctional Ca2+/calmodulin-dependent protein kinase isoforms. Biochim Biophys Acta 1221, 89–101

Ehrlund A, Mejhert N, Lorente-Cebrián S, Aström G, Dahlman I, Laurencikiene J, Rydén M (2013): Characterization of the Wnt inhibitors secreted frizzled-related proteins (SFRPs) in human adipose tissue. J Clin Endocrinol Metab 98, 503–508

Eisenberg CA, Gourdie RG, Eisenberg LM (1997): Wnt-11 is expressed in early avian mesoderm and required for the differentiation of the quail mesoderm cell line QCE-6. Dev Camb Engl 124, 525–536

Eisner DA, Caldwell JL, Kistamás K, Trafford AW (2017): Calcium and excitation-contraction coupling in the heart. Circ Res 121, 181–195

El-Battrawy I, Zhao Z, Lan H, Cyganek L, Tombers C, Li X, Buljubasic F, Lang S, Tiburcy M, Zimmermann WH, et al. (2018): Electrical dysfunctions in human-induced pluripotent stem cell-derived cardiomyocytes from a patient with an arrhythmogenic right ventricular cardiomyopathy. Europace 20, f46–f56

Eschenhagen T, Carrier L (2019): Cardiomyopathy phenotypes in human-induced pluripotent stem cell-derived cardiomyocytes-a systematic review. Pflugers Arch 471, 755–768

Frey N, Olson EN (2003): Cardiac hypertrophy: the good, the bad, and the ugly. Annu Rev Physiol 65, 45–79

Fujii M, Sakaguchi A, Kamata R, Nagao M, Kikuchi Y, Evans SM, Yoshizumi M, Shimono A, Saga Y, Kokubo H (2017): Sfrp5 identifies murine cardiac progenitors for all myocardial structures except for the right ventricle. Nat Commun 8, 14664

Fujio Y, Matsuda T, Oshima Y, Maeda M, Mohri T, Ito T, Takatani T, Hirata M, Nakaoka Y, Kimura R, et al. (2004): Signals through gp130 upregulate Wnt5a and contribute to cell adhesion in cardiac myocytes. FEBS Lett 573, 202–206

Gessert S, Kühl M (2010): The multiple phases and faces of wnt signaling during cardiac differentiation and development. Circ Res 107, 186–199

Go LO, Moschella MC, Watras J, Handa KK, Fyfe BS, Marks AR (1995): Differential regulation of two types of intracellular calcium release channels during end-stage heart failure. J Clin Invest 95, 888–894

Goldspink PH, Montgomery DE, Walker LA, Urboniene D, McKinney RD, Geenen DL, Solaro RJ, Buttrick PM (2004): Protein kinase Cε overexpression alters myofilament properties and composition during the progression of heart failure. Circ Res 95, 424–432

Gómez AM, Valdivia HH, Cheng H, Lederer MR, Santana LF, Cannell MB, McCune SA, Altschuld RA, Lederer WJ (1997): Defective excitation-contraction coupling in experimental cardiac hypertrophy and heart failure. Science 276, 800–806

Grimm M, Brown JH (2010): β-Adrenergic receptor signaling in the heart: role of CaMKII. J Mol Cell Cardiol 48, 322–330

Gutiérrez-Vidal R, Vega-Badillo J, Reyes-Fermín LM, Hernández-Pérez HA, Sánchez-Muñoz F, López-Álvarez GS, Larrieta-Carrasco E, Fernández-Silva I, Méndez-Sánchez N, Tovar AR, et al. (2015): SFRP5 hepatic expression is associated with non-alcoholic liver disease in morbidly obese women. Ann Hepatol 14, 666–674

Hagenmueller M, Riffel JH, Bernhold E, Fan J, Katus HA, Hardt SE (2014): Dapper-1 is essential for Wnt5a induced cardiomyocyte hypertrophy by regulating the Wnt/PCP pathway. FEBS Lett 588, 2230–2237

Hajjar RJ (2013): Potential of gene therapy as a treatment for heart failure. J Clin Invest 123, 53–61

Hamdani N, Krysiak J, Kreusser MM, Neef S, dos Remedios CG, Maier LS, Krüger M, Backs J, Linke WA (2013): Crucial role for ca2+/calmodulin-dependent protein kinase-II in regulating diastolic stress of normal and Failing hearts via titin phosphorylation. Circ Res 112, 664–674

Han Y, Chen YS, Liu Z, Bodyak N, Rigor D, Bisping E, Pu WT, Kang PM (2006): Overexpression of HAX-1 protects cardiac myocytes from apoptosis through caspase-9 inhibition. Circ Res 99, 415–423

Haq S, Michael A, Andreucci M, Bhattacharya K, Dotto P, Walters B, Woodgett J, Kilter H, Force T (2003): Stabilization of β-catenin by a Wnt-independent mechanism regulates cardiomyocyte growth. Proc Natl Acad Sci U S A <u>100</u>, 4610–4615

Hein S, Scholz D, Fujitani N, Rennollet H, Brand T, Friedl A, Schaper J (1994): Altered expression of titin and contractile proteins in failing human myocardium. J Mol Cell Cardiol <u>26</u>, 1291–1306

Henze S: Induced pluripotent stem cell-derived cardiomyocytes as model for studying CPVT caused by mutations in RYR2. Göttingen 2016

Herron TJ, McDonald KS (2002): Small amounts of α-myosin heavy chain isoform expression significantly increase power output of rat cardiac myocyte fragments. Circ Res <u>90</u>, 1150–1152

Hirotani S, Zhai P, Tomita H, Galeotti J, Marquez JP, Gao S, Hong C, Yatani A, Avila J, Sadoshima J (2007): Inhibition of glycogen synthase kinase 3β during heart failure is protective. Circ Res <u>101</u>, 1164–1174

Holly VL, Widen SA, Famulski JK, Waskiewicz AJ (2014): Sfrp1a and Sfrp5 function as positive regulators of Wnt and BMP signaling during early retinal development. Dev Biol <u>388</u>, 192–204

Hu MC, Rosenblum ND (2004): Smad1, β-catenin and Tcf4 associate in a molecular complex with the Myc promoter in dysplastic renal tissue and cooperate to control Myc transcription. Dev Camb Engl <u>132</u>, 215–225

Hu Z, Deng H, Qu H (2013): Plasma SFRP5 levels are decreased in Chinese subjects with obesity and type 2 diabetes and negatively correlated with parameters of insulin resistance. Diabetes Res Clin Pract <u>99</u>, 391–395

Hug N, Longman D, Cáceres JF (2016): Mechanism and regulation of the nonsense-mediated decay pathway. Nucleic Acids Res <u>44</u>, 1483–1495

Hurh S, Cho B, You DJ, Kim H, Lee EM, Lee SH, Park SJ, Park HC, Koo OJ, Yang J, et al. (2013): Expression Analysis of Combinatorial Genes Using a Bi-Cistronic T2A Expression System in Porcine Fibroblasts. PLoS ONE <u>8</u>, e70486

Järvinen K, Hotti A, Santos L, Nummela P, Hölttä E (2011): Caspase-8, c-FLIP, and caspase-9 in c-Myc-induced apoptosis of fibroblasts. Exp Cell Res <u>317</u>, 2602–2615

Jiang MT, Lokuta AJ, Farrell EF, Wolff MR, Haworth RA, Valdivia HH (2002): Abnormal Ca2+ release, but normal ryanodine receptors, in canine and human heart failure. Circ Res <u>91</u>, 1015–1022

Jin X, Guo B, Yan J, Yang R, Chang L, Wang Y, Miao C, Liu S, Zhang H, Li Y (2015): Angiotensin II increases secreted frizzled-related protein 5 (sFRP5) expression through AT1 receptor/Rho/ROCK1/JNK signaling in cardiomyocytes. Mol Cell Biochem <u>408</u>, 215–222

Joiner MA, Koval OM, Jingdong L, He BJ, Allamargot C, Gao Z, Luczak ED, Hall DD, Fink BD, Chen B, et al. (2012): CaMKII determines mitochondrial stress responses in heart. Nature <u>491</u>, 269–273

Jones SE, Jomary C (2002): Secreted frizzled-related proteins: searching for relationships and patterns. Bioessays <u>24</u>, 811–820

Jung YS, Lee HY, Kim SD, Park JS, Kim JK, Suh PG, Bae YS (2013): Wnt5a stimulates chemotactic migration and chemokine production in human neutrophils. Exp Mol Med <u>45</u>, e27

Kannel WB, Gordon T, Offutt D (1969): Left ventricular hypertrophy by electrocardiogram. Prevalence, incidence, and mortality in the Framingham study. Ann Intern Med <u>71</u>, 89–105

Kawakami K, Yamamura S, Hirata H, Ueno K, Saini S, Majid S, Tanaka Y, Kawamoto K, Enokida H, Nakagawa M, Dahiya R (2011): Secreted frizzled-related protein-5 (sFRP-5) is epigenetically downregulated and functions as a tumor suppressor in kidney cancer. Int J Cancer J Int Cancer 128, 541–550

Ke HY, Yang HY, Francis AJ, Collins TP, Surendran H, Alvarez-Laviada A, Firth JM, MacLeod KT (2019): Changes in cellular Ca2+ and Na+ regulation during the progression towards heart failure in the guinea pig. J Physiol 598, 1339–1359

Khadjeh S, Hindmarsh V, Weber F, Cyganek L, Vidal RO, Torkieh S, Streckfuss-Bömeke K, Lbik D, Tiburcy M, Mohamed BA, et al. (2020): CRISPLD1: a novel conserved target in the transition to human heart failure. Basic Res Cardiol 115, 27

Khoo MSC, Li J, Singh MV, Yang Y, Kannankeril P, Wu Y, Grueter CE, Guan X, Oddis CV, Zhang R, et al. (2006): Death, cardiac dysfunction, and arrhythmias are increased by calmodulin kinase II in calcineurin cardiomyopathy. Circulation 114, 1352–1359

Kim D, Bae S, Park J, Kim E, Kim S, Yu HR, Hwang J, Kim JI, Kim JS (2015): Digenome-seq: genome-wide profiling of CRISPR-Cas9 off-target effects in human cells. Nat Methods 12, 237–243

Kim NH, Kang PM (2010): Apoptosis in cardiovascular diseases: mechanism and clinical implications. Korean Circ J 40, 299–305

Kohlhaas M, Zhang T, Seidler T, Zibrova D, Dybkova N, Steen A, Wagner S, Chen L, Brown JH, Bers DM, Maier LS (2006): Increased sarcoplasmic reticulum calcium leak but unaltered contractility by acute CaMKII overexpression in isolated rabbit cardiac myocytes. Circ Res 98, 235–244

Kooij V, Boontje N, Zaremba R, Jaquet K, dos Remedios C, Stienen GJM, van der Velden J (2010): Protein kinase C α and ε phosphorylation of troponin and myosin binding protein C reduce Ca2+ sensitivity in human myocardium. Basic Res Cardiol 105, 289–300

Koval OM, Guan X, Wu Y, Joiner ML, Gao Z, Chen B, Grumbach IM, Luczak ED, Colbran RJ, Song L-S, et al. (2010): CaV1.2 beta-subunit coordinates CaMKII-triggered cardiomyocyte death and afterdepolarizations. Proc Natl Acad Sci U S A 107, 4996–5000

Kreiss P, Cameron B, Rangara R, Mailhe P, Aguerre-Charriol O, Airiau M, Scherman D, Crouzet J, Pitard B (1999): Plasmid DNA size does not affect the physicochemical properties of lipoplexes but modulates gene transfer efficiency. Nucleic Acids Res 27, 3792–3798

Kubota T, McTiernan CF, Frye CS, Slawson SE, Lemster BH, Koretsky AP, Demetris AJ, Feldman AM (1997): Dilated cardiomyopathy in transgenic mice with cardiac-specific overexpression of tumor necrosis factor α. Circ Res 81, 627–635

Kwong JQ, Molkentin JD (2015): Physiological and pathological roles of the mitochondrial permeability transition pore in the heart. Cell Metab 21, 206–214

Kwong JQ, Davis J, Baines CP, Sargent MA, Karch J, Wang X, Huang T, Molkentin JD (2014): Genetic deletion of the mitochondrial phosphate carrier desensitizes the mitochondrial permeability transition pore and causes cardiomyopathy. Cell Death Differ 21, 1209–1217

Lam CSP, Grewal J, Borlaug BA, Ommen SR, Kane GC, McCully RB, Pellikka PA (2010): Size, shape and stamina: the impact of left ventricular geometry on exercise capacity. Hypertension 55, 1143–1149

Levy D, Garrison RJ, Savage DD, Kannel WB, Castelli WP (1990): Prognostic implications of echocardiographically determined left ventricular mass in the Framingham Heart Study. N Engl J Med 322, 1561–1566

Li H, Zhu H, Xu Chi jie, Yuan J (1998): Cleavage of BID by Caspase 8 Mediates the Mitochondrial Damage in the Fas Pathway of Apoptosis. Cell 94, 491–501

Li Y, Kranias EG, Mignery GA, Bers DM (2002): Protein kinase A phosphorylation of the ryanodine receptor does not affect calcium sparks in mouse ventricular myocytes. Circ Res 90, 309–316

Li Y, Rankin SA, Sinner D, Kenny AP, Krieg PA, Zorn AM (2008): Sfrp5 coordinates foregut specification and morphogenesis by antagonizing both canonical and noncanonical Wnt11 signaling. Genes Dev 22, 3050–3063

Lian X, Zhang J, Azarin SM, Zhu K, Hazeltine LB, Bao X, Hsiao C, Kamp TJ, Palecek SP (2013): Directed cardiomyocyte differentiation from human pluripotent stem cells by modulating Wnt/β-catenin signaling under fully defined conditions. Nat Protoc 8, 162–175

Lieu DK, Fu JD, Chiamvimonvat N, Chan Tung KW, McNerney GP, Huser T, Keller G, Kong CW, Li RA (2013): Mechanism-based facilitated maturation of human pluripotent stem cell-derived cardiomyocytes. Circ Arrhythm Electrophysiol 6, 191–201

Lin K, Wang S, Julius MA, Kitajewski J, Moos M, Luyten FP (1997): The cysteine-rich frizzled domain of Frzb-1 is required and sufficient for modulation of Wnt signaling. Proc Natl Acad Sci 94, 11196–11200

Lindner M, Erdmann E, Beuckelmann DJ (1998): Calcium content of the sarcoplasmic reticulum in isolated ventricular myocytes from patients with terminal heart failure. J Mol Cell Cardiol 30, 743–749

Lino CA, Harper JC, Carney JP, Timlin JA (2018): Delivering CRISPR: a review of the challenges and approaches. Drug Deliv 25, 1234–1257

Lou Q, Janardhan A, Efimov IR (2012): Remodeling of calcium handling in human heart failure. Adv Exp Med Biol 740, 1145–1174

Lundy SD, Zhu WZ, Regnier M, Laflamme MA (2013): Structural and functional maturation of cardiomyocytes derived from human pluripotent stem cells. Stem Cells Dev 22, 1991–2002

Luo M, Anderson ME (2013): Ca2+ cycling in heart failure. Circ Res 113, 690–708

Lv C, Jiang Y, Wang H, Chen B (2012): Sfrp5 expression and secretion in adipocytes are up-regulated during differentiation and are negatively correlated with insulin resistance. Cell Biol Int 36, 851–855

Mali P, Yang L, Esvelt KM, Aach J, Guell M, DiCarlo JE, Norville JE, Church GM (2013): RNA-guided human genome engineering via Cas9. Science 339, 823–826

Martherus RSRM, Vanherle SJV, Timmer EDJ, Zeijlemaker VA, Broers JL, Smeets HJ, Geraedts JP, Ayoubi TAY (2010): Electrical signals affect the cardiomyocyte transcriptome independently of contraction. Physiol Genomics 42A, 283–289

Menasché P, Vanneaux V, Hagège A, Bel A, Cholley B, Cacciapuoti I, Parouchev A, Benhamouda N, Tachdjian G, Tosca L, et al. (2015): Human embryonic stem cell-derived cardiac progenitors for severe heart failure treatment: first clinical case report. Eur Heart J 36, 2011–2017

Mercadier JJ, Lompré AM, Duc P, Boheler KR, Fraysse JB, Wisnewsky C, Allen PD, Komajda M, Schwartz K (1990): Altered sarcoplasmic reticulum Ca2(+)-ATPase gene expression in the human ventricle during end-stage heart failure. J Clin Invest 85, 305–309

Meyer M, Schillinger W, Pieske B, Holubarsch C, Heilmann C, Posival H, Kuwajima G, Mikoshiba K, Just H, Hasenfuss G (1995): Alterations of sarcoplasmic reticulum proteins in failing human dilated cardiomyopathy. Circulation 92, 778–784

Michalak M, Agellon LB (2018): Stress coping strategies in the heart: an integrated view. Front Cardiovasc Med 5, 168

Mirotsou M, Zhang Z, Deb A, Zhang L, Gnecchi M, Noiseux N, Mu H, Pachori A, Dzau V (2007): Secreted frizzled related protein 2 (Sfrp2) is the key Akt-mesenchymal stem cell-released paracrine factor mediating myocardial survival and repair. Proc Natl Acad Sci 104, 1643–1648

Mishra S, Gupta RC, Tiwari N, Sharov VG, Sabbah HN (2002): Molecular mechanisms of reduced sarcoplasmic reticulum Ca(2+) uptake in human failing left ventricular myocardium. J Heart Lung Transplant Off Publ Int Soc Heart Transplant 21, 366–373

Miyoshi T, Doi M, Usui S, Iwamoto M, Kajiya M, Takeda K, Nosaka K, Nakayama R, Okawa K, Takagi W, et al. (2014): Low serum level of secreted frizzled-related protein 5, an anti-inflammatory adipokine, is associated with coronary artery disease. Atherosclerosis 233, 454–459

Mohamed BA, Hartmann N, Tirilomis P, Sekeres K, Li W, Neef S, Richter C, Zeisberg EM, Kattner L, Didié M, et al. (2018): Sarcoplasmic reticulum calcium leak contributes to arrhythmia but not to heart failure progression. Sci Transl Med 10, 0724

Mohamed TMA, Abou-Leisa R, Stafford N, Maqsood A, Zi M, Prehar S, Baudoin-Stanley F, Wang X, Neyses L, Cartwright EJ, Oceandy D (2016): The plasma membrane calcium ATPase 4 signalling in cardiac fibroblasts mediates cardiomyocyte hypertrophy. Nat Commun 7, 11074

Mohler PJ, Davis JQ, Bennett V (2005): Ankyrin-B Coordinates the Na/K ATPase, Na/Ca Exchanger, and InsP3 Receptor in a Cardiac T-Tubule/SR Microdomain. PLOS Biol 3, e423

Montgomery DE, Rundell VLM, Goldspink PH, Urboniene D, Geenen DL, de Tombe PP, Buttrick PM (2005): Protein kinase C ε induces systolic cardiac failure marked by exhausted inotropic reserve and intact Frank-Starling mechanism. Am J Physiol Heart Circ Physiol 289, H1881-1888

Moseley AE, Cougnon MH, Grupp IL, El Schultz J, Lingrel JB (2004): Attenuation of cardiac contractility in Na,K-ATPase α1 isoform-deficient hearts under reduced calcium conditions. J Mol Cell Cardiol 37, 913–919

Mozaffarian D, Anker SD, Anand I, Linker DT, Sullivan MD, Cleland JGF, Carson PE, Maggioni AP, Mann DL, Pitt B, et al. (2007): Prediction of mode of death in heart failure: the Seattle heart failure model. Circulation 116, 392–398

Mummery CL (2018): Perspectives on the use of human induced pluripotent stem cell-derived cardiomyocytes in biomedical research. Stem Cell Rep 11, 1306–1311

Nakamura K, Sano S, Fuster JJ, Kikuchi R, Shimizu I, Ohshima K, Katanasaka Y, Ouchi N, Walsh K (2016): Secreted frizzled-related protein 5 diminishes cardiac inflammation and protects the heart from ischemia/reperfusion injury. J Biol Chem 291, 2566–2575

Nakamura M, Sadoshima J (2018): Mechanisms of physiological and pathological cardiac hypertrophy. Nat Rev Cardiol 15, 387–407

Nakayama H, Bodi I, Maillet M, DeSantiago J, Domeier TL, Mikoshiba K, Lorenz JN, Blatter LA, Bers DM, Molkentin JD (2010): The IP3 receptor regulates cardiac hypertrophy in response to select stimuli. Circ Res 107, 659–666

Naqvi RU, Macleod KT (1994): Effect of hypertrophy on mechanisms of relaxation in isolated cardiac myocytes from guinea pig. Am J Physiol 267, H1851-1861

NCBI. https://www.ncbi.nlm.nih.gov/gene/6425; accessed on 18.05.2020

NEB. https://international.neb.com/protocols/0001/01/01/high-efficiency-transformation-protocol-c3019; accessed on 07.02.2019

Nichols M, Townsend N, Scarborough P, Rayner M (2014): Cardiovascular disease in Europe 2014: Epidemiological update. Eur Heart J 35, 2950–2959

Noubissi FK, Elcheva I, Bhatia N, Shakoori A, Ougolkov A, Liu J, Minamoto T, Ross J, Fuchs SY, Spiegelman VS (2006): CRD-BP mediates stabilization of βTrCP1 and c-myc mRNA in response to β-catenin signalling. Nature 441, 898–901

Ouchi N, Higuchi A, Ohashi K, Oshima Y, Gokce N, Shibata R, Akasaki Y, Shimono A, Walsh K (2010): Sfrp5 Is an anti-inflammatory adipokine that modulates metabolic dysfunction in obesity. Science 329, 454–457

Pandur P, Läsche M, Eisenberg LM, Kühl M (2002): Wnt-11 activation of a non-canonical Wnt signalling pathway is required for cardiogenesis. Nature 418, 636–641

Pattison JS, Waggoner JR, James J, Martin L, Gulick J, Osinska H, Klevitsky R, Kranias EG, Robbins J (2008): Phospholamban overexpression in transgenic rabbits. Transgenic Res 17, 157–170

Paul K, Ball NA, Dorn GW, Walsh RA (1997): Left ventricular stretch stimulates angiotensin II-mediated phosphatidylinositol hydrolysis and protein kinase C ε isoform translocation in adult guinea pig hearts. Circ Res 81, 643–650

Pavlović D, Fuller W, Shattock MJ (2007): The intracellular region of FXYD1 is sufficient to regulate cardiac Na/K ATPase. FASEB J Off Publ Fed Am Soc Exp Biol 21, 1539–1546

Peng C, Xiao X, Kang B, He S, Li J (2014): Serum secreted frizzled-related protein 5 levels differentially decrease in patients with hepatitis B virus-associated chronic infection and hepatocellular carcinoma. Oncol Lett 8, 1340–1344

Piacentino V, Weber CR, Chen X, Weisser-Thomas J, Margulies KB, Bers DM, Houser SR (2003): Cellular basis of abnormal calcium transients of failing human ventricular myocytes. Circ Res 92, 651–658

Picht E, Zima AV, Blatter LA, Bers DM (2007): SparkMaster: automated calcium spark analysis with ImageJ. Am J Physiol Cell Physiol 293, C1073-1081

Pieske B, Maier LS, Bers DM, Hasenfuss G (1999): Ca2+ handling and sarcoplasmic reticulum Ca2+ content in isolated failing and nonfailing human myocardium. Circ Res 85, 38–46

Pieske B, Maier LS, Piacentino V, Weisser J, Hasenfuss G, Houser S (2002): Rate dependence of [Na+]i and contractility in nonfailing and failing human myocardium. Circulation 106, 447–453

Ping P, Takano H, Zhang J, Tang XL, Qiu Y, Li RC, Banerjee S, Dawn B, Balafonova Z, Bolli R (1999): Isoform-selective activation of protein kinase C by nitric oxide in the heart of conscious rabbits: a signaling mechanism for both nitric oxide-induced and ischemia-induced preconditioning. Circ Res 84, 587–604

Ping P, Zhang J, Pierce WM, Bolli R (2001): Functional proteomic analysis of protein kinase C ε signaling complexes in the normal heart and during cardioprotection. Circ Res 88, 59–62

Ponikowski P, Anker SD, AlHabib KF, Cowie MR, Force TL, Hu S, Jaarsma T, Krum H, Rastogi V, Rohde LE, et al. (2014): Heart failure: preventing disease and death worldwide. ESC Heart Fail 1, 4–25

Primessnig U, Schönleitner P, Höll A, Pfeiffer S, Bracic T, Rau T, Kapl M, Stojakovic T, Glasnov T, Leineweber K, et al. (2016): Novel pathomechanisms of cardiomyocyte dysfunction in a model of heart failure with preserved ejection fraction. Eur J Heart Fail 18, 987–997

Protze SI, Liu J, Nussinovitch U, Ohana L, Backx PH, Gepstein L, Keller GM (2017): Sinoatrial node cardiomyocytes derived from human pluripotent cells function as a biological pacemaker. Nat Biotechnol 35, 56–68

Rapti K, Stillitano F, Karakikes I, Nonnenmacher M, Weber T, Hulot JS, Hajjar RJ (2015): Effectiveness of gene delivery systems for pluripotent and differentiated cells. Mol Ther Methods Clin Dev 2, 14067

Ren X, Yang Z, Xu J, Sun J, Mao D, Hu Y, Yang SJ, Qiao HH, Wang X, Hu Q, et al. (2014): Enhanced specificity and efficiency of the CRISPR/Cas9 system with optimized sgRNA parameters in Drosophila. Cell Rep 9, 1151–1162

Roderick HL, Higazi DR, Smyrnias I, Fearnley C, Harzheim D, Bootman MD (2007): Calcium in the heart: when it's good, it's very very good, but when it's bad, it's horrid. Biochem Soc Trans 35, 957–961

Satoh W, Matsuyama M, Takemura H, Aizawa S, Shimono A (2008): Sfrp1, Sfrp2, and Sfrp5 regulate the Wnt/β-catenin and the planar cell polarity pathways during early trunk formation in mouse. Genesis 46, 92–103

Schirone L, Forte M, Palmerio S, Yee D, Nocella C, Angelini F, Pagano F, Schiavon S, Bordin A, Carrizzo A, et al. (2017): A review of the molecular mechanisms underlying the development and progression of cardiac remodeling. Oxid Med Cell Longev 2017, 3920195

Schmidt U, Hajjar RJ, Kim CS, Lebeche D, Doye AA, Gwathmey JK (1999): Human heart failure: cAMP stimulation of SR Ca(2+)-ATPase activity and phosphorylation level of phospholamban. Am J Physiol 277, 474–480

Schröder M, Kaufman RJ (2006): Divergent roles of IRE1α and PERK in the unfolded protein response. Curr Mol Med 6, 5–36

Schumann H, Holtz J, Zerkowski HR, Hatzfeld M (2000): Expression of secreted frizzled related proteins 3 and 4 in human ventricular myocardium correlates with apoptosis related gene expression. Cardiovasc Res 45, 720–728

Schwinger RH, Böhm M, Schmidt U, Karczewski P, Bavendiek U, Flesch M, Krause EG, Erdmann E (1995): Unchanged protein levels of SERCA II and phospholamban but reduced Ca2+ uptake and Ca(2+)-ATPase activity of cardiac sarcoplasmic reticulum from dilated cardiomyopathy patients compared with patients with nonfailing hearts. Circulation 92, 3220–3228

Sedej S, Schmidt A, Denegri M, Walther S, Matovina M, Arnstein G, Gutschi EM, Windhager I, Ljubojević S, Negri S, et al. (2014): Subclinical abnormalities in sarcoplasmic reticulum Ca(2+) release promote eccentric myocardial remodeling and pump failure death in response to pressure overload. J Am Coll Cardiol 63, 1569–1579

Segura AM, Frazier OH, Buja LM (2014): Fibrosis and heart failure. Heart Fail Rev 19, 173–185

Shannon P, Markiel A, Ozier O, Baliga NS, Wang JT, Ramage D, Amin N, Schwikowski B, Ideker T (2003): Cytoscape: a software environment for integrated models of biomolecular interaction networks. Genome Res 13, 2498–2504

Sigma-Aldrich. https://www.sigmaaldrich.com/technical-documents/articles/biology/tips-for-cell-engineering-crispr-cas9.html; accessed on 18.05.2020

Silberbach M, Gorenc T, Hershberger RE, Stork PJS, Steyger PS, Roberts CT (1999): Extracellular signal-regulated protein kinase activation is required for the anti-hypertrophic effect of atrial natriuretic factor in neonatal rat ventricular myocytes. J Biol Chem 274, 24858–24864

Sklepkiewicz P, Shiomi T, Kaur R, Sun J, Kwon S, Mercer B, Bodine P, Schermuly RT, George I, Schulze PC, D'Armiento JM (2015): Loss of secreted frizzled-related protein-1 leads to deterioration of cardiac function in mice and plays a role in human cardiomyopathy. Circ Heart Fail 8, 362–372

Song LS, Sobie EA, McCulle S, Lederer WJ, Balke CW, Cheng H (2006): Orphaned ryanodine receptors in the failing heart. Proc Natl Acad Sci U S A 103, 4305–4310

Spiegelman VS, Slaga TJ, Pagano M, Minamoto T, Ronai Z, Fuchs SY (2000): Wnt/β-catenin signaling induces the expression and activity of βTrCP ubiquitin ligase receptor. Mol Cell 5, 877–882

Stuckenholz C, Lu L, Thakur PC, Choi TY, Shin D, Bahary N (2013): Sfrp5 modulates both Wnt and BMP signaling and regulates gastrointestinal organogenesis in the zebrafish. PloS One 8, e62470

Su Z, Zou A, Nonaka A, Zubair I, Sanguinetti MC, Barry WH (1998): Influence of prior Na+ pump activity on pump and Na+/Ca2+exchange currents in mouse ventricular myocytes. Am J Physiol-Heart Circ Physiol 275, H1808–H1817

Su Z, Sugishita K, Ritter M, Li F, Spitzer KW, Barry WH (2001): The sodium pump modulates the influence of INa on [Ca2+]i transients in mouse ventricular myocytes. Biophys J 80, 1230–1237

Sun M, Chen M, Dawood F, Zurawska U, Li JY, Parker T, Kassiri Z, Kirshenbaum LA, Arnold M, Khokha R, Liu PP (2007): Tumor necrosis factor-α mediates cardiac remodeling and ventricular dysfunction after pressure overload state. Circulation 115, 1398–1407

Suzuki H, Watkins DN, Jair KW, Schuebel KE, Markowitz SD, Dong Chen W, Pretlow TP, Yang B, Akiyama Y, van Engeland M, et al. (2004): Epigenetic inactivation of SFRP genes allows constitutive WNT signaling in colorectal cancer. Nat Genet 36, 417–422

Takahashi K, Tanabe K, Ohnuki M, Narita M, Ichisaka T, Tomoda K, Yamanaka S (2007): Induction of pluripotent stem cells from adult human fibroblasts by defined factors. Cell 131, 861–872

Takeishi Y, Ping P, Bolli R, Kirkpatrick DL, Hoit BD, Walsh RA (2000): Transgenic overexpression of constitutively active protein kinase C ε causes concentric cardiac hypertrophy. Circ Res 86, 1218–1223

Tamura N, Ogawa Y, Chusho H, Nakamura K, Nakao K, Suda M, Kasahara M, Hashimoto R, Katsuura G, Mukoyama M, et al. (2000): Cardiac fibrosis in mice lacking brain natriuretic peptide. Proc Natl Acad Sci U S A 97, 4239–4244

Teliewubai J, Ji H, Lu Y, Bai B, Yu S, Chi C, Xu Y, Zhang Y (2018): SFRP5 serves a beneficial role in arterial aging by inhibiting the proliferation, migration and inflammation of smooth muscle cells. Mol Med Rep 18, 4682–4690

Thomson JA, Itskovitz-Eldor J, Shapiro SS, Waknitz MA, Swiergiel JJ, Marshall VS, Jones JM (1998): Embryonic stem cell lines derived from human blastocysts. Science 282, 1145–1147

Tiburcy M, Hudson JE, Balfanz P, Schlick S, Meyer T, Chang Liao ML, Levent E, Raad F, Zeidler S, Wingender E, et al. (2017): Defined engineered human myocardium with advanced maturation for applications in heart failure modeling and repair. Circulation 135, 1832–1847

Tohyama S, Hattori F, Sano M, Hishiki T, Nagahata Y, Matsuura T, Hashimoto H, Suzuki T, Yamashita H, Satoh Y, et al. (2013): Distinct metabolic flow enables large-scale purification of mouse and human pluripotent stem cell-derived cardiomyocytes. Cell Stem Cell 12, 127–137

Torre-Amione G, Kapadia S, Lee J, Durand JB, Bies RD, Young JB, Mann DL (1996): Tumor necrosis factor-α and tumor necrosis factor receptors in the failing human heart. Circulation 93, 704–711

Torres R, Martin MC, Garcia A, Cigudosa JC, Ramirez JC, Rodriguez-Perales S (2014): Engineering human tumour-associated chromosomal translocations with the RNA-guided CRISPR-Cas9 system. Nat Commun 5, 3964

Toyofuku T, Hong Z, Kuzuya T, Tada M, Hori M (2000): WNT/Frizzled-2 signaling induces aggregation and adhesion among cardiac myocytes by increased cadherin–β-catenin complex. J Cell Biol 150, 225–242

Ueno S, Weidinger G, Osugi T, Kohn AD, Golob JL, Pabon L, Reinecke H, Moon RT, Murry CE (2007): Biphasic role for Wnt/β-catenin signaling in cardiac specification in zebrafish and embryonic stem cells. Proc Natl Acad Sci U S A 104, 9685–9690

Vakili BA, Okin PM, Devereux RB (2001): Prognostic implications of left ventricular hypertrophy. Am Heart J 141, 334–341

van Oort RJ, Respress JL, Li N, Reynolds C, De Almeida AC, Skapura DG, De Windt LJ, Wehrens XHT (2010): Accelerated development of pressure overload-induced cardiac hypertrophy and dysfunction in an RyR2-R176Q knockin mouse model. Hypertens Dallas Tex 1979 55, 932–938

Veeck J, Geisler C, Noetzel E, Alkaya S, Hartmann A, Knüchel R, Dahl E (2008): Epigenetic inactivation of the secreted frizzled-related protein-5 (SFRP5) gene in human breast cancer is associated with unfavorable prognosis. Carcinogenesis 29, 991–998

Vincent F, Duquesnes N, Christov C, Damy T, Samuel JL, Crozatier B (2006): Dual level of interactions between calcineurin and PKC-ε in cardiomyocyte stretch. Cardiovasc Res 71, 97–107

Wang D, Zhang Y, Shen C (2020): Research update on the association between SFRP5, an anti-inflammatory adipokine, with obesity, type 2 diabetes mellitus and coronary heart disease. J Cell Mol Med 24, 2730–2735

Wang X, Peng Q, Jiang F, Xue L, Li J, Fan Z, Chen P, Chen G, Cai Y (2017): Secreted frizzled-related protein 5 protects against oxidative stress-induced apoptosis in human aortic endothelial cells via downregulation of Bax. J Biochem Mol Toxicol 31, 12

Wang Y, Sano S, Oshima K, Sano M, Watanabe Y, Katanasaka Y, Yura Y, Jung C, Anzai A, Swirski FK, et al. (2019): Wnt5a-mediated neutrophil recruitment has an obligatory role in pressure overload-induced cardiac dysfunction. Circulation 140, 487–499

Weinberger F, Breckwoldt K, Pecha S, Kelly A, Geertz B, Starbatty J, Yorgan T, Cheng KH, Lessmann K, Stolen T, et al. (2016): Cardiac repair in guinea pigs with human engineered heart tissue from induced pluripotent stem cells. Sci Transl Med 8, 363ra148

Weisberg SP, McCann D, Desai M, Rosenbaum M, Leibel RL, Ferrante AW (2003): Obesity is associated with macrophage accumulation in adipose tissue. J Clin Invest 112, 1796–1808

Wu Y, MacMillan LB, McNeill RB, Colbran RJ, Anderson ME (1999): CaM kinase augments cardiac L-type Ca2+ current: a cellular mechanism for long Q-T arrhythmias. Am J Physiol 276, 2168–2178

Xiao A, Wang Z, Hu Y, Wu Y, Luo Z, Yang Z, Zu Y, Li W, Huang P, Tong X, et al. (2013): Chromosomal deletions and inversions mediated by TALENs and CRISPR/Cas in zebrafish. Nucleic Acids Res 41, e141

Xu H, Barnes GT, Yang Q, Tan G, Yang D, Chou CJ, Sole J, Nichols A, Ross JS, Tartaglia LA, Chen H (2003): Chronic inflammation in fat plays a crucial role in the development of obesity-related insulin resistance. J Clin Invest 112, 1821–1830

Yamamoto T, Su Z, Moseley AE, Kadono T, Zhang J, Cougnon M, Li F, Lingrel JB, Barry WH (2005): Relative abundance α2 Na(+) pump isoform influences Na(+)-Ca(2+) exchanger currents and Ca(2+) transients in mouse ventricular myocytes. J Mol Cell Cardiol <u>39</u>, 113–120

Yang L, Katchman A, Morrow JP, Doshi D, Marx SO (2011): Cardiac L-type calcium channel (Cav1.2) associates with γ subunits. FASEB J <u>25</u>, 928–936

Yang X, Pabon L, Murry CE (2014): Engineering adolescence: maturation of human pluripotent stem cell-derived cardiomyocytes. Circ Res <u>114</u>, 511–523

Yu J, Vodyanik MA, Smuga-Otto K, Antosiewicz-Bourget J, Frane JL, Tian S, Nie J, Jonsdottir GA, Ruotti V, Stewart R, et al. (2007): Induced pluripotent stem cell lines derived from human somatic cells. Science <u>318</u>, 1917–1920

Yue DT, Herzig S, Marban E (1990): Beta-adrenergic stimulation of calcium channels occurs by potentiation of high-activity gating modes. Proc Natl Acad Sci U S A <u>87</u>, 753–757

Zhao C, Bu X, Zhang N, Wang W (2009): Downregulation of SFRP5 expression and its inverse correlation with those of MMP-7 and MT1-MMP in gastric cancer. BMC Cancer <u>9</u>, 224

Acknowledgment

I would first like to thank my thesis advisor Prof. Dr. Gerd Hasenfuß of the clinic for cardiology, University medical center of Göttingen, who gave me the opportunity to work on the thesis. Especially, I want to thank both of my supervisors Dr. Lukas Cyganek from the Stem Cell Unit who enabled the work with the fascinating hiPSC- and CRISPR/Cas9-technology and Dr. Sara Klas from the Hasenfuß lab, who taught me to use AAVs and how to analyze the huge data set of mRNA sequencing. They always had an open door, whenever I ran into a trouble spot or had a question about my research or writing. They consistently allowed this thesis to be my own work but steered me in the right the direction whenever they thought I needed it. I would also like to thank these experts who were further involved in this research project:

- The Stem Cell Unit team for lab skill teaching and the warm and friendly atmosphere where I always felt welcome
- Nadine Gotzmann from the Stem Cell Unit for the support to generate the SFRP5^{KO} hiPSC-line and Vanessa Hindmarsh from the Hasenfuß lab for her support of its characterization
- Orr Shomroni from the NGS-facility for integrative genomics (University medical center Göttingen) for the analysis of the raw mRNA sequencing data set
- Dr Ulf Diekmann for yielding many suggestions and points for reflection and for the support in transcribing the thesis
- Hannah Neuenhofer and Moritz Stelter for the support to finalize my thesis

Without their passionate participation and input, the validation survey could not have been successfully conducted.

I would also like to acknowledge Prof. Dr Michael Zeisberg of the clinic for nephrology and rheumatology at the University medical center of Göttingen as the second reader of this thesis and his impulses during my thesis committee, and I am gratefully indebted for his very valuable comments on this thesis.

For the encouragement to apply for the *Kaltenbach-Doktorandenstipendium* of the *Deutsche Herzstiftung*, I want to thank Dr. Cyganek. The scholarship helped me to intensively focus on my thesis for one year.

Lebenslauf

Am 21.09.1994 wurde ich als Tochter von Heike Weber, geborene Paduch und Michael Weber in Gehrden geboren. Gemeinsam mit meiner Schwester Mareike Diekmann, geborene Weber, wuchs ich in Eldagsen auf und besuchte dort die Grundschule. In meiner Weiterführenden Schule, das Otto-Hahn-Gymnasium in Springe, wurde mein Interesse für die Naturwissenschaften und die Medizin geweckt. Nach meinem Abitur 2013 absolvierte ich ein Praktikum in der *REBIRTH Unit for Translational Hepatology and Stem Cell Biology* der Medizinischen Hochschule Hannovers in der Arbeitsgruppe von Prof Dr. Tobias Cantz in dem mein Interesse an der Wissenschaft geweckt wurde und ich das erste Mal mit der Technologie der induzierten pluripotenten Stammzellen in Berührung kam. Nach dem Beginn des Medizinstudiums an der Universität Göttingen im Wintersemester 2013 suchte ich nach erfolgreichem 1. Abschnitt der Ärztlichen Prüfung 2015 eine Doktorarbeit, welche auch mit dieser neuen Technologie arbeitete. Über die *Stem Cell Unit* unter der Leitung von Dr. Lukas Cyganek in Kooperation mit der AG Hasenfuß entstand so mein Promotionsthema „*The role of SFRP5 in cardiomyocyte function*". Ich begann im August 2016 mit der Arbeit an der Promotion. Um mich ausführlich auf das Promotionsvorhaben zu konzentrieren nahm ich mir zwei Freisemester in meinem Studium. Weitere zwei Semester neben dem Studium erforderte es noch meine Experimente zu vervollständigen. Durch die intensive Unterstützung von Dr. Lukas Cyganek war es mir zudem möglich, das Kaltenbach-Doktorandenstipendium der Deutschen Herzstiftung im Jahre 2017 zu erwerben. Den 2. Abschnitt der Ärztlichen Prüfung absolvierte ich im Oktober 2019. Mein Medizinstudium beendete ich im November 2020 erfolgreich mit dem 3. Abschnitt der Ärztlichen Prüfung.